DESIGN AND DEVELOPMENT OF A NEW GENERATION OF UV-VISIBLE-LIGHT-DRIVEN NANOSIZED CODOPED TITANIUM DIOXIDE PHOTOCATALYSTS AND BIOCIDES/SPOROCIDES, AND ENVIRONMENTAL APPLICATIONS

by

DAMBAR B. HAMAL

B.S., TRIBHUVAN UNIVERSITY, KATHMANDU, NEPAL, 1993

M. S., TRIBHUVAN UNIVERSITY, KATHMANDU, NEPAL, 1995

AN ABSTRACT OF A DISSERTATION

submitted in partial fulfillment of the requirements for the degree

DOCTOR OF PHILOSOPHY

Department of Chemsitry
College of Arts and Sciences

KANSAS STATE UNIVERSITY
Manhattan, Kansas

2009

Abstract

For solar environmental remediation, a new generation of nanosized (< 10 nm) titanium dioxide photocatalysts codoped with metals and nonmetals, or metals only were prepared by the xero-gel and aero-gel methods. For silver or cobalt-based xero-gel titanium dioxide photocatalysts, photoactivities tests revealed that codoping of titanium dioxide with a metal (1% Ag or 2% Co) and nonmetals (carbon and sulfur) is necessary to achieve high-activities for acetaldehyde degradation under visible light (wavelength > 420 nm). It was concluded that high visible-light-activities for acetaldehyde degradation over codoped titanium dioxide were attributed to an interplay of anatase crystallinity, high-surface area, reduced band-gap (< 3.0 eV), uniform dispersion of doped metal ions, and suppressed recombination rate of photogenerated electron-hole pairs. Moreover, the nature and amount of codoped metals play a significant role in visible-light-induced photocatalysis.

Metals (Al, Ga, and In) doped/codoped titanium dioxide photocatalysts were prepared by the aero-gel method. The photocatalytic studies showed that activities of metal doped/codoped photocatalysts under UV light (wavelength < 400 nm) were found to be dependent on pollutants. Indium demonstrated beneficial effects in both textural and photocatalytic properties. Gallium and indium codoped titanium dioxide photocatalysts displayed even better performance in the CO oxidation reaction under UV light. Notably, titanium dioxide codoped with Ga, In, and Pt, exhibited unique photoactivities for the CO oxidation under both UV and visible light irradiation,

indicating that this system could have promise for the water-gas shift reaction for hydrogen production.

Silver-based nanostructured titanium dioxide samples were developed for killing human pathogens (*Escherichia coli* cells and *Bacillus subtilis* spores). Biocidal tests revealed that silver, carbon, and sulfur codoped titanium dioxide nanoparticles (< 10 nm) possess very strong antimicrobial actions on both *E. coli* (logarithmic kill > 8) and *B. subtilis* spores (logarithmic kill > 5) for 30 minute exposures in dark conditions compared with Degussa P25. It was believed that the carbon and sulfur codoped titanium dioxide support and Ag species acted synergistically during deactivation of both *E. coli* and *B. subtilis* spores. Thus, titanium dioxide codoped with silver, carbon, sulfur can serve as a multifunctional generic biocide and a visible- light-active photocatalyst.

DESIGN AND DEVELOPMENT OF A NEW GENERATION OF UV-VISIBLE-LIGHT-DRIVEN NANOSIZED CODOPED TITANIUM DIOXIDE PHOTOCATALYSTS AND BIOCIDES/SPOROCIDES, AND ENVIRONMENTAL APPLICATIONS

by

DAMBAR B. HAMAL

B. S.; TRIBHUVAN UNIVERSITY, KATHMANDU, NEPAL, 1993

M. S.; TRIBHUVAN UNIVERSITY, KATHMANDU, NEPAL, 1995

A DISSERTATION

submitted in partial fulfillment of the requirements for the degree

DOCTOR OF PHILOSOPHY

Department of Chemistry
College of Arts and Sciences

KANSAS STATE UNIVERSITY
Manhattan, Kansas

2009

Approved by:

Major Professor
Kenneth J. Klabunde

Copyright

Abstract

For solar environmental remediation, a new generation of nanosized (< 10 nm) titanium dioxide photocatalysts codoped with metals and nonmetals, or metals only were prepared by the xero-gel and aero-gel methods. For silver or cobalt-based xero-gel titanium dioxide photocatalysts, photoactivities tests revealed that codoping of titanium dioxide with a metal (1% Ag or 2% Co) and nonmetals (carbon and sulfur) is necessary to achieve high-activities for acetaldehyde degradation under visible light (wavelength > 420 nm). It was concluded that high visible-light-activities for acetaldehyde degradation over codoped titanium dioxide were attributed to an interplay of anatase crystallinity, high-surface area, reduced band-gap (< 3.0 eV), uniform dispersion of doped metal ions, and suppressed recombination rate of photogenerated electron-hole pairs. Moreover, the nature and amount of codoped metals play a significant role in visible-light-induced photocatalysis.

Metals (Al, Ga, and In) doped/codoped titanium dioxide photocatalysts were prepared by the aero-gel method. The photocatalytic studies showed that activities of metal doped/codoped photocatalysts under UV light (wavelength < 400 nm) were found to be dependent on pollutants. Indium demonstrated beneficial effects in both textural and photocatalytic properties. Gallium and indium codoped titanium dioxide photocatalysts displayed even better performance in the CO oxidation reaction under UV light. Notably, titanium dioxide codoped with Ga, In, and Pt, exhibited unique photoactivities for the CO oxidation under both UV and visible light irradiation,

indicating that this system could have promise for the water-gas shift reaction for hydrogen production.

Silver-based nanostructured titanium dioxide samples were developed for killing human pathogens (*Escherichia coli* cells and *Bacillus subtilis* spores). Biocidal tests revealed that silver, carbon, and sulfur codoped titanium dioxide nanoparticles (< 10 nm) possess very strong antimicrobial actions on both *E. coli* (logarithmic kill > 8) and *B. subtilis* spores (logarithmic kill > 5) for 30 minute exposures in dark conditions compared with Degussa P25. It was believed that the carbon and sulfur codoped titanium dioxide support and Ag species acted synergistically during deactivation of both *E. coli* and *B. subtilis* spores. Thus, titanium dioxide codoped with silver, carbon, sulfur can serve as a multifunctional generic biocide and a visible- light-active photocatalyst.

Table of Contents

List of Figures

List of Tables

Acknowledgements

First of all, I would like to express my sincere and heartfelt gratitude to my doctorate advisor, Professor Kenneth J. Klabunde, at Kansas State University, for his honor to work under his guidance. I greatly appreciate the freedom he gave me and the opportunity to pursue my research in my own way. It is noteworthy to mention that I decided to pursuemy doctorate degree in Chemistry at KSU due to his priceless guidance and encouragement that have made my life richer and my research better. I also would like to thank him for the opportunities to participate conferences held inside and outside USA.

Secondly, I would like to thank my Graduate Committee Members: Professor Kenneth J. Klabunde, Professor Christopher J. Levy, Professor Takashi Ito, Professor Keith Hohn and Professor Thomas E. Roche. Thank you very much for you valuable time, suggestions and discussions. Thank you very much Professor Thomas E. Roche to be my outside chairperson of my graduate committee.

I sincerely would like to thank Dr. Shyamala Rajagopalan, Dr. David Jones, and other members of NanoScale Incorporation for their friendly help. I really enjoy working with you guys. A special thank goes to Dr. Ravi Mulukutla for his suggestions in the beginning of the project work.

I would like to thank my Master's Degree advisor, Professor Raja Ram Pradhananga, Tribhuvan University, Nepal. I also would like to thank Professor Tetsuo Saji, Tokyo Institute of Technology, Japan, for his honor to accept me as a UNESCO Fellow for "The 36th International Course for Advanced Research in Chemistry and Chemical Engineering", and to work under his guidance (2000 – 2001). A special thanks to Professor Christer B. Aakeroy and other chemistry faculty members for the opportunity to come to K-State and attend graduate school.

A special thanks to all the present and former group members of the KJK group during my time here: Dr. Shalini Rodrigues, Dr. Uma Sitharaman, Dr. Jeevanandam Pethaiyan, Dr. Ranjit Koodali, Dr. Igor Martyanov, Dr. Alexander Smetana, Dr. Dmytro Demydov, Dr. Aaron Yang, Dr. Johanna A. Haggstrom, Dr. Xiangxin Yang, Dr. Kennedy K. Kalebaila, Erin Beavers, Sreeram Cingarapu, Luther Mahoney, Yen-Ting Kuo, Khadga Man Shrestha, Manindu, and Sheila. Dr. Ranjit Koodali, Dr. Shalini Rodrigues and Dr. Dmytro Demydov are especially acknowledged for their help in kicking off TiO_2 photocatalysis. Additonally, I would like to thank Dr. Johanna and Dr. Azadeh Lalezari for their friendly help at KSU.

I sincerely would like to thank Earline Dikeman for help in teaching courses. Thank you to all the ladies in the office for helping with all kinds of things! Thank you very Richard Bachamp, Tobe Eggers and Jim Hodgson for fixing my equipment whenever needed! I would like to thank late Dr. George Marchin at the Division of Biology for providing lab facilities for biocidal tests of my samples. In addition, I would like to thank Dr. Dan Boyle and the Division of Biology for the assistance and use of the Transmission Electron Microscope. I am also thankful to Myles Ikenberry and Dr. Keith Hohn for the XPS measurements of the samples.

I would like to acknowledge NanoScale Incorporation, Manhattan, KS, and US Army Research Office for funding the present research works and paying my stipend.

I sincerely would like to thank my wife, Shanti Singh, for her enormous love and moral support. Thanks to my daughter, Smriti Hamal, and Son, Darshan Hamal for making me as a happy dad! Lastly, I also would like to thank my Father-in-law and mother-in-law (Dr. Surya B. Singh and Narayani Singh), elder sister and brother-in-law (Ramu Shah and Ravi B. Shah) and nephew (Mohan Malla) for their unlimited love, encouragement and support to come to the United States of America for advanced degree.

Dedication

To my parents

Mother Ran Kumari Hamal and Late Father Sher Bahadur Hamal

To my wife

Shanti Singh

And

To my brothers

Khushbi Ram Hamal and Late Binod Kumar Hamal

For their endless love and support in my life

Preface

Environmental issue concerned! Nanosized Anatase TiO_2 photocatalyst (1 nm = 10^{-9}m)

CHAPTER 1 - Introduction

1.1 Relevance of TiO_2 Heterogeneous Photocatalysis in Environmental Applications

The need to design and develop visible-light-driven photocatalysts is an important scientific research forum from the perspective of solar energy conversion and environmental remediation. According to the late Nobel laureate Richard Smalley (in his presentation on energy and nanotechnology conference, Rice University, Texas, 2003), for the next 50 years, we will face the most difficult problems in energy, food, water, environment, poverty, terrorism & war, disease, education, democracy and population.[1] Given the priority of the environmental issue, it is important for us to discuss the reasons for this. Of course, one explicit reason is based on the fact that the quality of human life depends largely on the quality of the environment. Unfortunately, rapid growth of world population and the emission of hazardous chemicals into the atmosphere, particularly from expanding industries in developing countries, have created serious environmental problems in natural air/water qualities. Therefore it is important that scientific research efforts rapidly advance in design and development of cost-effective, nontoxic and highly stable materials focused on advanced remediation technologies.

Further, in order to keep the environment safe, there is a growing demand for effective, economic, and benign air/water treatment technology. In this context, over the past decades, much research effort has been directed toward TiO_2 materials for the removal of toxic pollutants

from air, soil and water.[2] These efforts implied that heterogeneous photocatalysis based on titanium dioxide-based new nanomaterials could have great promise for the environmental remediation campaign. Before delving into the wide applicability of TiO_2 for a remediation campaign, it seems relevant to mention from a historic viewpoint that TiO_2 photocatalysis emerged as a new scientific area since the discovery of the Honda-Fujishima effect on photoelectrochemical splitting of water.[3] The other chronological milestones in the development of TiO_2 photoactivated phenomena include: reduction of CN^- in water (1977);[4] ammonia synthesis with Fe-doped TiO_2 (1977);[5] organic photosynthesis (1978);[6] organic pollutant mineralization (1983);[7] TiO_2 as microbiocide (1985);[8] treatment of tumor cells (1986);[9] solar cells (1991);[10] anti-fogging and self-cleaning materials (1998).[11] Above all, these chronological developments provide evidences for displaying the most important and versatile properties of TiO_2. Figure 1.1 shows the wide range of opportunity for research and development topics in TiO_2 heterogeneous photocatalysis due to its intrinsic photoinduced activities.[12]

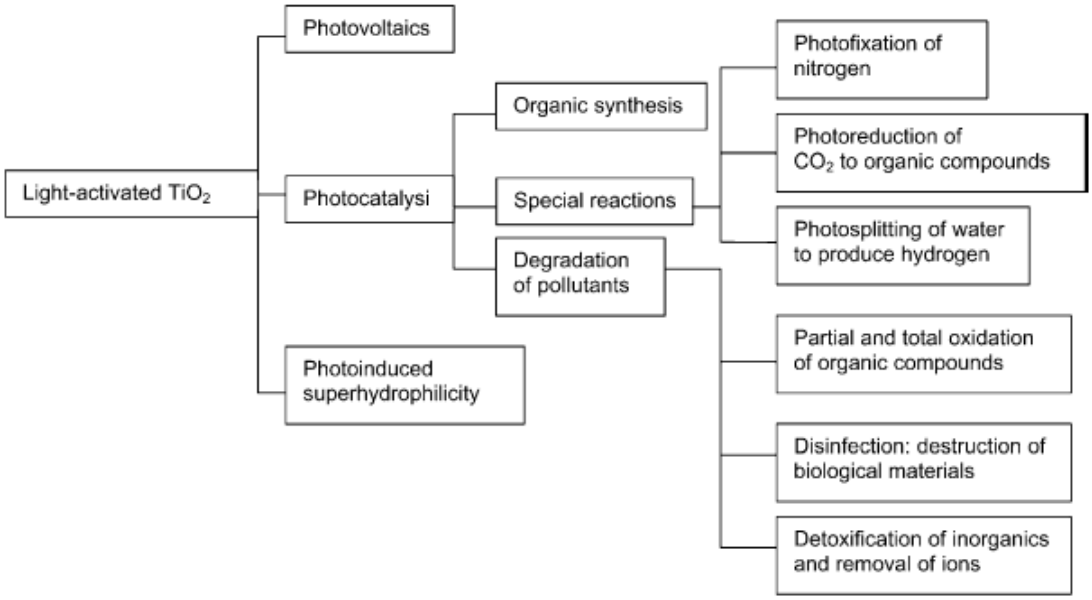

Figure 1.1 Photoinduced processes on TiO_2 [12]

Now from the environmental viewpoint, it is very important to mention that for air or water purification, titanium dioxide (TiO_2) photooxidation treatment has inexhaustible abilities to offer many distinctive advantages over well-known traditional technologies (carbon adsorption, biofiltration, incineration and chemical oxidation with chlorine) that are either inefficient or expensive to some extent. These distinctions include: (a) oxidation of pollutants at parts per million (ppm) levels under ambient conditions, (b) use of solar energy as the only input; (c) exhibition of reduction-oxidation properties, (d) use of oxygen as the only oxidant, and (e) design simplicity. Most intriguingly, TiO_2 exhibits inherent photoactivity, photochemical stability, nontoxicity and cost-effectiveness as priceless attributes that make it a foremost choice for researchers from both academe and industry.

1.2 Mechanistic Insights and Charge-Carrier Dynamics in TiO_2 Photocatalysis

Broadly defined, semiconductor-based heterogeneous photocatalysis involves the combination of photochemistry and catalysis, implying that both light and semiconductor catalysts are inevitable to enhance the rate of kinetically slow reactions. In contrast to metallic conductors and insulators, inorganic semiconductor catalysts are characterized by their specific electronic band structures known as the valence band (VB) and the conduction band (CB). The energy gap between the conduction band and valence band is referred to as band gap energy (E_g) that is usually measured in the order of few electron-volts. Figure 1.2 depicts the electronic band structures of some selected inorganic semiconductors. [13]

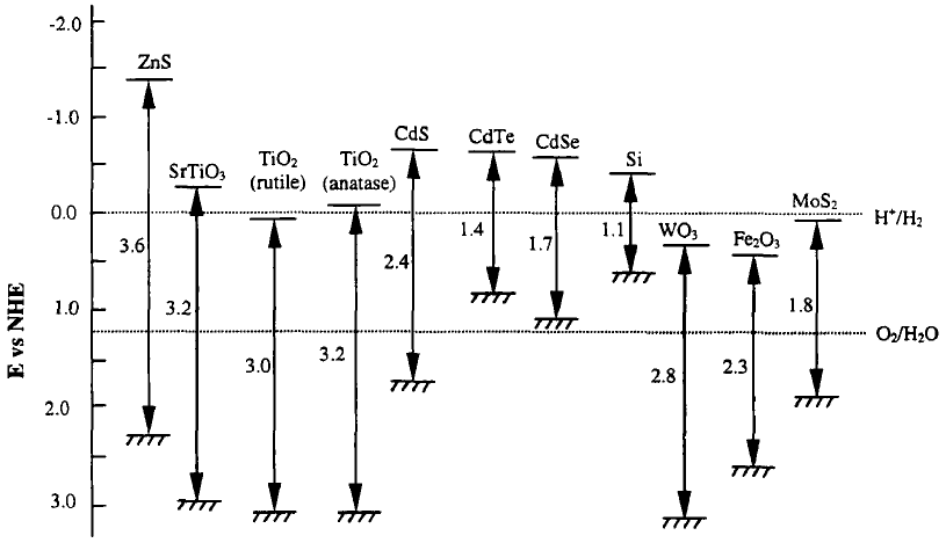

Figure 1.2 Valence and conduction band positions of semiconductors at pH = 0[13]

From a mechanistic viewpoint, input of the incident photons with energy greater than the band gap activate these semiconductors by exciting an electron (e^-) from the valence band into the conduction band, leaving a vacancy called a hole (h^+) in the valence band. These are known as photoinduced charge-carriers, which can move independently or remain as a bound pair (an exciton) due to the Columbic force of attractions. The generation and separation of photoinduced charge carriers (electrons/holes) are the first and foremost steps of all semiconductor-based photocatalytic reactions. In principle, these photoinduced electrons and holes behave as strong reducing and oxidizing agents respectively, and no sooner do they migrate to the surface of the photocatalysts than they can avail themselves for successive reduction and oxidation reactions. However, in reality, the surface and bulk properties of a photocatalyst actually determine the fate

and reaction pathway of the photogenerated electron-hole pairs. Figure 1.3 shows some major processes and their characteristic times for understanding mechanistic insights and charge-carriers dynamics in TiO_2 photocatalyzed degradation of organic pollutants.[12] It is obvious that both reduction and oxidation reactions go side by side on the TiO_2 photocatalyst particles due to the charge-carrier (electron-hole) generation. However, it must be noted that two critical processes- (i) the competition between charge-carrier recombination and trapping, and (ii) the competition between charge-carrier recombination and interfacial charge transfer- determine the overall activity of the TiO_2 photocatalyst. Naturally, it turns out that the faster the interfacial charge transfer, the higher the activity.

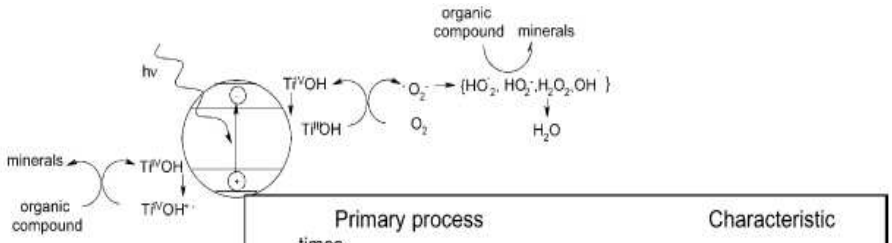

Primary process	Characteristic times
1. Charge-carrier generation:	
$TiO_2 + h\nu \rightarrow e_{CB}^- + h_{VB}^+$	fast
2. Charge-carrier trapping:	
a. $h_{VB}^+ + >Ti^{IV}OH \rightarrow \{>Ti^{IV}OH^{\bullet}\}^+$	fast (10ns)
b. $e_{CB}^- + >Ti^{IV}OH \leftrightarrow \{>Ti^{III}OH\}$ (shallow traps,dynamic equilibrium)	(100ps)
c. $e_{CB}^- + >Ti^{IV} \rightarrow >Ti^{III}$ (deep traps, irreversible)	(10ns)
3. Surface charge-carrier recombination:	
a. $e_{CB}^- + \{>Ti^{IV}OH^{\bullet}\}^+ \rightarrow >Ti^{IV}OH$	slow (100ns)
b. $h_{VB}^+ + \{>Ti^{III}OH\} \rightarrow >Ti^{IV}OH$	fast (10ns)
4. Interfacial charge transfer:	
a. $\{>Ti^{IV}OH^{\bullet}\}^+ + Red \rightarrow >Ti^{IV}OH + Red^{\bullet+}$	slow (100ns)
b. $e_{CB}^- + Ox \rightarrow >Ti^{IV}OH + Ox^{\bullet-}$	very slow (ms)

Figure 1.3 Major processes and their characteristic times for TiO_2-sensitized photooxidative mineralization of organic compounds by dissolved oxygen in aqueous solution[12]

Besides the direct participation of electron-hole pairs in the surface- bound redox reaction, it is known that depending upon the experimental conditions, the generation of other reactive oxygen species- hydroxyl radicals ($^{\bullet}OH$), superoxide anion (O_2^-), and hydrogen peroxide (H_2O_2) – do play crucial roles in the overall photocatalysis mechanism. Now, it seems reasonable to have an understanding on the oxidizing power of some common oxidants used in oxidation processes. It is known that the oxidizing power of an oxidant is intrinsically related to the magnitude of its standard reduction potential. Thus, the more positive reduction potential implies the more powerful oxidant. Table 1.1 shows that the molecular fluorine is the most powerful oxidizing agent due to its highest positive value of the oxidation potential (3.03 V *vs* NHE) compared with other chemical oxidants.[13]

Table 1.1 Oxidation potentials of some oxidants[13]

Species	Oxidation Potential (V)
Fluorine	3.03
Hydroxyl Radical	2.80
Atomic Oxygen	2.42
Ozone	2.07
Hydrogen Peroxide	1.78
Perhydroxyl Radical	1.70
Permanganate	1.68
Hypobromous Acid	1.59
Chlorine Dioxide	1.57
Hypochlorous Acid	1.49
Hypoiodous Acid	1.45
Chlorine	1.36
Bromine	1.09
Iodine	0.54
Molecular Oxygen	-0.56

But, the use of fluorine as an oxidant can be very unfortunate due to its toxic effects and dangers of explosions. On the other hand, Table 1.2 shows that the valence band holes (h^+) in photoactivated TiO_2 can exhibit nearly the same oxidizing power (2.96 V *vs* NHE) as compared with that of the fluorine, but much higher than that of hydroxyl radicals ($^{\bullet}OH$) and other chemical oxidants.[14] Therefore the use of the TiO_2 photocatalysis has been considered both the safest and the best alternative for the environmental remediation campaign.

Table 1.2 Oxidation potentials of oxidizing species during TiO_2 photocatalytic one-electron oxidation reaction[14]

Oxidizing Species	Eox/V versus NHE
h_{VB}^+	+ 2.96
h_{tr}^+	+ 1.6-1.7
$\bullet OH_{free}$	+ 2.72
$\bullet OH_{trap}$	+ 1.5, > +1.6

1.3 Second-Generation TiO_2 Photocatalysts in Environmental Applications

In accordance with the above-mentioned mechanism, it is relevant to mention that a variety of highly toxic and hazardous pollutants such as CO,[15] As(III),[16] NO,[17] N_2O,[18] HCHO,[19] CH_3CN,[20] CH_3COOH,[21] DMMP,[22] 2CEES,[23] benzene,[24] phenol,[25] aromatic esters[26] and dyes[27] have been degraded with UV light activated TiO_2 photocatalyst. Miyauchi et al.[28] reported that except for ZnO, anatase TiO_2 demonstrated superior activities to that of other single metal oxides (CeO_2, Cr_2O_3, CuO, Fe_2O_3, In_2O_3, SnO_2, V_2O_5 and WO_3) for methylene blue dye degradation under UV

light irradiation. All these examples indicate that the photomineralization of highly toxic and hazardous pollutants with the TiO_2 photocatalyst can be feasible only with UV light (3-5%) as energy input but not with visible light (40-45%) (Figure 1.4).[29] Consequently, pure TiO_2 is a less efficient photonic material due to its wide band gap energy (3.2 eV). Furthermore, in most cases, the TiO_2 photocatalyst seems to be incapable of discriminating between pollutants of high and low toxicities owing to the non-selective nature of highly reactive hydroxyl radicals (formed by hole oxidation of the hydroxyl anion). Attempts to overcome these shortcomings eventually led to second-generation TiO_2 photocatalysts of modified electronic and optical properties, particularly prepared by doping either nonmetals or metals.

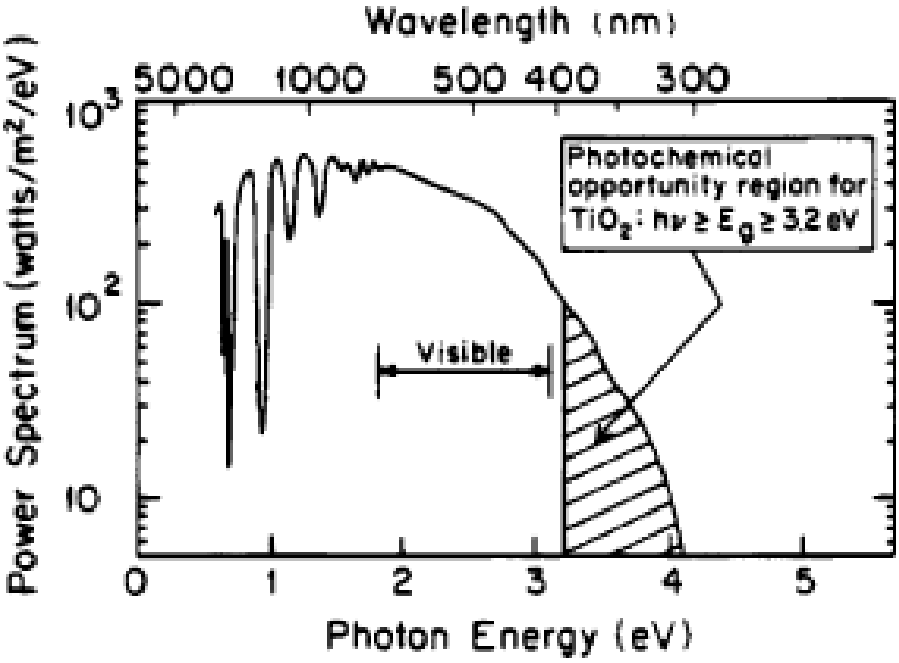

Figure 1.4 Solar spectrum at sea level with the sun at zenith[29]

There are a number of recent reports on TiO_2 photocatalysts particularly doped with carbon,[30] nitrogen,[31] phosphorus,[32] sulfur,[33] fluorine,[34] and iodine.[35] These research works have evidenced that nonmetal doping is very effective in narrowing the band gap of TiO_2 (< 3.0 eV). The reduction in band gap basically emanates from the incorporation of the nonmetal impurity into the Ti-O lattice or the formation of the intra-band states within the band gap of TiO_2. As a consequence, the photons of lower energy (λ> 400 nm) can excite TiO_2 particles to generate electron–hole pairs, which migrate to the surface and eventually engage in surface redox reactions, directly or indirectly. If the doped nonmetal forms intra-band trap states, the lifetime of charge-carrier separation predominates over the fast charge-recombination, thereby resulting in an enhanced visible light activity. Additionally, many authors reported that further enhancement in visible light activity can be achieved by codoping TiO_2 with two nonmetals such as C-S,[36] C-N,[37] N-F,[38] and N-Si.[39] A marked improvement in the visible light activity of the codoped TiO_2 occurs in comparison to pure and single nonmetal doped titania due to the synergetic effect of the two nonmetals.

Besides doping and codoping nonmetals only, various transition metals like V, Cr, Mn, Co, Ni and Cu have been doped into the bulk of pure TiO_2 substituting Ti^{4+} ions in the lattice through the ion-implantation technique to design second-generation visible light active TiO_2 photocatalysts.[40] The results show that the conduction band (3d) of TiO_2 overlap with the 3d-orbital of the doped transition metals results a in red shift of the band edge of TiO_2, and this shift is seen more pronounced in the cases of V and Fe.[40, 41] Although the ion-implantation technique produces a pronounced shift in the band edge of TiO_2 into the visible region, this method requires more expensive and more sophisticated equipment as compared to chemical methods,

which are economical and can be conducted at or near ambient temperatures. For example, the sol-gel prepared Fe-doped TiO_2 photocatalysts have been reported to be active for the degradation dye pollutants under visible light irradiation.[42] However, the transition metal ion-doped TiO_2 suffers from some serious drawbacks, such as thermal instability and low quantum efficiency of the photoinduced charge carriers (electron-hole pairs).[43] In addition to transition metal-ion doping, other researchers [44-51] have reported the effect of doping TiO_2 with main group metal ions like alkaline ions (Li^+, Na+, K^+), alkaline-earth ions (Be^{2+}, Mg^{2+}, Ca^{2+}, Sr^{2+}, Ba^{2+}), Ga^{3+}, In^{3+}, Sb^{3+}, Bi^{3+}, La^{3+}, and Ce^{4+}. The overall effect is that doping TiO_2 with these metal ions could not induce visible light activity, but enhanced the UV light activity. Apart from doping TiO_2 with a single metal or nonmetal, further design and development in visible light active photocatalysts have been achieved by codoping TiO_2 with a metal and a nonmetal such as (Sr, N)/TiO_2,[52] (Ni, B)/TiO_2,[53] (La, N)/TiO_2,[54] (La, S)/TiO_2,[55] (Fe, C)/TiO_2,[56] and (V, B)/TiO_2.[57] Interestingly, these new photocatalytic systems exhibited higher photocatalytic activities for degrading organic pollutants than that of the single metal or nonmetal - doped TiO_2. In these systems, it is noticed that the codoped nonmetal induces visible light absorption due to the band gap reduction of titania while the codoped metal suppress the photoinduced charge-carrier (electron-hole pairs) recombination.

In addition to the photomineralization of both inorganic and organic pollutants, the use of the TiO_2 photocatalysts in killing pathogenic organisms from air, soil and water represent a top priority since its historic discovery in 1985. Over the past years, researchers have shown that pathogenic bacteria could be killed effectively and efficiently with S-TiO_2,[58] N-TIO_2,[59] (C, N)-

TiO_2,[60] AgBr-TiO_2,[61] and AgI-TiO_2[62] photobiocides. Unlike organic and pure silver biocides, however, these photobiocides are inactive in killing of human pathogens in the dark condition.

1.4 Goals of the Current Research

From the above discussion, it is obvious that significant effort and progress have been made in metal and or/nonmetal codoped titanium dioxide photocatalysts for the degradation of highly toxic and hazardous organic pollutants, as well as killing of human pathogens under visible light. Most importantly, doping or codoping nonmetal(s) has been the best strategy to reduce band gap and shift the optical absorption edge of TiO_2 into the visible region. Further improvement in photoactivity seems to be highly promising for TiO_2 photocatalysts codoped with a metal and nonmetal. Now, what is the next step for design and development of visible light active photocatalysts that can be selectively used in a specific or multi-purpose? Up to now, there has been no research works reported in regard to design and development of TiO_2 photocatalysts prepared with an appropriate combination of different metals and/or nonmetals. However, there are several avenues for enhancing the photoresponse and photocatalytic activity of pure TiO_2 both under UV light and visible light. Firstly, the amount and the nature of metal dopant can be widely varied as per the experimental need; so doping of TiO_2 with metals of different electronic configurations together still deserves further attention. Therefore, it could be an appealing avenue for synthesizing highly active, nontoxic and stable TiO_2 photocatalysts for numerous photocatalytic applications. Secondly, metal ions have the abilities to modify both acidic and basic sites on the photocatalytic surfaces, depending upon their concentration. Thirdly, the doped

metals ions are good electron-scavengers and help suppress charge-carrier recombination. Therefore, we envision that metal-nonmetal-nonmetal or metal-metal-metal codoping would be new strategies to design and develop a new generation of UV – Visible light active TiO_2 photocatalyst as well as biocide/sporocide. Therefore, the current research study has been focused on achieving the following goals:

- To design and develop one metal (Ag) and two nonmetals (C, S) – codoped TiO_2 photocatalyst for degrading acetaldehyde, an indoor pollutant
- To design and develop one metal (Co) and two nonmetals (C, S) – codoped TiO_2 photocatalyst for degrading acetaldehyde, an indoor pollutant
- To design and develop three metals (Ga, In, Pt) – codoped TiO_2 photocatalyst for carbon monoxide photooxidation.
- To design and develop a multifunctional biocide/sporocide for killing human pathogens (*E. coli* and *Bacilus subtilis* spores)

It was discovered that materials in the nano-domain exhibit a unique surface chemical reactivity for the destructive absorption of acid gas and chemical warfare agents.[63, 64] This unique surface reactivity of nanomaterials was attributed to the high surface areas and the presence of defects, edges and corners. To further increase the performance of TiO_2 systems, the sol-gel [65-67] synthesis method has been used to prepare nanostructured gels (xerogels or aerogels) with appreciable surface area and porosity relative to bulk TiO_2. A high surface area is expedient to adsorb a large quantity of probe materials and porosity allows pollutants and by-products to diffuse in and out of the photocatalyst. Furthermore, the sol-gel synthesis method has the ability

to offers excellent control for achieving homogeneous multicomponent photocatalysts by varying the synthesis conditions. Also, preparing TiO_2 on the nanosize-domain increases the number of reactive sites per unit mass on the surface of the catalyst.

1.5 References

1. Graetzel, M., *Chem. Lett.* **2005**, 34, 8-13.
2. Hoffmann, M. R; Martin, S. T; Choi, W; Bahnemann, D. W., *Chem. Rev.***1995**, 95, 69-96.
3. Fujishima A, Honda K., *Nature* **1972**, 238, 37.
4. Frank, S. N; Bard, A. J., *J. Am. Chem. Soc* **1977**, 99, 303.
5. Kreutler B; Bard, A. J., *J. Am. Chem. Soc.* **1978**, 100, 4317.
6. Schrauzer, G. N; Guth, T. D., *J. Am. Chem. Soc.* **1977**, 99, 7189.
7. Pruden, A. L; Ollis, D. F., *J. Catal.* **1983**, 82, 404.
8. Matsunaga, T; Tomato, R; Nakajima, T; Wake, H., *FEMS Microbiol. Lett.* **1985**, 29, 211.
9. Fujishima, A; Ohtsuki, J; Yamashita, T; Hayakawa, S., *Photomed. Photobiol.* **1986,** 8, 45.
10. O'Regan, B; Gra¨tzel, M., *Nature* **1991,** 353, 737.
11. Wang, R; Hashimoto, K; Fujishima, A; Chikuni, M; Kojima, E; Kitamura, A., *Nature* **1997**, 388, 431.
12. Carp, O; Huisman, C. L; Reller, A., *Prog. Solid State Chem.* **2004**, 32, 33-177.
13. Chen, D; Shivakumar, M; Ray, A. K., Dev. *Chem. Mineral Process* 2000, 8, 505-550.
14. Tachikawa, T; Fujitsuka, M; Majima, T., *J. Phys. Chem. C* **2007**, 111, 5259-5275.
15. Vorontsov, A. V; Savinov, E. N; Kurkin, E. N; Torbova, O. D; Parmon, V. N., *React. Kinet. Catal. Lett.* **1997**, 62, 83-88.
16. Lee, H; Choi, W., *Environ. Sci. Technol.* **2002**, 36, 3872-3878.
17. Rusu, C. N; Yates, J. T. Jr., *J. Phys. Chem. B* **2000**, 104, 1729-1737.
18. Rusu, C. N; Yates, J. T. Jr., *J. Phys. Chem. B* **2001**, 105, 2596-2603.
19. Noguchi, T.; Fujishima, A; Sawunyama, P; Hashimoto, K., *Environ. Sci. Technol.* **1998**, 32, 3831-3833.
20. Zhuang, J; Rusu, C. N; Yates, J. T. Jr., *J. Phys. Chem. B* **1999**, 103, 6957-6967.
21. Wilson, J. N; Idriss, H., *J. Am. Chem. Soc.* **2002**, 124, 11284-11285.
22. Rusu, C. N; Yates, J. T. Jr., *J. Phys. Chem. B* **2000**, 104, 12299-12305.
23. Martyanov, I. N; Klabunde, K. J., *Environ. Sci. Technol*. **2003**, 37, 3448-3453.

24. Einaga, H; Futamura, S; Ibusuki, T., *Appl. Catal. B: Environ.* **2002**, 38, 215-225.

25. Colon, G.; Sanchez-Espana, J. M; Hidalgo, M. C; Navio, J. A., *J. Photochem. Photobiol. A: Chem.* **2006**, 179, 20-27.

26. Muneer, M; Theurich, J; Bahnemann, D., *J. Photochem. Photobiol. A: Chem.* **2001**, 143, 213-219.

27. Zainal, Z; Hui, L. K; Hussein, M. Z; Taufiq-Yap, Y. H; Abdullah, A. H; Ramli, I., *J. Hazar. Mater.* **2005**, 125, 113-120.

28. Miyauchi, M; Nakajima, A; Watanabe, T; Hashimoto, K., *Chem. Mater.* **2002**, 14, 2812-2816.

29. Linsebigler, A. L; Lu, G; Yates, J. T. Jr., *Chem. Rev.* **1995**, 95,735-58.

30. Nagaveni, K; Hegde, M. S; Ravishankar, N; Subbanna, G. N.; Madras, G., *Langmuir* **2004**, 20, 2900-2907.

31. Asahi, R; Morikawa, T; Ohwaki, T; Aoki, K; Taga, Y., *Science* **2001**, 293, 269-271.

32. Lin, Li; Lin, W; Zhu, Y; Zhao, B; Xie, Y., *Chem. Lett.* **2005**, 34, 284-285.

33. Ohno, T; Mitsui, T; Matsumura, M., *Chem. Lett.* **2003**, 32, 364-365.

34. Li, Di; Haneda, H; Labhsetwar, N. K; Hishita, S; Ohashi, N., *Chem. Phys. Lett.* **2005**, 401, 579-584.

35. Hong, X; Wang, Z; Cai, W; Lu, F; Zhang, J; Yang, Y; Ma, N; Liu, Y., *Chem. Mater.* **2005**, 17, 1548-1552.

36. Sun, H; Bai, Y; Cheng, Y; Jin, W; Xu, N., *Ind. Eng. Chem. Res.* 2006, 45, 4971-4976.

37. Cong, Y; Chen, F; Zhang, J; Anpo, M., *Chem. Lett.* **2006**, 35, 800-801.

38. Li, D; Haneda, H; Hishita, S; Ohashi, N., *Chem. Mater.* **2005**, 17, 2588-2595.

39. Ozaki, H; Iwamoto, S; Inoue, M., *Chem. Lett.* **2005**, 34, 1082-1083.

40. Yamashita, H; Harada, M; Misaka, J; Takeuchi, M; Ikeue, K; Anpo, Ma., *J. Photochem. Photobiol. A: Chem.* **2002**, 148, 257-261.

41. Anpo, M; Takeuchi, M., *J. Catal.* **2003**, 216, 505-516.

42. Wang, X. H; Li, J. G; Kamiyama, H; Moriyoshi, Y; Ishigaki, T., *J. Phys. Chem. B* **2006**, 110, 6804-6809.

43. Choi, W; Termin, A; Hoffmann, M. R., *J. Phys. Chem.* **1994**, 98, 13669-79.

44. Bessekhouad, Y; Robert, D; Weber, J. V; Chaoui, N., *J. Photochem. Photobiol. A: Chem.* **2004**, 167, 49-57.

45. Li, Y; Peng, S; Jiang, F; Lu, G; Li, S., *J. Serb. Chem. Soc.* **2007**, 72, 393-402.

46. Zhou, J; Zhang, Y; Zhao, X. S; Ray, A. K., *Ind. Eng. Chem. Res.* **2006**, 45, 3503-3511.

47. Shchukin, D; Poznyak, S; Kulak, A; Pichat, P. *J. Photochem. Photobiol. A: Chem.* **2004**, 162, 423-430.

48. Moon, J; Takagi, H; Fujishiro, Y; Awano, M., *J. Mater. Sci.* **2001**, 36, 949-955.

49. Zuo, H; Sun, J; Deng, K; Su, R; Wei, F; Wang, D., *Chem. Eng. Technol.* **2007**, 30, 577-582.

50. Jin, M; Nagaoka, Y; Nishi, K; Ogawa, K; Nagahata, S; Horikawa, T; Katoh, M; Tomida, T; Hayashi, J., *Adsorption* **2008**, 14, 257-263.

51. Galindo, F; Gomez, R; Aguilar, M., *J. Mol. Catal. A: Chem.* **2008**, 281, 119-125.

52. Sakatani, Y; Ando, H.; Okusako, K; Koike, H; Nunoshige, J; Takata, T; Kondo, J. N; Hara, M; Domen, K., *J. Mater. Res.* **2004**, 19, 2100-2108.

53. Zhao, W; Ma, W; Chen, C; Zhao, J; Shuai, Z., *J. Am. Chem. Soc.* **2004**, 126, 4782-4783.

54. Sakatani, Y; Nunoshige, J; Ando, H; Okusako, K; Koike, H; Takata, T; Kondo, J. N; Hara, M; Domen, K., *Chem. Lett.* **2003**, 32, 1156-1157.

55. Liu, H; Gao, L., *Chem. Lett.* **2004**, 33, 730-731.

56. Tryba, B; Morawski, A. W; Inagaki, M; Toyoda, M., *J. Photochem. Photobiol. A: Chem.* **2006**, 179, 224-228.

57. Bettinelli, M; Dallacasa, V; Falcomer, D; Fornasiero, P; Gombac, V; Montini, T; Romano, L; Speghini, A., *J. Hazar.Mater.* **2007**, 146, 529-534.

58. Yu, J. C; Ho, W; Yu, J; Yip, H; Wong, P. K; Zhao, J., *Environ. Sci. Technol*. **2005**, 39, 1175-1179.

59. Wong, M. S; Chu, W. C; Sun, D. S; Huang, H. S; Chen, J. H; Tsai, P. J; Lin, N. T; Yu, M. S; Hsu, S. F; Wang, S. L; Chang, H. H., *Appl. Environ. Microbiol*. **2006**, 72, 6111-6116.

60. Li, Qi; Xie, R.; Li, Y. W.; Mintz, E. A.; Shang, J. K., *Environ. Sci. Technol*. **2007**, 41, 5050-5056.

61. Hu, C.; Guo, J.; Qu, J.; Hu, X., *Langmuir* **2007**, 23, 4982-4987.

62. Lan, Y; Hu, C; Hu, X; Qu, J., *Appl. Catal. B* **2007**, 73, 354-360.

63. Corrie L. C; Klabunde, K. J., *Chem. Mater*. **2002**, 14, 1807.

64. Medine, G. M; Zaikovskii, V; Klabunde, K. J., *J. Mater. Chem.* **2004**, 14, 757.

65. Hench, L. L; West, J. K., *Chem. Rev.* **1990**, 90, 33-72.

66. Rolison, D. R; Dunn, B., *J. Mater. Chem.* **2001**, 11, 963-980.

67. Pierre, A. C; Pajonk, G. M., *Chem. Rev.* **2002**, 102, 4243-4265.

CHAPTER 2 - Synthesis, Characterization and Visible Light Activity of New Nanoparticle Photocatalysts Based on Silver, Carbon and Sulfur-Doped TiO_2

2.1 Introduction

The phenomenon of photocatalysis is defined as the combination of photochemistry and catalysis. More precisely, the term "photocatalysis" herein implies that the light and a catalyst are essential to enhance the rates of thermodynamically favored but kinetically slow photophysical and photochemical transformations. Indeed, photocatalysis emerged as a new scientific area when Fujishima and Honda carried out photolysis of water into environmentally clean fuels (hydrogen and oxygen) using a titanium dioxide electrode in an electrochemical cell.[1] Ever since, heterogeneous photocatalysis by means of TiO_2 has been widely accepted and exploited as an efficient technology for killing bacteria and degrading organic and inorganic pollutants.[2-13] Moreover, titanium dioxide (TiO_2) has been regarded as an excellent semiconductor photocatalyst because of its performance, low cost, nontoxicity, stability and availability. Unfortunately, because of its wide band gap (Anatase: 3.2 eV; Rutile: 3.0 eV), the extensive exploitation of TiO_2 created an expectation to use merely 3-4% UV light of the whole radiant solar energy.

Fortunately, there are, however, a number of empirical ways to design and develop a second generation of visible-light-sensitive photocatalysts of titanium dioxide by means of physical and chemical processes.[14, 15] Of the various processes cited in the literature, ion implantation methods require more expensive and more sophisticated equipment, whereas chemical methods are more

economical and can be conducted at or near ambient temperatures. In context, a great deal of effort has shown that doping with transition metals, such as Cr, Co, V and Fe, extends the spectral response of TiO_2 well into the visible region and enhances the photoreactivity.[16-19] However, transition metal ion-doped TiO_2 suffers from some serious drawbacks, such as thermal instability and low quantum efficiency of the photoinduced charge carriers (electron-hole pairs).[20] Besides metal ion-doped TiO_2 systems, there are numerous recent reports on nonmetal-doped TiO_2, for example, carbon, nitrogen, phosphorus, sulfur and fluorine doped photocatalysts.[21-33] Basically, doping with carbon, nitrogen and sulfur effectively narrows the band gap of TiO_2 (<3.0 eV).[34-36] Moreover, band gap narrowing emanates from the electronic perturbations caused by change of the lattice parameters and/or the presence of the trap states within conduction and valence bands of TiO_2. Consequently, the photons of lower energy (λ> 420 nm) can induce electron–hole pairs in TiO_2. These photoinduced electrons and holes, which are in fact very powerful reducing and oxidizing agents, migrate to the surface of TiO_2 and eventually become available for direct or indirect consecutive reduction and oxidation reactions. Furthermore, because of the presence some trap states within the band gap of titanium dioxide, the lifetime of the so-called photoinduced charge-carriers increases in such a way that it predominates over the fast charge-recombination process, thereby resulting in an enhanced visible light reactivity.

Apart from doping TiO_2 with a single metal or nonmetal, it is highly anticipated that doping TiO_2 with an appropriate combination of metals and/or nonmetals would, of course, result in more visible light sensitive photocatalysts for a desired application. In this context, Di Li et al. synthesized N-F-codoped TiO_2 photocatalysts by spray pyrolysis (SP) using $TiCl_3$ and NH_4F precursors and observed an enhanced photoreactivity of the materials in visible light.[37] Hongmei

Luo et al. prepared a Br and Cl-codoped TiO_2 system and demonstrated the efficiency of the material for photocatalytic splitting of water into H_2 and O_2 in the presence of Pt co-catalyst and UV light irradiation.[38] These recent efforts and strategies have revealed that codoping TiO_2 with a metal and a nonmetal can result in the development of additional visible active photocatalysts.[39-41]

It is well known that noble metals such as Ag, Au and Pt possess unique electronic and catalytic properties. For example, X. Z. Li reported that Au^{3+}-doped TiO_2 exhibited visible light reactivity for the photodegradation of methylene blue.[42] Likewise, Soonhyun Kim et al. prepared Pt ion-doped TiO_2, and examined its visible light activity for the photodegradation of chlorinated organic compounds.[43] From an economic viewpoint, gold and platinum are very expensive and unaffordable metals for extensive use in photocatalysis. Compared to gold and platinum, silver is a more affordable metal and deserves further investigation. Munevver et al. reported a Ag-TiO_2 system for killing E. *coli* under UV light illumination.[44] There have been some reports on the preparation of Ag^+-doped TiO_2 films and nanoparticlesthat degrade some textile dyes (methyl orange, crystal violet, and methyl red) in aqueous medium.[45-47] Furthermore, silver halides, such as AgBr/SiO_2 and AgCl catalysts, have also been used in photocatalysis.[48, 49] It appears that doping with Ag^+ ions makes a dramatic improvement in the performance of TiO_2 photocatalysts; however, the aforementioned silver based photocatalysts function only under UV light. Earlier, researchers in our group have reported the synthesis and characterization of some nanocrystalline metal oxides and mixed metal oxides. It was discovered that materials in the nano-domain exhibit a unique surface chemical reactivity for the destructive absorption of acid gas and

chemical warfare agents.[50, 51] Moreover, this unique surface reactivity of nanomaterials was attributed to the high surface areas and the presence of defects, edges and corners.

Therefore, it is rationally more desirable to synthesize new nanoparticle visible-light-driven photocatalysts based on silver, carbon and/or sulfur-doped TiO_2. To accomplish the desired work, a quest for a suitable precursor material seems indispensable for carbon and sulfur dopants. On this line of research, J. H. Park et al. prepared carbon-doped TiO_2 nanotube arrays at an elevated temperature range of 500^o-800^oC by using carbon monoxide precursor, and tangibly demonstrated the catalytic efficiency of the C-doped TiO_2 nanotubes for water splitting under visible light irradiation.[52] Further, Y. Choi et al. fabricated C-doped TiO_2 photocatalysts by oxidative annealing of TiC and ended up with the conclusion that C-doped TiO_2 powder exhibited superior photoactivity for the photodecomposition of methylene blue and water under UV light.[53] Thus, carbon monoxide can be used, but it is rather dangerous and is not a suitable precursor for carbon dopant on a large-scale synthesis. Also, oxidative annealing of TiC requires hundreds of hours or progressively very high temperatures (600^o–750^o C) for optimal activity of the materials and such a high temperature synthesis results in materials inclusive of anatase-rutile phases and lower surface areas, thereby making them less worthwhile for photocatalysis. We thus realize, in essence, the need for a more suitable precursor for carbon and sulfur dopants other than TiC, CO and NH_2CSNH_2. Herein, we express a strong preference for carbon and sulfur as nonmetal dopants, because these elements can stabilize Ag^+ ions in doped TiO_2 systems. Moreover, the well-dispersed Ag^+ ions trap photoinduced electrons, leading to a substantial increase in electron-hole separation and a concomitant decrease in charge-carrier recombination.

In this chapter, we focus on synthesis and characterization of silver, carbon and sulfur -codoped nanosized anatase TiO_2 photocatalysts, and the photoreactivity of the synthesized materials was evaluated for the degradation of gaseous acetaldehyde (a major indoor pollutant) under UV and visible light.

2.2 Experimental

2.2.1 Materials Required

Ethanol (Absolute, 200 Proof, Aaper Alcohol and Chemical Co.), titanium (IV) isopropoxide (97% Sigma-Aldrich), Ammonium thiocyanate (97.5% Alfa Aesar), thiourea (99%, Alfa Aesar), silver nitrate (99.9+%, Alfa Aesar), and ammonium hydroxide (29.9%, Fisher) were used as received without further purification.

2.2.2 Catalyst Synthesis

Herein, we chose two different nonmetal precursors, ammonium thiocyanate (hereafter the samples are designated as-01) and thiourea (hereafter the samples are designated as-02) to elucidate the effect of precursor materials on the photoreactivity of the doped TiO_2.

In a typical procedure, 0.031 moles (8.5 g) of titanium (IV) isopropoxide and 0.124 moles (9.44 g) of ammonium thiocyanate or thiourea (9.42 g) were dissolved 200 mL ethanol under vigorous stirring followed by drop-wise addition of 0.125 moles (2.25 g) of de-ionized water containing 0.62 mL (0.00031 moles) of $AgNO_3$ (0.5 M) and one mL (0.0015 moles) of NH_4OH for complete hydrolysis. After stirring for five minutes at room temperature, the solvent was

completely evaporated in a rotavapor. The as-synthesized samples (11.5-12 g, 92.6 % – 96 % yield) were kept over night in a drying cabinet, and calcined at 500^{o}C for two hours in air at a heating rate of 5^{o}C/min using a Chamber Furnace (Carbolite, CWF-1100). The resulting yellow product was ground well into fine particles. For comparison, the same experimental procedure was used for the synthesis of only nonmetal doped-TiO_2.

2.2.3 Catalyst Characterization

A Scanning Electron Microscope-S-3500N and Absorbed Electron Detector- S-6542 (Hitachi Science Systems, Ltd.), EDXA (Inca Energy, Oxford Instruments Microanalysis Ltd.) were used to determine the surface composition of the samples under the specified conditions of 20 keV, 15 mm working distance and 4000X magnification. X-ray diffraction (XRD) patterns of samples were recorded on a Scintag XDS 2000 D8 diffractometer with Cu-Kα radiation of wavelength of 1.5406 Å and were analyzed from 15^{o}–75^{o} (2θ) with a step size of 0.05^{o} and step time of 3s to assess the crystallinity of the catalysts under study. Nitrogen adsorption–desorption isotherms were recorded at liquid nitrogen temperature (77K) on a Quantachrome Instrument (NOVA 1000 Series) and the specific surface areas were determined by the Brunauer-Emmett- Teller (BET) method. The Barrett-Joyner- Halenda (BJH) method was used to determine the pore size distributions derived from the BJH desorption isotherms. IR spectra were recorded on a Nicolet NEXUS 670 FTIR instrument to detect the presence of carbonate and sulfate by pelletizing with KBr as a reference. Raman spectra were measured to assess the anatase crystallinity. The UV-Vis absorption spectra were recorded from 200 nm to 800 nm on a Cary 500 Scan UV-Vis NIR Spectrometer with an integrating sphere attachment using PTFE powder as a reference.

2.2.4 Kinetics of Photocatalysis

Kinetic study of the photocatalysts for the photodegradation of gaseous acetaldehyde was performed in a 305 mL cylindrical air-filled static glass reactor with a quartz window at room temperature. 103 mg of the catalyst was placed in a circular glass dish and mounted into the reactor. 100 μL of liquid acetaldehyde was added into the reactor, which vaporized, and the gaseous mixture of acetaldehyde and air was constantly stirred. Prior to light illumination, the concentration of the probe molecule was allowed to equilibrate for 40 minutes, and 35 μL of gaseous aliquot from the reactor was periodically extracted and analyzed on a GC-MS port (Shimadzu GCMS-QP 5000). The temperatures of the column, injector and detector were maintained at 40^{o}, 200^{o} and 280^{o}C, respectively. For the visible light experiment, the sample was illuminated with a 1000 W high-pressure mercury lamp (Oriel Corp.) at a distance of 20 cm from the top using combined filters, one VIS-NIR long pass filter (400 nm) and another colored glass filter (> 420 nm). Exactly, the same procedure was followed for the UV light experiment by using two cut-off filters (320 nm < λ < 420 nm).

2.3 Results and Discussion

2.3.1 Characterization

Table 2.1 shows the EDXA measurements of the doped TiO_2 samples annealed at 500^oC/2h in air. It is worthwhile to note that both carbon (5.5 at. %) and sulfur (1.7 at. %) were simultaneously incorporated into TiO_2 from NH_4SCN precursor, whereas only sulfur (1.6 atm %) could be incorporated into TiO_2 from NH_2CSNH_2. Besides carbon and sulfur, no nitrogen and hydrogen were detected in Energy Dispersive X-ray Analysis spectrum (EDXA). However, amount of silver determined from EDX is less than the initial loading of silver (1 at. %), indicating that only a small fraction of the doped silver remained on the surface and the rest of it could be present in the interstitial space of the TiO_2 lattice.

Table 2.1 EDX measurement of the various samples annealed at 500^o C/2h in air

Samples[a, b]	Ag (at. %)	C (at. %)	S (at. %)
(C, S)-TiO_2-01-500^oC	0.0	5.5	1.7
S-TiO_2-02-500^oC	0.0	0.0	1.6
Ag/(C, S)-TiO_2-01-500^oC	0.19	7.7	0.4
Ag/(C, S)-TiO_2-02-500^oC	0.24	5.8	1.5

(a)-01 is designation for ammonium thiocyanate precursor

(b)-02 is designation for thiourea precursor

The simultaneous incorporation of carbon and sulfur from the NH_4SCN precursor is explained as follows. Ammonium thiocyanate, on the one hand, is an ionic compound and it is highly soluble in ethanol and, on the other hand, thiourea is an organic compound and is comparatively less soluble in the same volume of ethanol. Because of its ionic nature and the high solubility in the chosen solvent, NH_4SCN forms electrically charged NH_4^+ and SCN^- ions, whereas NH_2CSNH_2 does not form electrically charged ions. For the time being, in case of NH_4SCN, we can surmise that some of the NH_4^+ and SCN^- ions might have participated in forming a stable complex with Ti^{4+} during solvent evaporation. This assumption might be correlated with the appearance of the yellow color of the as-synthesized sample after the complete evaporation of the solvent and its disappearance when dissolved into solvent again. On this basis, a portion of the yellow colored complex thus formed is formulated as [NH_4] [Ti (SCN) $_4$ .OH. H_2O].[54] Now, it is likely that during the calcination process, the combustion of the thiocyanate complex of Ti (IV) might, in part, lead to the substitution of carbon and sulfur for oxygen sites into TiO_2. In contrast, because of a weaker ligand property of NH_2CSNH_2, the thiourea complex of Ti (IV) being very unstable undergoes a rapid combustion and decomposition, thereby resulting in only substitution of sulfur for oxygen sites into TiO_2. Meanwhile, doping of TiO_2 with Ag^+ ions boosted the amount of the doped carbon along with a little amount of the doped sulfur from both the precursor materials. This is attributable to the greater affinity of Ag^+ ions to exist in the forms of carbonate than sulfate. Moreover, we do believe that the nature and amounts of the doped nonmetals entirely depend upon the source of the non-metal precursors as well as the metal ions.

Figure 2.1a illustrates the X-ray diffraction (XRD) profiles of carbon and/or sulfur–doped TiO_2 ($500^oC/2h$). Compared to Degussa P25, which contains anatase ($2\theta = 25.25^o$) and rutile (2θ =

27.5°) phases, the XRD patterns of the nonmetal-doped TiO_2 samples revealed anatase as the predominant homogeneous crystalline phase (2θ = 25.25°). Figure 2.1b illustrates the XRD patterns of Ag/(C, S)-TiO_2-01 sample annealed progressively at 400°, 500° and 600°C. Again, the analysis of the observed peaks corroborated the homogeneous anatase crystalline phase. Now, it is reasonable to infer that the doping with silver, carbon and sulfur prevents the phase transformation of TiO_2 up to 600°C, whereas the polycrystalline TiO_2 prepared by a sol-gel technique undergoes phase transformation above 500°C.[55, 56] Moreover, NH_4SCN and Ag^+ ions precursor materials promote the formation of the anatase in preference to rutile. Further, no noticeable peaks of silver carbonate and silver metal were observed in the X-ray diffractograms.

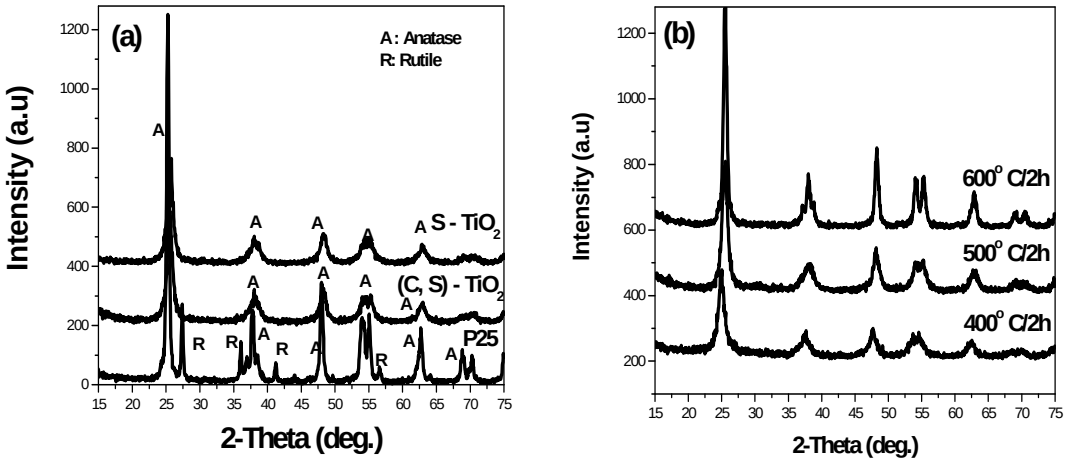

Figure 2.1 XRD profiles of (a) C and/or S-doped TiO_2 and (b) Ag/(C, S)-TiO_2 -01

Table 2.2 Surface area and crystallite size of the catalysts

Catalysts samples	BET Surface Area (m^2/g)	XRD Crystallize size (nm)
Degussa P25-TiO_2	51	23
(C, S)-TiO_2-01	75	8.5
S-TiO_2-02	67	7.0
Ag/(C, S)-TiO_2-01	86	5.3
Ag/(C, S)-TiO_2-02	71	6.8
Ag/(C, S)-TiO_2-01	36	17

Table 2.2 shows the BET surface area and average crystallite size of the various catalysts compared to Degussa P25. Obviously, the specific surface areas of the doped TiO_2 samples are higher than that of the undoped P-25. The average crystallite sizes of the doped samples were determined by analyzing the most intense (101) XRD peaks and using the well known Scherrer's equation, $t\ (size) = 0.9\lambda/\beta\cos\theta$ [1], where λ is the wavelength of the X-ray (nm), and β is the full width (radians) at half maximum of the signal. Up to 500^oC, the doped samples are nanoparticles of average crystallite size of 5-9 nm, whereas at 600^oC, the average crystallite size of the samples was 17 nm. The BJH desorption isotherm shows that the doped TiO_2 samples have microporous structures with an average pore diameter of 2-2.5 nm. Of the various preparation parameters, the calcination temperature has a profound effect on the BET surface areas. It is understandable that the higher the temperature and the longer the calcination time, the lower the BET surface area because of sintering of the smaller particles into the bigger particles. That is why Ag/(C, S)-TiO_2-01 catalysts at 600^oC/ 2h have the least surface area (36 m^2/g). On the other hand, (C, S)-TiO_2-01 samples (with and without Ag^+) calcined at 500^oC/2h have a little bit higher surface

areas than S-TiO_2-02 samples. This suggests that the ammonium thiocyanate precursor prevents the sintering of particles more effectively than does thiourea during the calcination step. For the moment, we assume that this might be due to the differences in reducing properties, doping modes and heats of reactions of ammonium thiocyanate and thiourea.

The IR measurement of the Ag/(C, S)-TiO_2-01 sample annealed at 500^{o}C/2h shows the appearance of bands at 1236 cm^{-1}, 1143 cm^{-1}, 1038 cm^{-1}, 761 cm^{-1} and 493 cm^{-1}. Slager et al. carried out the FT-IR study of a pure silver (I) carbonate and observed four bands at 1410, 1020, 880, and 690 cm^{-1} for Ag_2CO_3 and only one band at 535 cm^{-1} for Ag_2O.[57] They also investigated that the reaction of silver (I) carbonate with water vapor resulted in the formation of basic silver carbonate ($AgOHAg_2CO_3$) having two characteristic bands at 1460 and 1480 cm^{-1}. Compared to Slager's results, the infrared spectrum of the Ag/(C, S)-TiO_2-01 catalyst revealed that the two weak peaks appearing at 1236 cm^{-1}, 1038 cm^{-1} and one shoulder peak at 761 cm^{-1} could be from the presence of doped carbonate species. The other infrared bands at 1038 cm^{-1} and 493 cm^{-1} are assigned to the presence of characteristic bands of sulfate (v3) and Ti-O-Ti-O species. This implies that the carbon and sulfur doped into TiO_2 are present, to some extent, in the form of carbonate and sulfate respectively. However, for future work, a meticulous FTIR study of the carbon and sulfur-doped TiO_2 samples seems indispensable for a comprehensive understanding and a precise explanation of doping mechanisms.

Additionally, of the several spectroscopic techniques used to characterize TiO_2, Raman spectroscopy has been employed, because this technique provides a rapid way of understanding the doping mechanisms and obtaining the surface crystal morphologies of the TiO_2

nanoparticles.[58-60] Figure 2.2 presents the Raman spectra of (C, S)-TiO_2-01 and Ag/(C, S)-TiO_2-01 catalysts after heat treatment at 500^{o}C/2h. For comparison, the Raman spectrum of Degussa P25 is also shown in the same figure. Obviously, the observed Raman peaks of the doped and undoped TiO_2 samples match pretty well with each other. Compared to P25-TiO_2, a slight shift of some peak values is caused by the smaller crystallite sizes of the doped samples. Nevertheless, these results confirmed codoping of TiO_2 with carbon, silver and sulfur.

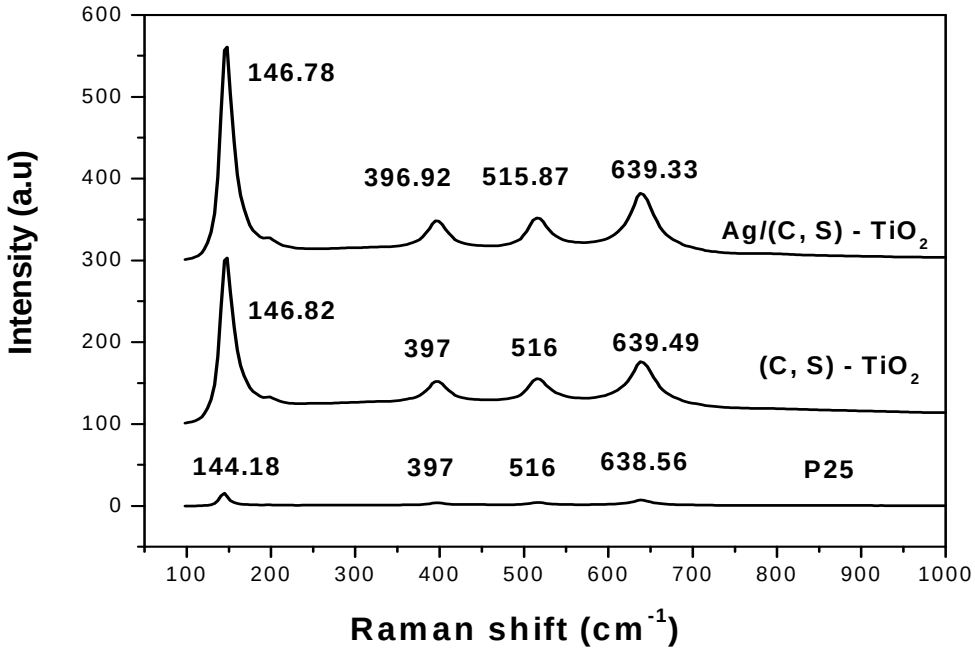

Figure 2.2 Raman profiles of (a) (C, S)-TiO_2-01 and (b) Ag/(C, S)-TiO_2-01 catalysts annealed at 500^o C/2h in air (The precursors for Ti, Ag, and C and S are $Ti[OCH(CH_3)_2]_4$, $AgNO_3$ and NH_4SCN, respectively)

UV-Vis diffuse reflectance spectroscopy directly provides some insight into the interactions of the photocatalyst materials with photon energies. Therefore, it is absolutely imperative to include this technique to examine for the visible light reactivity of synthesized photocatalysts. Figure 2.3a demonstrates the UV-Vis absorption profiles of carbon and/or sulfur-doped titanium dioxide (calcined at 500^{o}C/2h in air) compared to P25-TiO_2. Here, we perceived a noticeable shift of the optical absorption edges of the doped TiO_2 systems towards the visible regions of the solar spectrum. Notably, this shift towards the longer wavelengths originates from the band gap narrowing of titanium dioxide by carbon and/ or sulfur doping[34, 36] and the band gap energy of the doped samples was determined from the equation, Eg = 1239.8/λ [2], where λ is the wavelength (nm) of the exciting light.[61] The band gap energies of the (C, S)-TiO_2-01, S-TiO_2-02, Ag/(C, S)-TiO-01 and Ag/(C, S)-TiO_2-02 samples were found to be 2.77 eV, 2.79 eV, 2.75 eV and 2.76 eV respectively. Because the doped samples have lower band gap energies than the undoped TiO_2 (3.00-3.2 eV), these photocatalysts are, therefore, likely to operate under visible light illumination. Again, comparing the band gap energy, we notice that only carbon and sulfur effectively contribute to the band gap narrowing of TiO_2. Despite somewhat lower band gap values of the silver, carbon and sulfur-doped system, it clearly shows that doping of Ag^+ ions has, at most, a small contribution to the band gap reduction. Furthermore, doping TiO_2 with carbon and/or sulfur introduces some trap states (impurity levels) within the valence and conduction bands of titanium dioxide. Consequently, we observed a shoulder peaks in the UV–Vis absorption profiles of the nonmetal-doped TiO_2 samples. Figure 2.3b represents the profound effect of the calcination temperature in UV-Vis absorption spectra of the Ag/(C, S)–TiO_2-01 catalysts.

Compared to standard P25, Ag/(C, S)–TiO_2-01 samples retain a substantial amount of the visible light absorption (λ > 400 nm) in the temperature range of 400^o–600^{o}C. However, the ability of these samples to absorb visible light effectively decreases as the annealing temperature progressively increases. Therefore, Ag/(C, S)–TiO_2 sample calcined at 600^{o}C/2h shows the least visible light absorption compared to the other samples annealed below 600^{o}C. In contrast, the sample heat-treated at 400^{o}C/2h showed a greatest shift of absorption edge towards the visible region and should be the most active catalyst in visible light. In fact, this could be due to the presence of some residual organic impurities left in doped TiO_2. On the other hand, the magnitude of the UV-vis absorption intensity depends on various factors such as crystal structures, band gap energy, thickness, and the presence and absence of defects and foreign elements in concerned semiconducting materials. Therefore we noticed that a difference between the UV-vis absorption intensities of the doped samples and P-25 (Figures 2.3a and 3b) in the wavelength region less than 400 nm. Herein, we assumed that the smaller UV-vis absorption intensity of the doped samples could be ascribed to the smaller band gap excitation energies (less than 3.0 eV) whereas the higher the absorption intensity of the undoped P-25 was attributed to a higher band gap excitation energy (3.0 -3.2 eV).

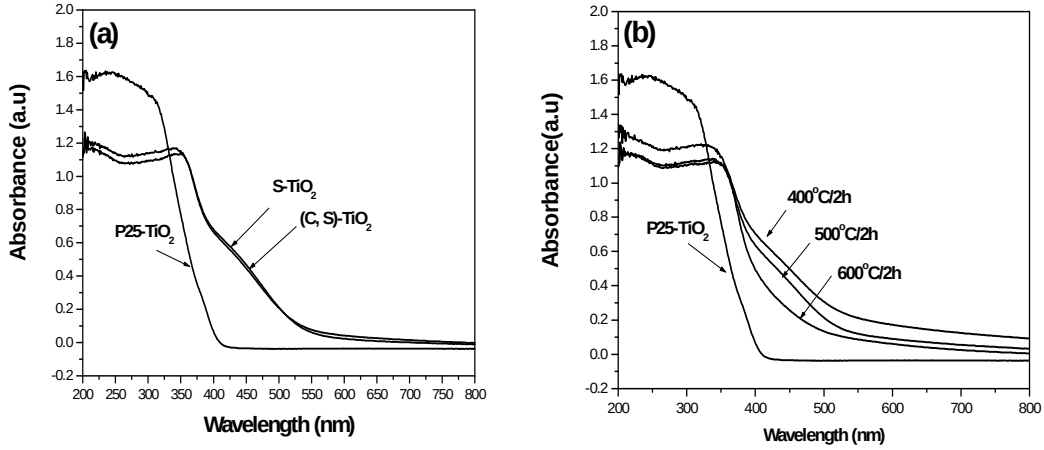

Figure 2.3 UV–Visible absorption profiles of (a) C and/or S doped-TiO_2, and (b) Ag/(C, S)-TiO_2 -01 catalysts at various temperatures compared to P25-TiO_2

2.3.2 Kinetics of Photocatalysis

In order to assess the photocatalytic activity of the new synthesized materials, the photodegradation of gaseous acetaldehyde by artificial light was performed at room temperature (298K). Figure 2.4 depict the photomineralization of the ubiquitous air pollutant acetaldehyde on Ag/(C, S)–TiO_2-01 under both visible light ($\lambda > 420$ nm) and UV light (320 nm $< \lambda <$ 420 nm) illuminations. From the concentration profiles, it is now clearly seen that there was a noticeable consumption of acetaldehyde (Figure 2.4a and c) and a subsequent production of carbon dioxide (Figure 2.4b and d) under both visible and UV light irradiations. Both from the qualitative and quantitative viewpoints, the probe molecules degrade faster under UV light than under visible light illumination.

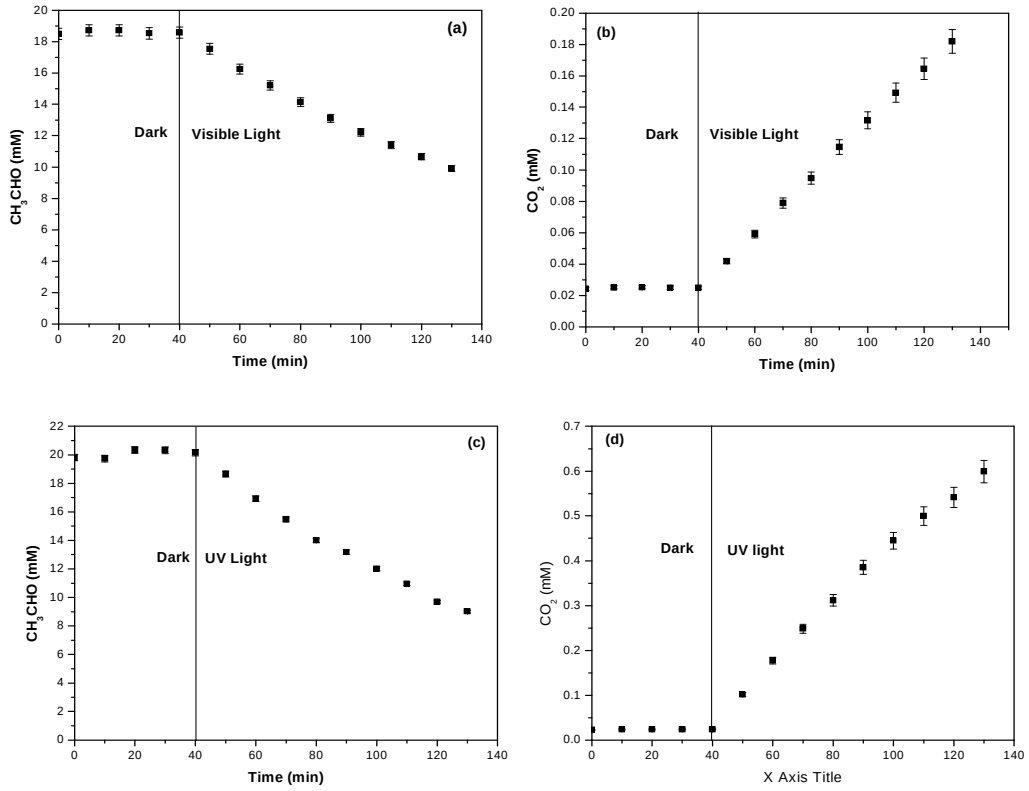

Figure 2.4 Degradation of gaseous acetaldehyde (a and b) and evolution of carbon dioxide (c and d) over Ag/(C, S)-TiO_2-01 catalyst (annealed at 500^{o}C/2h in air) under visible and UV light

This is, indeed, because of the fact that the UV photons are more energetic and more penetrating (can pass into the sample deeply), and produce more photoexcited electrons and holes for the surface catalysis from the doped TiO_2 than the visible photons. On the other hand, no dark reaction was observed for the systems under study, indicating that the reaction was basically photocatalytic in nature. Besides the photon energies, several other experimental parameters,

especially the annealing temperature and dopant concentration, could affect the photocatalytic performance of the materials.

Figure 2.5a shows the profound effect of annealing temperature on the production of carbon dioxide from the photodegradation of gaseous acetaldehyde under visible light irradiation. Based on the amount of CO_2 produced, it is inferred that the visible light reactivity of Ag/(C, S)–TiO_2-01 catalyst is enhanced as the annealing temperature increases from 400^o to 500^oC, and thereafter the photocatalytic activity decreases further while rising the temperature above 500^oC. The optimal visible light activity of the sample at 500^oC attributes to an improvement in crystallinity of the homogeneous anatase phase, whereas the lowest photoactivity at 600^oC was because of the simultaneous effects of the low surface area and the removal of some dopants from the doped catalysts. Figure 2.5b illustrates a similar effect of Ag^+ ion concentration on the production of CO_2 from CH_3CHO on Ag/(C, S)–TiO_2-01 under visible light illumination. The concentration of silver ion was varied from 0.5–10 at%. The optimal visible light reactivity of the catalyst was achieved for 1 atm % of Ag^+ ion. This means that 1 mole% Ag^+ ion concentration effectively suppresses the recombination of the photogenerated charge-carriers on the surface of the catalyst in order that a large number of reactant molecules are absorbed and undergo subsequent oxidation and reduction reactions. Unfortunately, an increase in Ag^+ ion concentration from 2 to 10 at% has a deleterious effect on the photoactivity of the catalysts. Conceivably, this happens because of the creation of recombination centers of charge-carriers at a higher loading of dopant concentration. Figure 2.5c demonstrates a similar effect of SCN^- ion concentration on the production of CO_2 from acetaldehyde on Ag/(C, S)–TiO_2-01 catalyst. Here, we observed a marginal effect of SCN^- ion concentration. The optimum visible light reactivity of the sample

was observed for 1: 4 mole ratio of Ti: SCN and samples containing the other mole ratios of Ti: SCN showed a little lower reactivity. Based on EDX analysis, carbon and sulfur have been introduced into TiO_2 lattices from the NH_4SCN precursor. Of course, as the concentration of ammonium thiocyanate increases, the amount of carbon and sulfur contents in doped TiO_2 also increases accordingly, thereby accelerating the rate of the recombination of photoinduced charge-carriers in the framework of titania.

Figures 2.6a and 6b compare the amount of carbon dioxide produced from the photomineralization of gaseous acetaldehyde on various catalysts under visible and UV light respectively. Upon visible light illumination, it turns out that both Ag/(C, S)–TiO_2-01 and Ag/(C, S)-TiO_2-02 catalysts exhibit similar but higher photoactivity than P25, (C, S)–TiO_2-01 and S-TiO2-02 in regard to the evolution of CO_2 from CH_3CHO. In contrast, Degussa P25 showed the highest photocatalytic performance pertaining to the production of CO_2 under the UV light, compared to the doped TiO_2. Specifically, P25-TiO_2 is an accredited photocatalyst and it possesses a very good photoactivity. Therefore, it seems that the production of carbon dioxide from the photodegradation of acetaldehyde was more favored. Empirically, we have found that the photodegradation of acetaldehyde not only involved the formation of carbon dioxide but also some other products, such as acetic and formic acids, which are not minor products. Therefore, for simplicity, the amounts of CH_3CHO and CO_2 expressed in mM have been shown in Figures 2.4a and 4b whereas only the amount of carbon dioxide produced in mM was shown in other figures (5a - 6b).

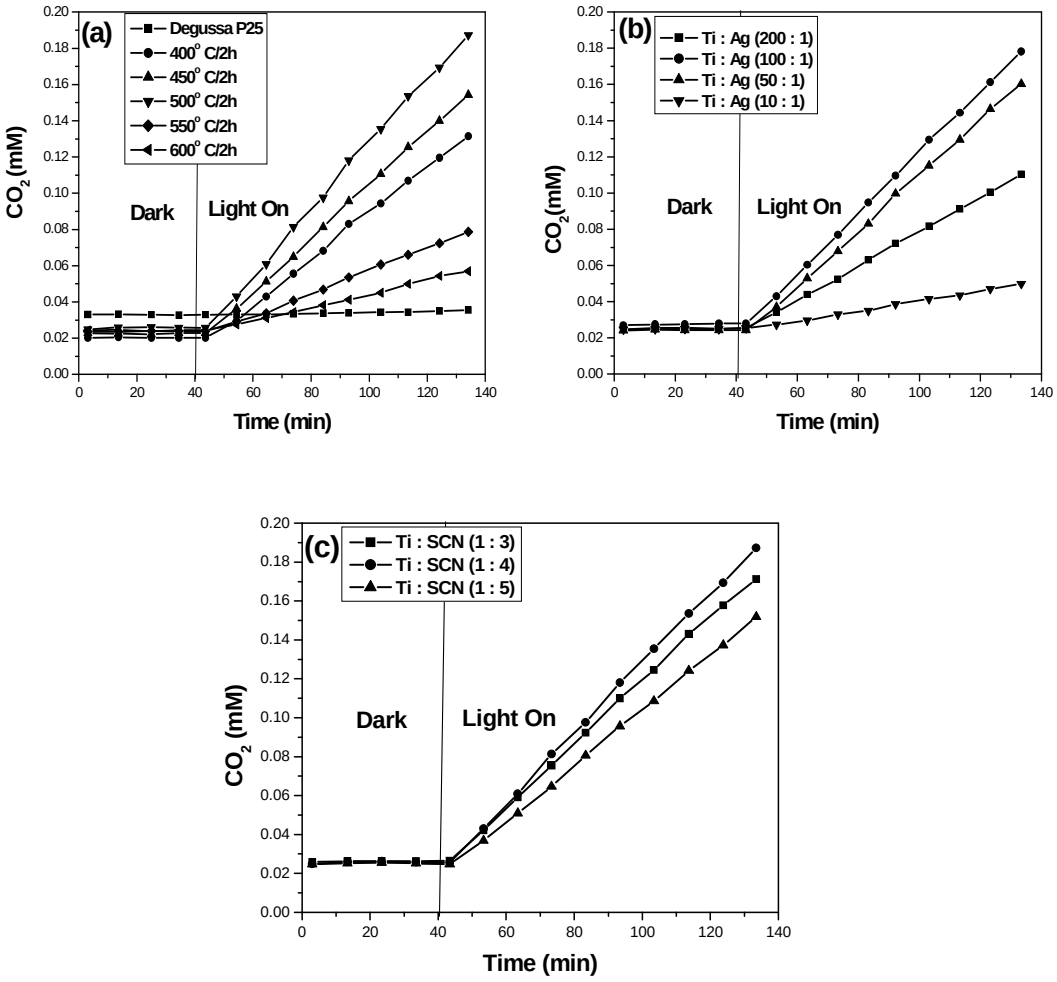

Figure 2.5 Effect of (a) calcination temperature, (b) Ag^+ ion and (c) SCN^- ion on CO_2 production from CH_3CHO on Ag/(C, S)–TiO_2-01 catalyst under visible light

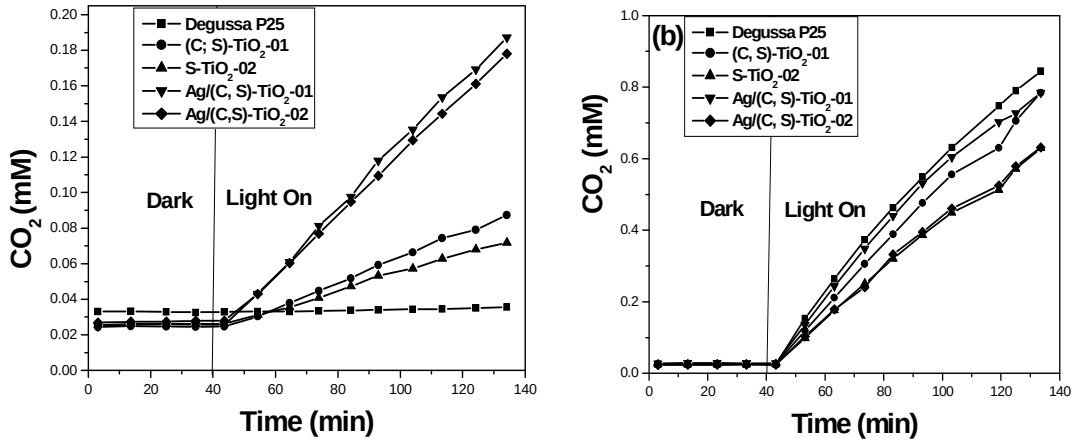

Figure 2.6 Production of CO_2 from CH_3CHO on various catalysts under (a) visible and (b) UV light

However, in photocatalysis, it would be more worthwhile to determine and compare the initial rates of the degradation of acetaldehyde and the subsequent production of carbon dioxide (Table 2.3). On comparing the initial rates, it is clearly seen that Ag/ (C, S)–TiO_2-01 catalyst prepared by using NH_4SCN as a nonmetal precursor degrades gaseous acetaldehyde 10 and 3 times faster in visible light and UV light respectively than P25. Still, other doped TiO_2 catalysts have higher initial rates of degradation of CH_3CHO and production of CO_2 than P25 both under UV and visible light.

The origin of the superior photoactivity of the doped TiO_2 catalysts might be explained as follows. Herein, regardless of the magnetic and thermal properties, we consider that all photocatalyst materials are assumed to be comprised of mainly two interlinked parts: the photopart and the catalysis part.[62] The photopart is intrinsically concerned with the interaction of

the semiconducting materials with light, for example, absorption of light, band gap, formation of electrons- holes, their dynamics and surface trapping, whereas the catalysis part includes surface area, surface reactivity, radical formation and the heterogeneous interaction of the chemical species with catalyst surface. More importantly, the better the crystalline quality and the lower the band gap, the more improvement on the photopart leading to the higher visible light reactivity of the catalysts. On the other hand, the higher the surface area, the higher the reactivity. Fundamentally, photocatalysis is an interfacial reaction and a higher surface area of the material, of course, produces a greater number of accessible active sites, thereby yielding an enhanced reactivity. Moreover, the photocatalytic activity of any semiconductor photocatalyst is, in fact, the result of a compromise and combination of these two structural parameters. In the case of pure TiO_2, the crystalline anatase is the most active catalyst compared to rutile and brookite phases. Keeping this principle in mind, the doped TiO_2 catalysts under present study have high surface areas, low band gaps and only the anatase crystalline phases as confirmed by the BET, UV-Vis, Raman and XRD measurement respectively. As a result, these photocatalysts exhibit better reactivity than P25-TiO_2 for the degradation of gaseous acetaldehyde under UV and visible light. Meanwhile, on comparing activity of the doped TiO_2 systems, it unequivocally shows that the Ag/(C, S)-TiO_2-01 catalyst exhibits the highest photoactivity because of its highest surface area (86 m^2/g) and lowest band gap (2.75 eV). Nonetheless, the superior photoactivity of Ag/(C, S)-TiO_2 catalysts is also attributed to good dispersion of Ag^+ ions, synergistic effects of dopants, nature and source of precursor materials. However, it is interesting to note that doping TiO_2 only with Ag^+ ions by using $AgNO_3$ or Ag_2O results in materials of almost no visible activity.

Table 2.3 Initial rates (mM/min) of production of CO_2 and degradation of CH_3CHO on various catalysts under visible and UV light

Catalysts	$[CO_2]$vis	$[CH_3CHO]$vis	$[CO_2]$uv	$[CH_3CHO]$uv
P25 (TiO_2)	0.0002	0.009	0.01	0.05
Ag/(C, S)-TiO_2-01	0.002	0.110	0.008	0.16
Ag/(C, S)-TiO_2-02	0.002	0.060	0.008	0.11
(C, S)-TiO_2-01	0.0007	0.053	0.009	0.20
S-TiO_2-02	0.0005	0.046	0.007	0.12

2.3.3 Mechanism for enhancing effect of silver dopant in photocatalysis

For a better understanding, we can propose a mechanism for the enhancing effect of silver ion dopant in photocatalysis. The chemical state of the Ag^+ ion in doped TiO_2 was determined by measuring the XPS of the best Ag/(C, S)-TiO_2-01 catalyst before and after UV and visible light reactions. The XPS profile of the Ag/(C, S)-TiO_2-01 sample (not shown here) showed the presence of both Ag^0 and Ag^+ species before and after reaction. Before the light reaction, the presence of metallic silver particles was likely due to the thermal reduction of silver ions during calcination step at 500^{o}C/2h.[63, 64] In general, Ag^+ ions were easily reduced to Ag^0 particles by the photoexcited conduction band electrons (e^-_{CB}) of Ag/(C, S)-TiO_2-01 catalyst thereby resulting in the formation of more Ag^0 particles; however, the XPS spectra of the Ag/(C, S)-TiO_2-01 sample remain almost the same even after UV and visible light reactions. This implied that during photocatalytic reaction the reduced Ag^0 particles were oxidized back to Ag^+ ions by the valence band holes (h^+_{VB}). Thus we can say that the presence of both Ag^0 and Ag^+ species facilitate the

charge separation (electron-hole) and suppress the recombination of the photoexcited charge carriers thereby enhancing the catalytic property of the material. Based on these facts, the following mechanism was proposed to show a real photocatalytic activity of the Ag/(C, S)-TiO_2-01 catalyst for acetaldehyde photodegradation in gas phase.

$$TiO_2 + hv \rightarrow e^- (CB) + h^+ (VB) \quad (3)$$

$$Ag^0 + h^+ (VB) \rightarrow Ag^+ \quad (4)$$

$$Ag^+ + e^- (CB) \rightarrow Ag^0 \quad (5)$$

2.4 Conclusions

For the first time, we report the synthesis and characterization of highly active (in visible light) new nanoparticle photocatalysts based on silver, carbon and sulfur-doped TiO_2. XRD and the BET measurements corroborate that these doped materials are made up of the homogeneous anatase crystalline phase and have high surface areas. Furthermore, the UV-Vis absorption spectra substantiate the band gap tapering of TiO_2 by the doped carbon and/or sulfur along with a very little contribution from the doped Ag^+ ions. Notably, the well-dispersed Ag^+ ions in (C, S)-doped TiO_2 significantly promote the electron-hole separation and subsequently enhance the photoactivity. Moreover, Ag/(C, S)-TiO_2 new nanoparticle photocatalysts degrade the gaseous acetaldehyde 10 and 3 times faster than P25-TiO_2 under visible and UV light, respectively. Compared to P25-TiO_2, the commendable visible light activity of Ag/(C, S)-TiO_2 nanoparticle photocatalysts is predominantly attributed to an improvement in anatase crystallinity, high surface area, low band gap and effect of precursor materials. Herein, we also report on codoping TiO_2 with carbon and sulfur from a single nonmetal precursor (NH_4SCN) and this result is important for future photocatalyst preparations.

2.5 References

1. Fujishima, A.; Honda, K., *Nature* 1**972**, 238, 37-38

2. Maness, P. C.; Smolinski, S.; Blake, D. M.; Huang, Z.; Wolfrum, E. J.; Jacoby, W. A., *Appl. Environ. Microbiol.* **1999**, 65, 4094-4098

3. Thomson, L.; Panayotov, A.; Yates, J.; Martyanov, I.; Klabunde, K. J., *J. Phys. Chem. B* **2004**, 108, 17875-17865

4. Einaga, H.; Futamura, S.; Ibusuki, T., *Appl. Catal. B* **2002**, 38, 215-225

5. Hongmin, L.; Zhiwei, L.;Xiaojiang,Ye.;Wenfeng, S., *Chemosphere* **2005,** 60**,** 630

6. Driessen, D.; Goodman, L.; Miller, M.; Zaharias, A.; Grassian, H., *J. Phys. Chem. B* **1998**, 102, 549-556

7. Zhuang, J.; Rusu, C. N.; Yates, J. T., *J. Phys. Chem. B* **1999**, 103, 6957-6967

8. Brown, G. T.; Darwent, J. R., *J. Phys. Chem.* **1984**, 88, 4955-4959

9. Rusu, C. N.; Yates, John T., *J. Phys. Chem. B* **2000**, 104, 12299-12305

10. Stylidi, M.; Kondarides, D. I.; Verykios, X. E., *Int. J. Photoenergy* **2003**, 5, 59-67

11. Rusu, C. N.; Yates, J. T., *J. Phys. Chem. B* **2000**, 104, 1729-1737

12. Rusu, C. N.; Yates, J. T., *J. Phys. Chem. B* **2001**, 105, 2596-2603

13. Lee, H.; Choi, W., *Environ. Sci. Technol.* **2002**, 36, 3872-3878

14. Anpo, M.; Takeuchi, M., *J. Catal.* **2003**, 216, 505-516

15. Yamashita, H.; Takeuchi, Anpo, M., *Enc Nanosci Nanotechnol* **2004**, 10, 639-654

16. Borgarello, E.; Kiwi, J.; Gratzel, M.; Pelizzetti, E.; Visca, M., *J. Am. Chem. Soc.* ***1*982**, 104, 2996-3002

17. Iwasaki, M.; Hara, M.; Kawada, H.; Tada, H.; Ito, S., *J. Colloid Interf. Sci.* **2000**, 224, 202-204

18. Klosek, S.; Raftery, D., *J. Phys. Chem. B* **2001**, 105, 2815-2819

19. Zhu, J.; Chen, F.; Zhang, J.; Chen, H.; Anpo, M., *J. Photochem. Photobiol. A* **2006**, 180, 196-204

20. Choi, W.; Termin, A.; Hoffmann, M. R., *J. Phys. Chem. B* **1994**, 98, 13669-13679

21. Irie, H.; Watanabe, Y.; Hashimoto; K., *Chem. Lett.* **2003**, 32, 772-773

22. Sakthivel, S.; Kisch, H., *Angew. Chem. Int. Ed.* **2003**, 42, 4908-4911

23. Ashashi, R.; Morikawa, T.; Ohwaki, T.; Aoki, K.; Taga Y., *Science* **2001**, 293, 269-271

24. Burda, C.; Lou, Y.; Chen, X.; Samia, A. C. S., Stout, J.; Gole, J. L., *Nano lett.* **2003**, 3, 1049-1051

25. Kuroda, Y.; Mori, T.; Yagi, K.; Makihata, N.; Kawahara, Y.; Nagao, M.; Kittaka , S., *Langmuir* **2005**, 21, 8026-8034

26. Lin, L.; Lin, W.; Zhu, Y.; Zhao, B.; Xie, Y., *Chem. Lett.* **2005**, 34, 284-285

27. Umebayashi, T.; Yamaki, T.; Tanaka, S.; Asai, K., *Chem. Lett.* **2003**, 32, 330-331

28. Ohno, T.; Mitsui, T.; Matsumura; M., *Chem. Lett.* **2003**, 32, 364-365

29. Ohno, T., *Water Sci. Technol.* **2004**, 49, 159-163

30. Hattori, A.; Yamamoto, M.; Tada, H.; Ito, S., *Chem. Lett.* **1998**, 707-708

31. Yu, J. C; Yu, J.; Ho, W.; Jiang, Z.; Zhang. L., *Chem. Mater.* **2002**, 14, 3808-3816

32. Yamaki, T.; Sumita, T.; Yamamoto, S., *J. Mater. Sci. Lett.* **2002**, 21, 33-35

33. Li, D.; Haneda, H.; Hishita, S.; Ohashi, N.; Labhsetwar, N. K., *J. Fluorine Chem.* **2005**, 126, 69-77

34. Nagaveni, K.; Hedge, M.S.; Ravishankar, N.; Subbanna, G.N.; Madras, G., *Langmuir* **2004**, 20, 2900-2907

35. Morikawa, T.; Asahi, R.; Ohwaki, T.; Aoki, K.; Taga, Y., *Jpn. J. Appl. Phys.* **2001**, 40, 561-563

36. Umebayashi, T.; Yamaki, T.; Itoh, H.; Asai, K., *Appl. Phys. Lett.* **2002**, 81, 454-456

37. Li, D.; Hajime, S. H.; Ohashi, N., *Chem. Mater.* **2005**, 17, 2596-2602

38. Luo, H.; Takata, T.; Lee, Y.; Zhao, J.; Domen, K.; Yan, Y., *Chem. Mater.* **2004**, 16, 846-849

39. Sakatani, Y.; Ando, H.; Okusako, K.; Koike; H., *J. Mater. Res.* **2004**, 19, 2100-2108

40. Sakatani, Y.; Nunoshiege, J.; Ando, H.; Okusako, K.; Koike, H.; Takata, T.; Kondo, J. N.; Hara, M.; Domen, K., *Chem. Lett.* **2003**, 32, 1156-1157

41. Zhao, W.; Ma, W.; Chen, C.; Zhao, J.; Shuai, Z., *J. Am. Chem. Soc.* **2004**, 126, 4782-4783

42. Li, X. Z.; Li, F. B., *Environ. Sci. Technol.* **2001**, 35, 2381-2387

43. Kim, S.; Hwang, S. J.; Choi, W., *J. Phys. Chem. B* **2005**, 109, 24260-24267

44. Sokmen, M.; Candan, F.; Sumer, Z., *J. Photochem. Photobiol. A* **2001**, 143, 241-244

45. Falaras, P.; Arabatzis, I. M.; Stergiopoulos, T.; Bernard, M. C., *Int. J. Photoenergy* **2003**, 5, 123-130

46. Gupta, K., Pal, A.; Sahoo, C., *Dyes Pigments* **2006**, 69, 224-232

47. Liu, Y.; Liu, C.; Rong, Q.; Zhang, Z., *Appl. Surf. Sci.* **2003**, 220, 7-11

48. Kakuta, N.; Goto, N.; Ohkita, H.; Mizushima, T., *J. Phys. Chem. B* **1999**, 103, 5917-5919

49. Currao, A.; Reddy, V. R.; Veen, M. K.; Schropp, R. E. I.; Calzferri, G., *Photochem. Photobiol. Sci.* **2004**, 3, 1017-1025

50. Carnes, C. L.; Klabunde, K. J., *Chem. Mater.* **2002**, 14, 1806-1811

51. Medine, M.; Zaikovskii, V.; Klabunde, K. J., *J. Mater. Chem.* **2004**, 14, 757-763

52. Park, J. H.; Kim, S.; Bard, A. J., *Nano Lett.* 2006, 6, 24-28

53. Choi, Y.; Umebayashi, T.; Yamamoto, S.; Tanaka, S., *J. Mater. Sci. Lett.* **2003**, 22, 1209-1211

54. Sutton, G. J., *Australian J. Chem.* **1959**, 12, 122-126

55. Tanaka, Y.; Suganuma, M., *J. Sol-Gel Sci. Technol.* **2001**, 22, 83-89

56. Jung, Y.; Park, B.; Anpo, M., *J. Photochem. Photobiol. A* **2005**, 170, 247-252

57. Slager, L.; Lindgren, J.; Mallmann, J.; Greenler, G., *J. Phys. Chem.* **1972**, 76, 940-943

58. Misook, K.; Yu-Ri, K.; Min-Kyu, J.; Sung-Chull, L.; Suk-Jin, C.; Jong-Yul, P.; Sun Kim, S. H. C., *J. Photochem. Photobiol. A* **2005**, 173, 128-136

59. Sean, K.; Fred, H. P.; Micha, T., *J. Phys. Chem. B* **1997**, 101, 2730-2734

60. Toshiaki, O.; Fujio, I.; Yoshinori, F., *J. Raman Spectrosc.* **1978**, 7, 321-324

61. Aditi, R. G.; Julio, B. F., *B. Catal. Soc. Ind.* **2005**, 4, 131

62. Kolen'ko, V.; Churagulov, R.; Kunst, M.; Mazerolles, L.; Colbeau-Justain, C., *Appl. Catal. B* **2004**, 54, 51-58

63. Lei, G.; Mingxia, X.; Haibo, F., *J. Sol-Gel Sci. Technol.* **2006**, 40, 6573

64. Enrico, T.; Maria, V.; Patrizia, N.; Silvia, L.; Jong, Y.; Takeshi, S.; Naoto, K., *J. Sol-Gel Sci. Technol.* **2001,** 22, 115-123

CHAPTER 3 - Synthesis and Characterization of Cobalt, Carbon and Sulfur-Codoped Nanosized Anatase TiO_2 for Enhanced Visible Light Photocatalysis

3.1 Introduction

Doping[1-6] and codoping[7-10] of nonmetals into ultraviolet-light-active titanium dioxide photocatalysts have been the most attractive strategies to design and develop efficient visible-light-active TiO_2 nanoparticle photoctatalysts for decontamination of toxic organic compounds in polluted air and water. Particularly, doping and codoping of nonmetals allow researchers to reduce the band gap of TiO_2 (< 3.0 eV) very effectively. The band gap reduction is a pre-requisite for TiO_2 – based heterogeneous photocatalysis to effectively and efficiently utilize solar energy. Consequently, nonmetal(s) doped/codoped - TiO_2 photocatalysts can be excited with photons of lower energy (λ> 400 nm) to generate electron–hole pairs, which can subsequently engage in surface redox reactions, contingent upon their lifetimes and recombination rates. Furthermore, it has been proven that codoping TiO_2 with two nonmetals rather than doping with a single nonmetal induces synergetic effects in accelerating photo-mineralization of toxic organic pollutants, primarily by suppressing both surface and bulk charge – carrier recombination processes. As a result, a marked improvement has been observed in the activity of the codoped TiO_2 photocatalyst under visible light irradiation compared with that of pure and single nonmetal doped TiO_2 photocatalysts.[9]

Besides doping a single metal or nonmetal, further improvements in visible- light-activities of TiO_2 photocatalysts have been achieved by codoping a metal and a nonmetal. On the basis of this design principle, visible-light-responsive new photocatalytic materials, such as (Sr, N)/TiO_2,[11] (Ni, B)/TiO_2,[12] (La, N)/TiO_2,[13] (La, S)/TiO_2,[14] (Fe, C)/TiO_2,[15] (V, B)/TiO_2[16], and (V, C)/TiO_2,[17] have been developed and investigated, especially for environmental remediation purposes. Moreover, these works have shown that new photocatalyst systems of TiO_2 derived by codoping a metal and a nonmetal displayed higher visible – light - activities for degradation of highly toxic organic pollutants than that the single metal, nonmetal – doped, and pristine TiO_2. From the mechanistic viewpoint, it turns out that in metal and nonmetal-codoped photocatalyst systems the codoped nonmetal actually reduces the band gap and induces visible light absorption to generate electron-hole pairs while the codoped metal suppresses the charge-carrier (electron-hole) recombination process.[13, 14] Thus codoping a metal and a nonmetal has been considered a good strategy for developing visible-light-driven new photocatalytic materials based on TiO_2.[12-14, 16, 17]

In recent work, we have shown that visible-light-activities of TiO_2 photocatalyst could be markedly improved by codoping TiO_2 with a noble metal (Ag) and two nonmetals (C and S).[18] This work actually motivated us with further interests to design visible-light-driven TiO_2 photocatalyst codoped with a transition metal and two nonmetals. In this context, several authors have reported TiO_2 photocatalysts doped with 3d-transition metals such as V,[19] Cr,[20] Mn,[21] Fe,[22] Co,[23] Ni,[24] Cu,[25] and Zn[26] for decontamination of hazardous organic pollutants. To our knowledge, there have been no research works so far done to study the effect of codoping 3d-transition metal and two nonmetals (C and S) on the photoactivity of TiO_2 for environmental applications. As compared with V and Cr, cobalt is less toxic, and cobalt-doped photocatalysts

have shown commendable activities for degradation of acetaldehyde[27, 28] and phenol,[29] and production of hydrogen[30] from aqueous ethanol solution. In this chapter, we have mainly focused our research goals on synthesis and characterization of a cobalt, carbon, and sulfur- codoped TiO_2 photocatalyst that exhibited exceptional activity enhancement for gas-phase acetaldehyde degradation under both UV– visible light irradiations. Moreover, the role of codopants (Co, C, S) in enhanced visible-light-driven photocatalysis over nanosized anatase TiO_2 photocatalyst is presented.

3.2 Experimental Section

3.2.1 Chemical Reagents

All chemical reagents, $Ti[OCH(CH_3)_2]_4$ (97% Sigma-Aldrich), NH_4SCN (97.5% Alfa Aesar), C_2H_5OH (200 Proof, Aaper Alcohol and Chemical Co.) and $Co(NO_3)_2$ (99.9+%, Alfa Aesar) were used without further purification.

3.2.2 Photocatalyst preparations

Typically, Co/(C, S)–TiO_2 photocatalyst preparation involves 0.031 moles (8.5 g) of $Ti[OCH(CH_3)_2]_4$ and 0.124 moles (9.44 g) of NH_4SCN dissolved 200 mL C_2H_5OH and stirred vigorously followed by drop-wise addition of 0.125 moles (2.25 g) of de-ionized water containing desired amount of $Co(NO_3)_2$ (0, 1 and 2 mole%). The contents of the reaction were stirred for 5 minutes for complete hydrolysis, and solvent was then removed by using a rotavap apparatus. After keeping in a drying cabinet over night, the samples were annealed in a Chamber

Furnace (Carbolite, CWF-1100) at 500^{o}C (5^{o}C/min) for 2h in air. The final product was ground well into fine particles. The same method was used to prepare TiO_2, (C, S)-TiO_2 and Co/TiO_2 as controls.

3.2.3 Characterizations

After annealing at 500^{o} C for 2h in air, the samples were characterized by various spectroscopic techniques. The powder X-ray diffraction (XRD) patterns of samples were recorded on a Scintag XDS 2000 D8 diffractometer with Cu-Kα radiation of wavelength of 1.5406 Å and were analyzed from 15^{o}–75^{o} (2θ) with a step size of 0.05^{o} and step time of 3s to determine the crystalline phase. The specific surface areas were determined from Nitrogen adsorption–desorption isotherms recorded at liquid nitrogen temperature (77K) on a Quantachrome Instrument (NOVA 1000 Series) by using the Brunauer-Emmett- Teller (BET) method. The pore size distributions was derived from the BJH desorption isotherms based on the Barrett-Joyner-Halenda (BJH) method. UV-Vis optical absorption spectra were collected on a Cary 500 Scan UV-Vis NIR Spectrometer from 200 nm to 800 nm by using PTFE as a reference. EDX measurement was performed on Scanning Electron Microscope-S-3500N and Absorbed Electron Detector- S-6542 (Hitachi Science Systems, Ltd.), EDXA (Inca Energy, Oxford Instruments Microanalysis Ltd.) to determine the surface composition of the samples under the specified conditions of 20 keV and 15 mm working distance.

3.2.4 Photoactivity Test

Photoactivity tests were performed in a 305 mL cylindrical air-filled static glass reactor with a quartz window at room temperature (Fig.3.1). 0.1025g (0.00128 moles) photocatalyst samples were placed in a circular glass dish sample holder. Then 100 μL liquid CH_3CHO was added into the bottom of the reactor and was constantly stirred for 40 minutes in order to allow acetaldehyde to vaporize and equilibrate. After 40 minutes stirred in dark conditions, 35 μL acetaldehyde-air mixtures were extracted periodically extracted (in every 10 min) and injected into the GC-MS port (Shimadzu GCMS-QP 5000). The temperatures of the column, injector and detector were maintained at 40^o, 200^o and 280^oC, respectively. The dark sampling was performed five times in order to examine the dark activity of the sample under study. For visible-light photocatalysis, the sample was irradiated with a 1000 W high-pressure mercury lamp (Oriel Corp.) at a distance of 20 cm from the top by using combined filters that contained one VIS-NIR long pass filter (400 nm) and another colored glass filter (> 420 nm) (See Figure 3.1). After visible light was turned on, nine injections (35 μL each time) from the reactor were made at every 10 minute interval to examine the photoactivity of the sample. The UV light photocatalysis was performed exactly in the same way by using two cut-off filters that transmit light of wavelength, 320 - 400 nm.

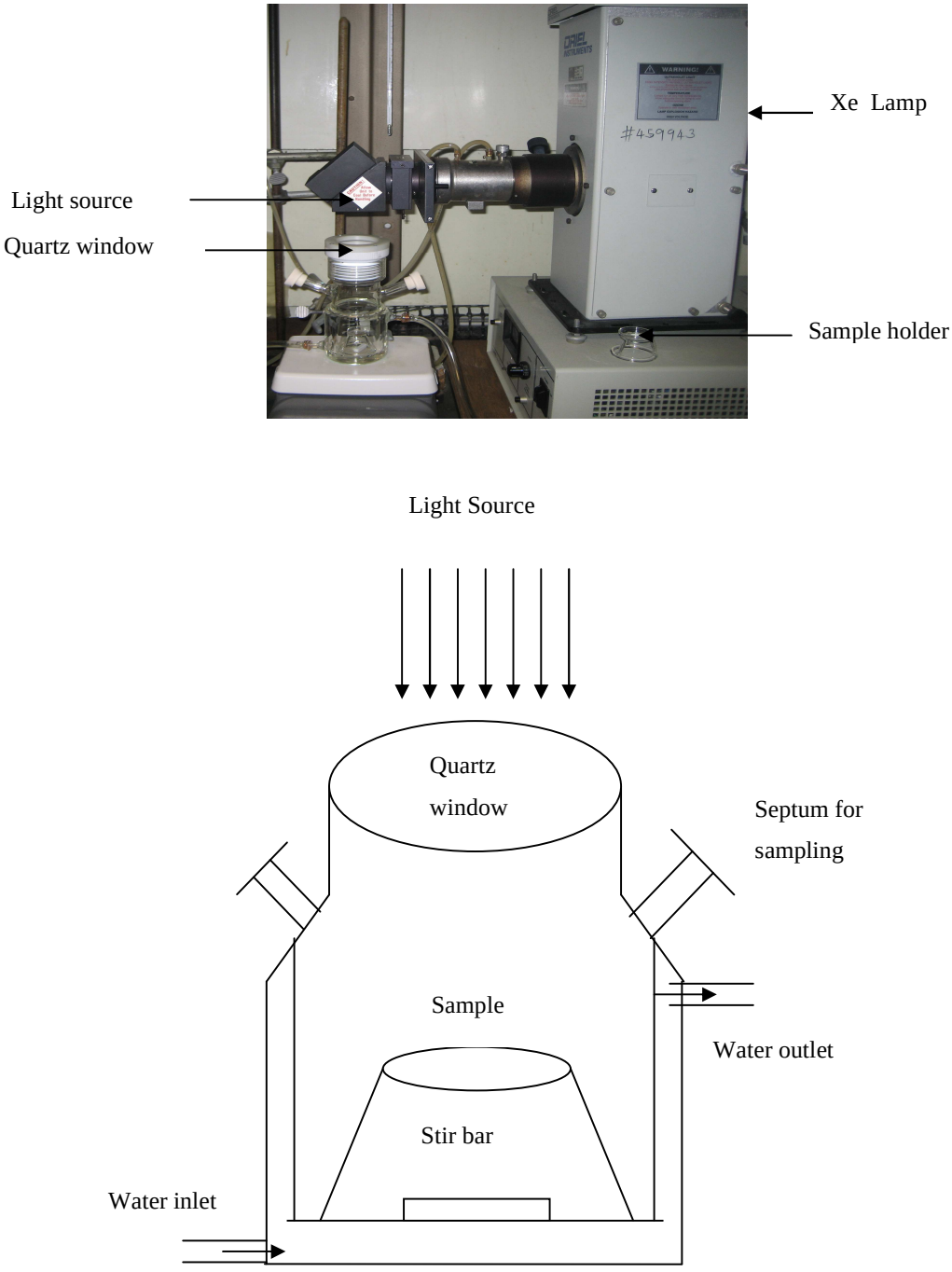

Figure 3.1 (Top) Actual reactor and (bottom) its schematic view

3.3 Results and Discussion

3.3.1 Characterizations

Energy dispersive x-ray spectral analysis showed the presence of codoped elements in various samples annealed at 500° C in air (Figure 3.2). During hydrolysis of titanium (IV) isopropoxide, the presence of ammonium thiocyanate as nonmetal precursor resulted in codoping of both carbon and sulfur into the TiO_2 photocatalyst (Figures 3.2a, c and d), whereas its absence resulted in only Co-TiO_2 without C and S (Figure 3.2b). Table 3.1 shows an average amount of codoped carbon and sulfur present on the surface of the annealed TiO_2 samples with 2% Co^{2+} loading. However, the amount of cobalt determined from the EDX is less than that of initial loading, suggesting that only a small fraction of the doped Co remains on the surface and the rest portion of it could have occupied the interstitial position of TiO_2 crystal lattice.

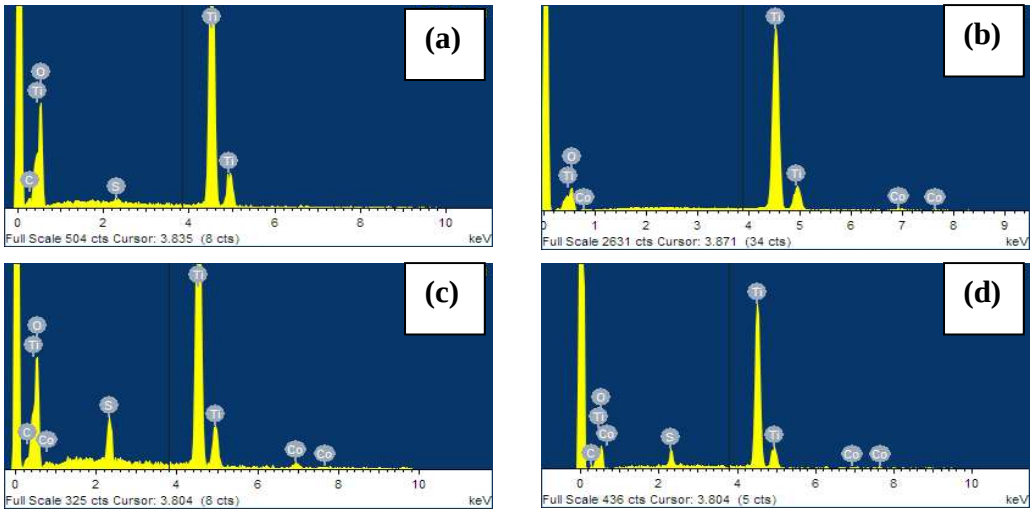

Figure 3.2 EDX spectra of (a) (C, S), (b) 2% Co(II)-TiO_2, (c) 2% CoII/(C, S)-TiO_2, and (d) 2% CoIII/(C, S)-TiO_2

Table 3.1 Average amount of codoped carbon and sulfur in TiO_2, when Co loading is 2%

Sample	Co (at. %)	C (at. %)	S (at. %)
(C, S)-TiO_2	0	4.2	0.2
2% CoII-TiO_2	0.48	0	0
2% CoII/(C, S)-TiO_2	0.45	4.1	2.1
2% CoIII/(C, S)-TiO_2	0.37	5.9	2.2

Powder X-ray diffraction analysis of the annealed samples confirmed the formation of only anatase TiO_2 (Figure 3.3). Further analysis of the XRD profile of cobalt-doped TiO_2 with or without codoped carbon and sulfur ruled out the formation of cobalt oxides and sulfides as separate phases. This indicates that codoped Co, C, and S are uniformly dispersed or coordinated in such a way that the X-rays are insensitive to detect them. This can be explained on the basis of the crystallite size of materials under study. The smaller the crystallite size, the higher is the dispersion of codoped elements, and this makes the X-ray beam insensitive to them. The crystallite size of each sample determined by using the Debye Scherrer equation (crystallite size = $0.89\lambda/\beta\text{Cos}\theta$, λ = wavelength of X-ray, β = full width at half maxima, and θ = diffraction angle) for the most intense (101) peak at around $2\theta = 25.25°$ is shown in the respective XRD pattern (Figure 3.3). Obviously, the crystallite size of the anatase TiO_2 codoped with C and S is smaller (8.4 nm) that that of Co-TiO_2 (15 nm and 17.5 nm) and undoped TiO_2 samples (20.4 nm and 21 nm), implying that codoping of C and S resists substantially the aggregation of the anatase TiO_2 nanoparticles during the annealing step at 500° C in air as compared with doping Co only. Still, this anti-sintering effect of the codoped nonmetals could be seen in the crystallite

sizes of 1% Co(II)/(C, S)-TiO_2 (8.5 nm), 2% Co(II)/(C, S)-TiO_2 (7.4 nm), 2% Co(III)/(C, S)-TiO_2 (6.6 nm). To confirm the existence of the nano-sized domains, we obtained the TEM image of 2% Co(II)/(C, S)-TiO_2 sample. Now, it is clear that this sample actually constitutes very small nanoparticles (Figure 3.4a) and the mean particle size is 5.7 ± 2 nm (Figure 3.4b). The formation of very small TiO_2 nanoparticles (< 10 nm) is advantageous for the migration of the photogenerated charge-carriers to the surface, where the photocatalytic reaction occurs. Therefore, it is anticipated that codoping cobalt, carbon and sulfur leads to the formation of codoped TiO_2 nanoparticle photocatalysts of high-activities for pollution remediation under visible light irradiation.

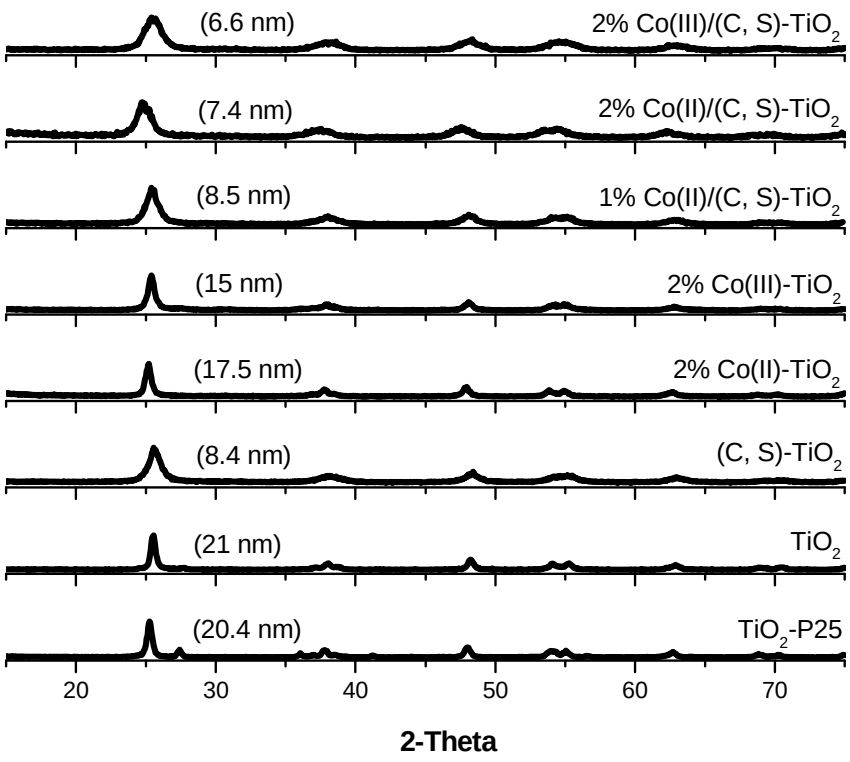

Figure 3.3 Powder X-ray diffraction patterns of undoped and codoped TiO_2

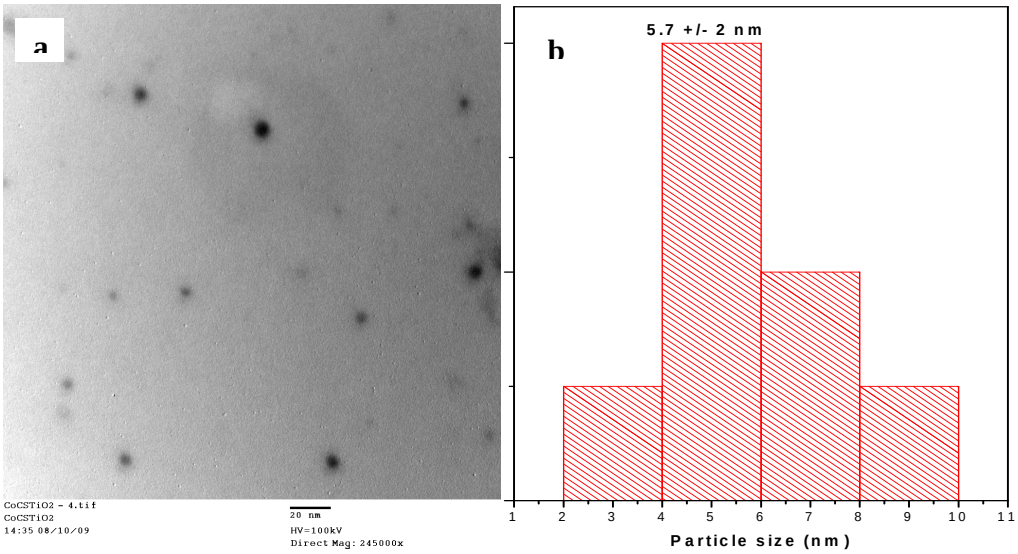

Figure 3.4 TEM image of (a) 2% Co/(C, S)-TiO_2 and (b) stacked histogram of particle size

The UV-visible diffuse reflectance measurements showed that codoping Co with or without C and S produces a pronounced red shift in the onset of the optical absorption edge of TiO_2 samples in visible region (Figure 3.5). These results indicate that all these codoped TiO_2 nanomaterials can induce visible-light photocatalysis for the degradation of organic pollutants.

The N_2 nitrogen adsorption-desorption isotherms (Figure 3.6a) and pore-size distribution (Figure 3.6b) showed that these nanomaterials exhibit mesoporous structures with uniform pore size distributions. Table 3.3 shows the other textural properties such as specific surface area, pore volume and pore diameter of TiO_2 based nanomaterials. Here we observed that Co, C, and S - codoped TiO_2 samples exhibit very high specific surface areas (88 m^2/g) as compared with (C, S)-TiO_2 (69.8 m^2/g), Co-TiO_2 (15 and 17.5 m^2/g) and undoped TiO_2 (5.4 m^2/g) samples prepared

by the same method. Therefore, codoping TiO_2 with a metal and nonmetals would be a good strategy to produce high-surface area TiO_2 nanoparticles for photocatalytic applications because high-surface provides more absorption/desorption sites for photocatalysis.

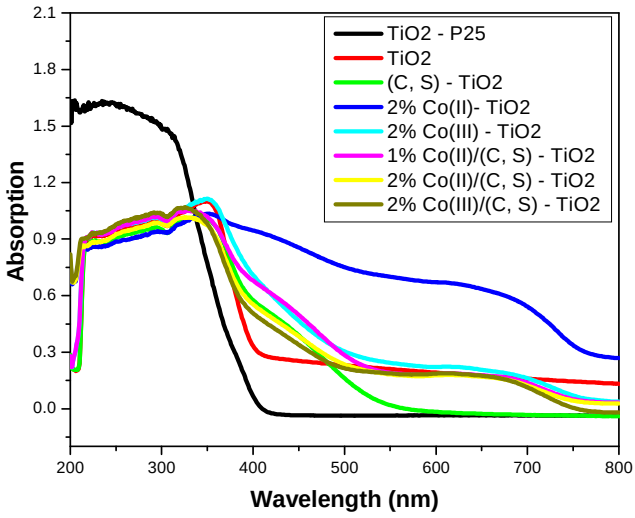

Figure 3.5 UV-vis absorption spectra of undoped, C and S-codoped, Co-doped, and Co, C, and S-codoped TiO_2 samples

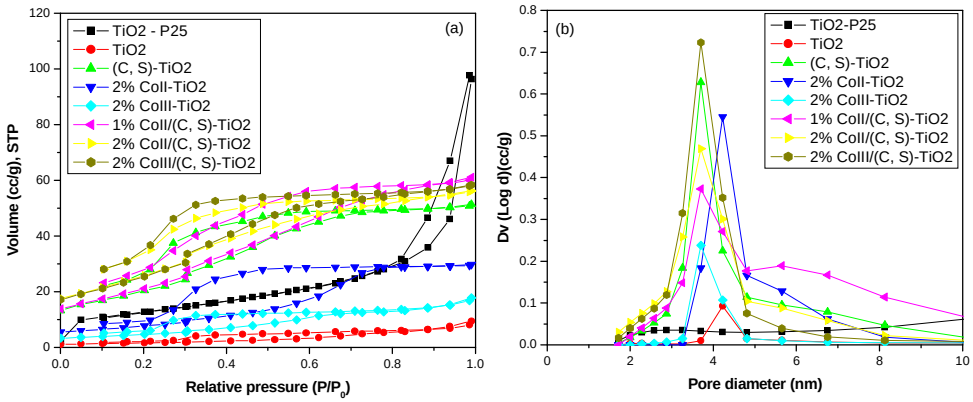

Figure 3.6 Nitrogen adsorption-desorption (a) isotherms and (b) pore-size distributions

Table 3.2 Textural properties of undoped and doped TiO_2 samples

Sample	BET area (m^2/g)	Pore volume (cc/g)	Pore diameter (nm)
TiO_2 – P25	45	0.15	2.3
TiO_2	5.4	0.02	3.8
CS-TiO_2	69.8	0.08	3.4
2% Co(II)/TiO_2	26	0.05	3.8
2% Co(III)/TiO_2	15.7	0.03	3.4
1% Co(II)/CS-TiO_2	73	0.1	3.3
2% Co(II)/CS-TiO_2	89	0.1	3.4
2% Co(III)/CS-TiO_2	88.6	0.1	3.4

3.3.2 Photoactivity studies

3.3.2.1 Photocatalytic degradation of gas-phase acetaldehyde

One indication of photomineralization of organic pollutants is the evolution of carbon dioxide as a major product, which indicates the efficiency of photocatalyzed reactions. In the present work, acetaldehyde (an indoor air pollutant) is chosen as a probe and its photodegradation is followed by measuring the amount of carbon dioxide evolved with respect to the irradiation time. Therefore, in most cases, the plot of the amount of CO_2 produced with time provides information on the activity of photocatalyst systems under study. Figure 3.7a clearly shows that the evolution of carbon dioxide increases linearly with time over visible-light-stimulated (C, S)-TiO_2 photocatalyst in the presence of acetaldehyde polluted air. This proves that the carbon and sulfur codoped TiO_2 system has the ability to degrade acetaldehyde to some extent under visible light illumination as compared with TiO_2-P25 and TiO_2, which are inactive for acetaldehyde degradation under the same condition. Obviously, the (C, S)-TiO_2 photocatalyst can be excited with visible light ($\lambda > 420$ nm) because the onset of its band edge is shifted to visible region at

about λ = 548.7 nm (Figure 3.5). Figure 3.7b compares the photoactivities for acetaldehyde degradation over TiO_2-P25, 1% Ag/(C, S)-TiO_2 and 1% Co/(C, S)-TiO_2 photocatalysts under visible light irradiation. It is obvious that 1% Co/(C, S)-TiO_2 system exhibits higher activities for CH_3CHO degradation under visible light than 1% Ag/(C, S)-TiO_2 system. This proves that the codoped metal has a significant effect on the photoactivities of nonmetals codoped TiO_2 systems. Therefore, we explored the photoactivity of Co, C, and S-codoped TiO_2 system in detail. Figure 3.8a depicts that codoping TiO_2 with cobalt, carbon, and sulfur markedly improved photoactivity for acetaldehyde degradation under visible light irradiation, and the optimum activity was obtained for 2% cobalt loading. This enhancement in activity could be attributed to the fact that cobalt introduces further red-shift of the onset of the absorption edge in visible region at about λ = 756.4 nm to 762.5 nm (Figure 3.5). In fact, this additional red-shift of absorption edge enables Co/(C, S)-TiO_2 photocatalyst to absorbs more visible light photons than (C, S)-TiO_2 and undoped TiO_2. Figure 3.8b displays photoactivities for acetaldehyde degradation under UV light irradiation over various photocatalysts. Still, we observed high activities of 1% and 2% Co/(C, S)-TiO_2 systems for CH_3CHO decomposition as compared with (C, S)-TiO_2, undoped TiO_2, and TiO_2-P25. Moreover, these photoactivity results prove that Co/(C, S)-TiO_2 nanoparticle photocatalysts have promise for harvesting abundant solar energy for environmental remediation.

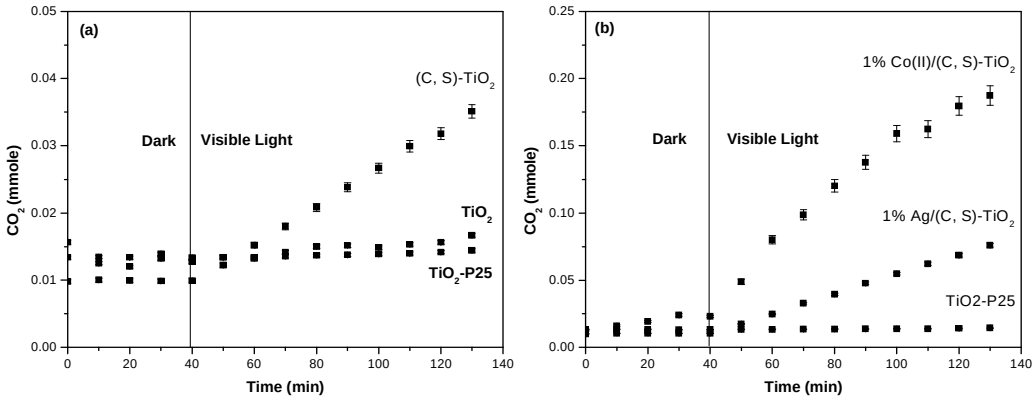

Figure 3.7 Evolution of CO_2 from CH_3CHO degradation over (a) naked and nonmetals (C and S) codoped TiO_2 systems, and (b) metals (silver and cobalt) and nonmetals (C, S) codoped TiO_2 systems under visible light irradiation

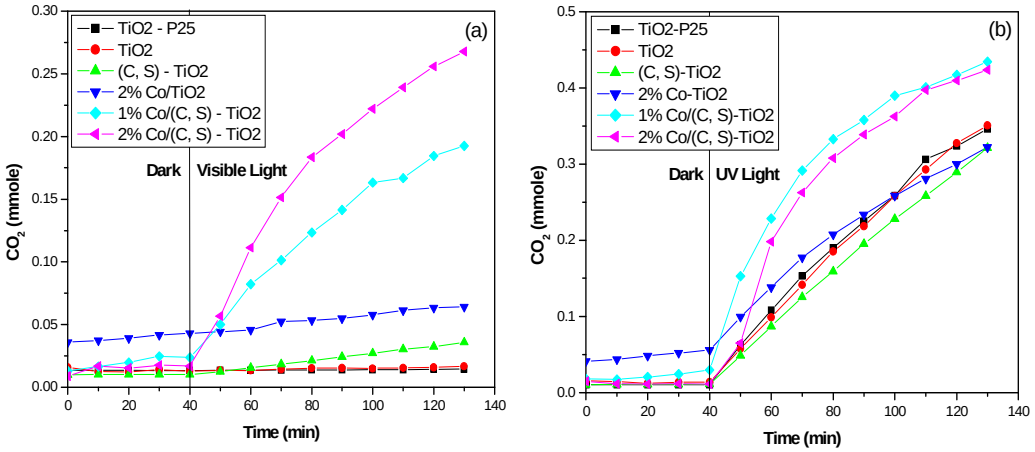

Figure 3.8 Effect of cobalt loading on concentration vs time profile for CO_2 evolution under (a) visible light and (b) under UV light irradiation

3.3.2.2 Photostability

Of the various attributes of ideal photocatalysts, the stability and reusability of the photocatalyst are also important for long-term applications. To investigate these two attributes of the photocatalyst, we performed two successive long-run experiments with the most active photocatalyst under visible light irradiation. Figure 3.9a shows that the concentration of gas-phase acetaldehyde decreases with irradiation time over 2% Co/(C, S)-TiO_2, indicating that acetaldehyde was degraded. This was further supported by the concurrent evolution of carbon dioxide as shown in Figure 3.9b. These results confirm that 2% Co/(C, S)-TiO_2 nanoparticle photocatalyst is stable and retains its visible-light-activity for a prolonged time period without any additional cost for activation.

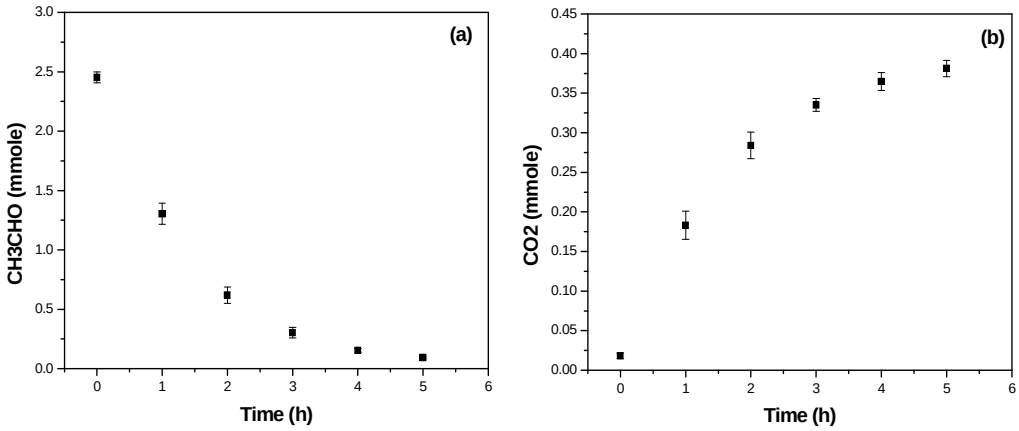

Figure 3.9 Long-run kinetic plot for (a) CH_3CHO degradation and (b) CO_2 evolution over 2% Co/(C, S)-TiO_2 visible light irradiation

3.3.2.3 Active sites recognition

Now, it is very important to know and understand about the active sites for enhanced visible-light-induced photodecomposition of gas-phase acetaldehyde over 2% Co/(C, S)-TiO_2 samples. To elucidate the active sites for visible-light-driven photocatalysis, we examined the activities of 2% Co(II) or Co(III)-doped TiO_2 systems with or without codoped C and S. Unfortunately, no photocatalysis was observed with 2% Co(II)-TiO_2 and 2% Co(III)-TiO_2 under visible light irradiation. However, TiO_2 codoped with 2% Co, C and S exhibited remarkable activities for CO_2 evolution from CH_3CHO decomposition under visible light irradiation, regardless of the initial valence state of cobalt in its precursors (Figure 3.10).

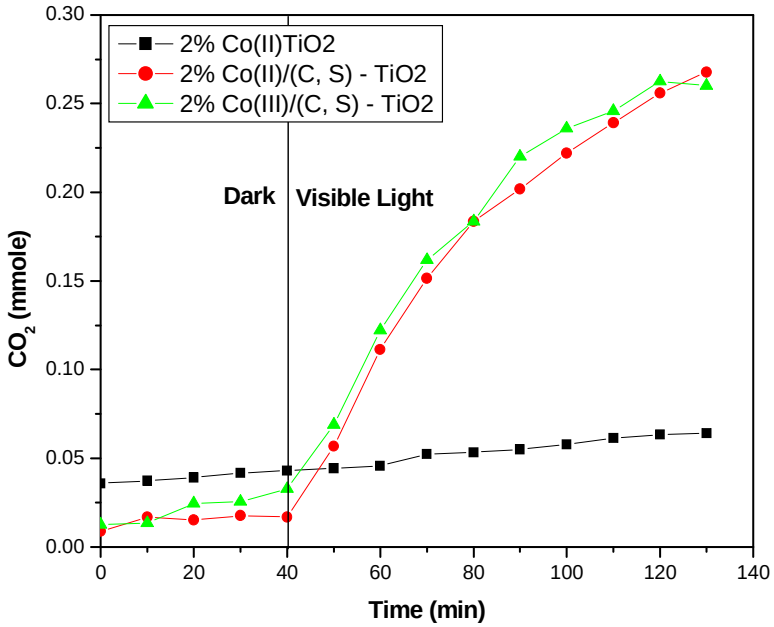

Figure 3.10 Effect of initial valence state of cobalt on CO_2 evolution from CH_3CHO degradation under visible light irradiation

Conceptually, one possible reason may be that active sites per unit mass of both 2% Co(II)/(C, S)-TiO_2 and 2% Co(III)/(C, S)-TiO_2 photocatalysts remain the same because both samples have almost equal BET surface areas (89 and 88.6 m^2/g). This implies that cobalt, carbon and sulfur are necessary for enhanced visible-light-activity of nanosized anatase TiO_2 photocatalyst.

To determine the chemical valence state of Ti, O, C, S and Co, we measured the X-ray photon spectroscopy (XPS) spectra of all samples and determined the core level binding energy for each element. For simplicity, a typical XPS spectrum of 2% Co(II)/(C, S)-TiO_2 is shown in Figure 3.11, and binding energy values of all constituent elements in Table 3.3. The Ti2p XPS spectrum (Figure 3.11a) and binding energy values for $Ti2p_{3/2}$ and $Ti2p_{1/2}$ spin-orbit doublet confirmed that titanium is present as Ti^{4+}.[4-6] The O1s XPS spectrum with a shoulder (Figure 3.11b) and B. E. values showed that oxygen is present as O^{2-} into the O-Ti lattice and as OH-M on the surface.[4-6] The C1s XPS spectrum (Figure 3.11c) and B. E values indicated that carbon is mostly present as graphitic carbon.[7] The $S2p_{3/2}$ XPS spectrum (Figure 3.11d) and B. E. values showed that sulfur is present as sulfate species.[8, 9] For cobalt, it is difficult to differentiate Co(II) and Co(III) species from the measured $Co2p_{3/2}$ core level binding energy values (Table 3.3). However, some clear features in the Co2p core level spectra will help us to differentiate Co(II) and Co(III) species. If Co(II) species is present, the Co2p XPS spectra exhibit strong shakeup satellite peaks at higher binding energies. Figure 3.12a shows the Co2p XPS spectrum of 2% Co(II)/(C, S)-TiO_2 sample before visible light photocatalysis. The shakeup satellite features obtained in the present study are in good agreement with reported ones,[31] confirming the presence of Co(II) species. Figure 3.12b shows the Co2p core level XPS spectrum of 2% Co(III)/(C, S)-TIO_2 sample before visible light photocatalysis. Since the shakeup satellite peaks

of Co(III) species are weaker than that of Co(II), the Co2p features in Figure 3.12b confirms the presence of Co(III) species. However, after visible light photocatalysis, the shakeup satellite features in Figure 3.12a became very weak, indicating the possible oxidation of Co(II) to Co(III). Interestingly, after visible light photocatalysis, no distinct shakeup satellite peaks appeared in Co2p XPS spectrum (Figure 3.12d). This ruled out the thermodynamically feasible reduction of Co(III) to Co(II) species. From these results, we conclude that Co(II) species act as first sacrificial sites, and then Co(III) species actually catalyze the degradation of acetaldehyde during photocatalysis with visible light. Even if we start with Co^{2+} precursor, the formation of Co^{3+} species is due to the oxidation of Co^{2+} to Co^{3+} to some extent during annealing of the codoped TiO_2 sample at 500° C in air. Also, the binding energy of Co in 2% Co(II) or Co(III)/(C, S)-TiO_2 samples before and after photocatalysis with visible light remains almost the same. This confirms that when codoped C and S are present, the Co^{3+} ions act as active sites for acetaldehyde degradation under visible light irradiation. If the Co(III) species were not the active sites in the presence of codoped C and S into TiO_2, the long-run kinetic results obtained for acetaldehyde degradation over 2% Co(II)/(C, S)-TiO_2 system under visible light irradiation could not have been the reproducible one (Figure 3.8).

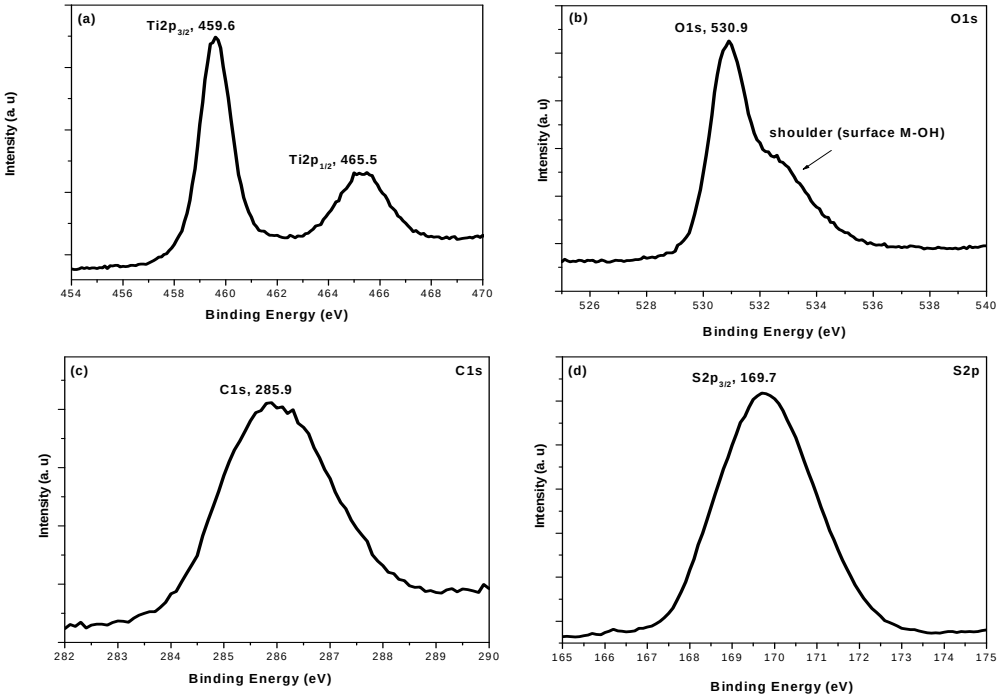

Figure 3.11 XPS spectra for (a) Ti, (b) O, (c) C, and (d) S present in 2% Co/(C, S)-TiO_2

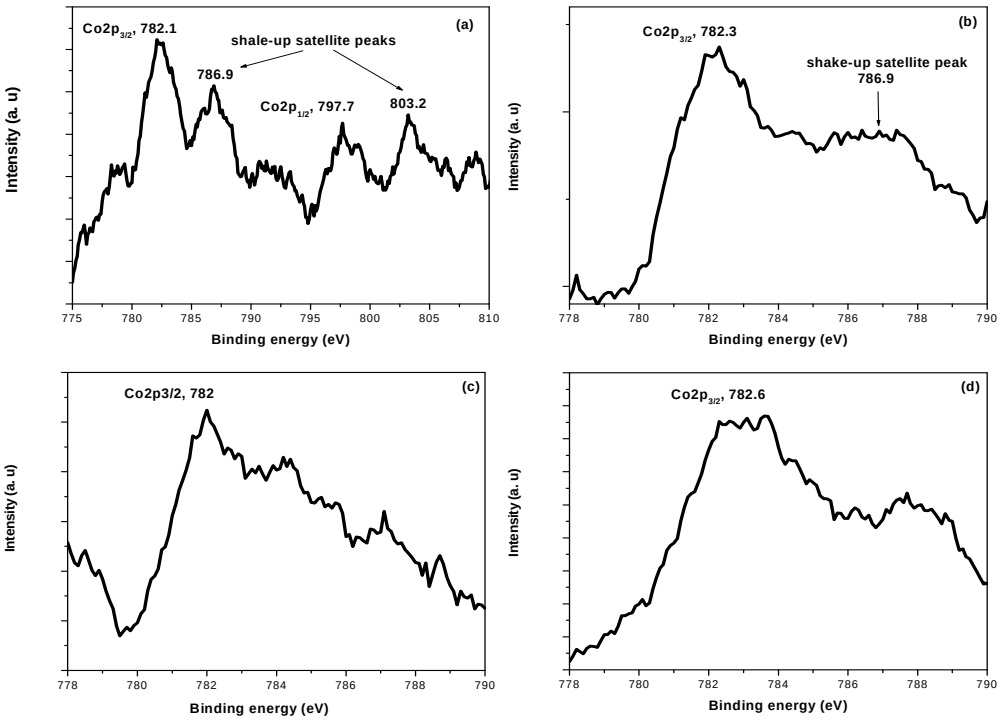

Figure 3.12 Co2p core level XPS spectral analysis. (a) Co(II) in 2% Co(II)/(C, S)-TiO_2 and (b) Co(III) in 2% Co(III)/(C, S)-TiO_2 samples before visible light reaction. (c) Co(II) in 2% Co(II)/(C, S)-TiO_2 and (d) Co(III) in 2% Co(III)/(C, S)-TiO_2 samples after visible light reaction

Table 3.3 Core level binding energies for Ti, O, C, S and Co

Sample	$Ti2p_{3/2}$	O1s	C1s	$S2p_{3/2}$	$Co2p_{3/2}$
(C, S)-TiO_2	458.6	529.9	284.7	168.9	
2% CoIITiO_2	459.5	530.8			782.6
2% CoII/(C, S)-TiO_2 before reaction	459.6	530.9	285.9	170.1	782.1
2% CoII/(C, S)-TiO_2 after reaction	459.6	531	285.5	170.1	782
2% CoIII/(C, S)-TiO_2 before reaction	459.6	530.9	285.2	169.9	782.3
2% CoIII/(C, S)-TiO_2 after reaction	459.6	530.9	285.3	169.9	782.6

3.3.2.4 Role of codopants (Co, C, and S) in enhanced visible light photocatalysis

Since photocatalytic reactions are complex, several factors, such as crystallinity, surface area, band gap, reactive oxygen species (OH radical, O^{2-} ion, H_2O_2 etc), and electron-hole recombination, affect the outcome. We have shown that low-surface area ($5.6m^2/g$) nanosized anatase TiO_2 demonstrated almost similar activity for acetaldehyde degradation under UV light illumination as compared with high-surface area ($45m^2/g$) mixed phase TiO_2-P25. However, surface area of pure TiO_2 nanomaterials depend upon the synthesis route. The present synthesis route resulted in very low-surface area of pure TiO_2, but however, shows UV light activity. The main goal of this study is to develop a visible-light-responsive TiO_2 photocatalyst that can be used for air purification. Fortunately, this goal has been partly achieved by codoping carbon and sulfur into TiO_2, and (C, S)-TiO_2 photocatalyst has a surface area of $69.8m^2/g$, much higher than $5.6m^2/g$ that of pure TiO_2. This proves that codoping carbon and sulfur can increase the surface area, which is also important for photocatalysis. Furthermore, codoping a metal (cobalt) and two

nonmetals (carbon and sulfur) into TiO_2 increased surface area to 89 m^2/g, which is higher than 15.7m^2/g and 26m^2/g those of only cobalt-doped TiO_2 samples.

Besides a surface area enhancement effect, carbon and sulfur codoping reduces the band gap of TiO_2 to 2.26 eV, a value far less than 3.2 eV (Table 3.4), allowing the utilization of abundant visible light. On the other hand, only cobalt doping into TiO_2 introduces an additional intra-band state of 1.61 eV (possibly due to $O^{2-} \rightarrow Co^{3+}$),[32] even less than that of 2.26 eV. Thus, by codoping TiO_2 with cobalt, carbon and sulfur results in the creation of two intra-band states or sites for visible light absorption. As a result, we observed enhanced visible-light-induced heterogeneous photocatalysis over Co/(C, S)-TiO_2 photocatalyst as compared with (C, S)-TiO_2 (Figure 3.8a).

Table 3.4 Band gap energies of photocatalyst samples

Sample	Band-gap (eV)	Intra-band state due to Co (eV)
TiO_2 – P25	3.17	
TiO_2	3.11	
CS-TiO_2	2.26	
2% Co(II)/TiO_2	2.32	1.62
2% Co(III)/TiO_2	2.69	1.61
1% Co(II)/CS-TiO_2	2.37	1.64
2% Co(II)/CS-TiO_2	2.4	1.63
2% Co(III)/CS-TiO_2	2.5	1.63

Hydroxyl radicals are generally considered as powerful oxidants for the decomposition of organic pollutants in most photooxidation reactions. Hopefully, the analysis of OH radicals will aid an understanding of photocatalysis mechanism. In order to elucidate the role of OH radicals, we used 1, 4-benzene dicarboxylic acid (terephthalic acid, TA) as a probe that scavenges OH radicals instantly to generate highly fluorescent molecules, 2-hydroxy terephthalic acid (TA-OH).[33, 34] Upon excitation by 315 nm light, TA-OH emits its photoluminescence (PL) signal at λ_{max} = 425 nm. Therefore the measurement of PL emission spectra of samples will provide an additional piece of information for OH radical analysis. Figure 3.13a shows the PL emission spectra from aqueous terephthalic acid solution excited at λ_{ex} = 315 nm. Even under dark conditions, it can be seen that the PL signal induced by 2% Co(II)/(C, S)-TiO_2 nanoparticles is much higher than that of a control. This observation suggests that 2% Co(II)/(C, S)-TiO_2 nanoparticle photocatalyst can readily generate OH radicals. When irradiated with visible light (λ > 420 nm, the PL signal (λ_{max} = 425 nm) increases linearly with time, indicating the formation and scavenging of OH radicals by TA. These results further prove the photostability and sustained visible-light-activity of 2% Co(II)/(C, S)-TiO_2 photocatalyst during gas-phase acetaldehyde photodegradation.

However, it seems indispensable to know whether or not OH radicals are the sole oxidants in photocatalysis. For this purpose, we measured the PL spectra of other photocatalysts (Figure 3.13b). Here, we noticed that the ability of (C, S)-TiO_2 nanoparticles to generate OH radicals on the photocatalyst/water interface is more than that of 2% Co(II)/(C, S)-TiO_2, 1% Co(II)/(C, S)-TiO_2, and 2% Co(II)-TiO_2. As a consequence, (C, S)-TiO_2 would be more visible-light-active photocatalyst for CH_3CHO decomposition than 2% Co(II)/(C, S)-TiO_2; however, the converse is

true. Also, 1% Co(II)/(C, S)-TiO_2, and 2% Co(II)-TiO_2 have the same abilities to generate OH radicals, but the former is visible-light-active and the latter is inactive. There could be two possible reasons for this inconsistency in the relationship between OH radicals and activity results. First, the gas-phase and aqueous-phase photocatalytic reactions markedly differ from each other. So, the gas-phase observed activity does not coincide with the results obtained for OH radicals in aqueous TA solution. Secondly, OH radicals might be only partly involved in photocatalysis.

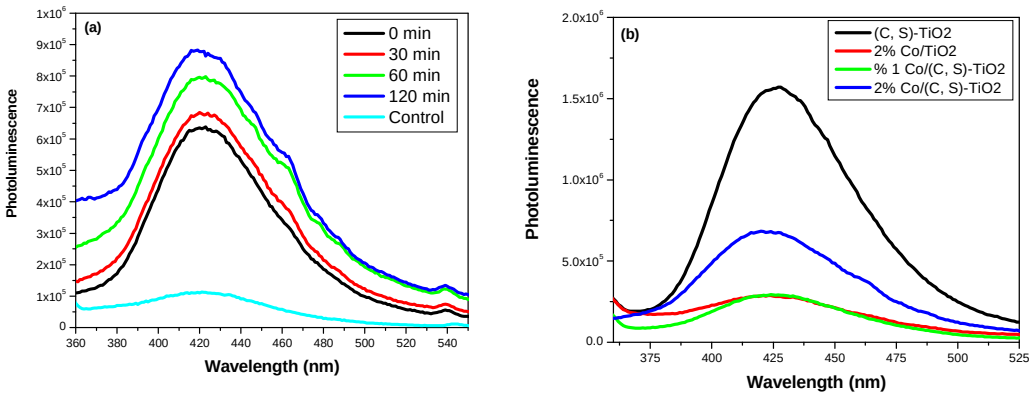

Figure 3.13 Photoluminescence (PL) spectra of (a) 2% Co/(C, S)-TiO_2 with visible light irradiation time, and (b) its comparative PL spectra for 30 minutes obtained in aqueous terephthalic acid solution (λ_{ex} = 315nm)

Another crucial factor that affects photocatalysis mechanism is the surface or bulk electron-hole recombination process that actually leads to a decline in photoactivity. Thus, the outcome of overall photocatalytic reaction depends largely upon the life-time of electron-hole separation, just opposite to the electron-hole recombination. The measurement of the photoluminescence

(PL) spectra emitted directly from pure photocatalysts excited with visible light ($\lambda > 420$ nm) will enable us to understand the why codoping TiO_2 with cobalt, carbon, and sulfur led to enhanced visible-light-activity for CH_3CHO degradation. Basically, photoluminescence is a process that involves emission of light when excited conduction-band electrons recombine with valence-band holes of semiconductors.[35] Thus, a high value of the PL signal would indicate a high rate of electron-hole recombination under light irradiation ($\lambda > 420$ nm), suggesting that the photoinduced charge-carriers (electrons-holes) do not engage in the surface-mediated redox reactions. In contrast, a low value of the PL signal will tell us that the electron-hole recombination rate is somehow suppressed, thereby resulting in the longer lifetime of photogenerated electron-hole pairs. As the probability of the separation of electron-hole pairs to engage in surface-mediated reactions increases, a high photocatalytic activity is expected. Figure 3.14 shows that the PL signal of cobalt-doped TiO_2 with or without C and S is lower than that of (C, S)-TiO_2, confirming that the doped cobalt has the ability to suppress the electron-hole recombination process. This is possible because Co^{3+} ions can scavenge or trap conduction electrons due to its high standard reduction potential ($Co^{3+} + e = Co^{2+}$, $E^0 = +1.81$ volts). That may be why 1% and 2% Co/(C, S)-TiO_2 photocatalysts demonstrated higher activities than (C, S)-TiO_2 for CH_3CHO degradation under visible light. Also, it can be seen that the electron-hole recombination is more suppressed in 1% Co/(C, S)-TiO_2 than in 2% Co/(C, S)-TiO_2. However, the observed photoactivity of the former is lower than that of the latter sample. The high activity of the latter sample could be attributed to the effect of other variables, such as surface area, OH radical generation and cobalt loading. Even though 2% Co(II)-TiO_2 sample has the abilities to generate OH radicals and suppress the electron-hole recombination to some extent, it does not work under visible light, and this is further supported by activity test with 2% Co(III)-TiO_2 (data

not shown). Overall, these results explain why codoping carbon and sulfur is necessary for cobalt-doped TiO_2 systems to be visible-light-active photocatalyst. We believe that high-surface area, anatase crystallinity, introduction of inter-band state, OH radical generation, and suppression of electron-hole recombination partly contributed to the optimum photoactivity of 2% Co/(C, S)-TiO_2 for acetaldehyde degradation under visible light (λ > 420 nm). In addition, we can only speculate that the codoped carbon may act a photosensitizer, and the codoped sulfur as sulfate may coordinate with the doped cobalt ions to facilitate the charge- transfer process in photocatalyst/air interfaces.

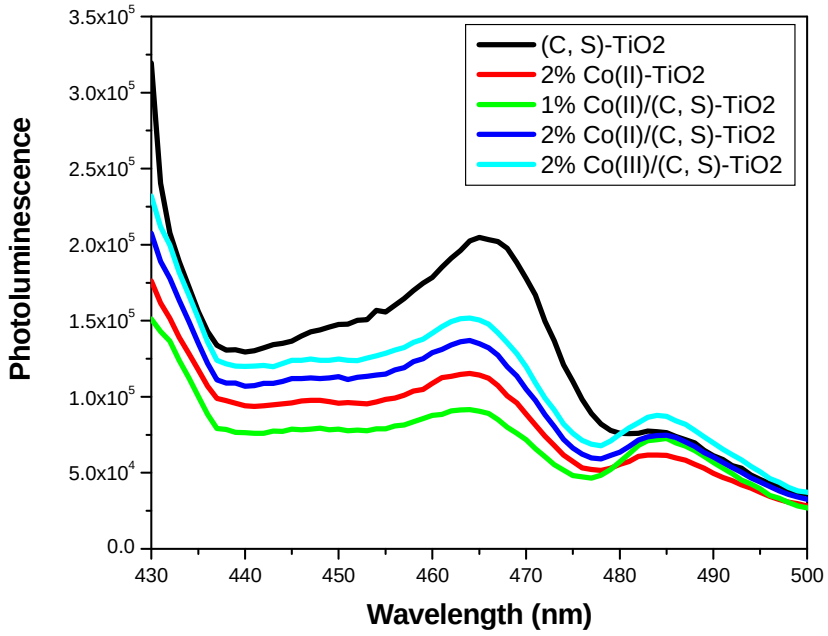

Figure 3.14 Photoluminescence spectra of codoped TiO_2 samples obtained at λ_{ex} = 420 nm

3.4 Conclusions

Effects of codoping 3d-transition metal ion, carbon and sulfur into nanosized anatase TiO_2 photocatalyst were investigated. Interestingly, Co/(C, S)-TiO_2 photocatalyst system exhibited commendable high-activity and long-term stability under visible light irradiation ($\lambda > 420$ nm) as compared with Ag/(C, S)-TiO_2 photocatalyst system. Characterization and activity results further imply that a compromised balance of several variables, such as crystallinity, particle size, surface area, band-gap reduction, hydroxyl radical generation, and electron-hole suppression, led to enhanced visible-light-activity of Co/(C, S)-TiO_2 system for air purification. Moreover, codoping a suitable metal and two nonmetals appears to be a good strategy for developing visible-light-driven nanosized anatase TiO_2 photocatalysts for environmental applications.

3.5 References

1. Nagaveni, K; Hegde, M. S; Ravishankar, N; Subbanna, G. N.; Madras, G., *Langmuir* **2004**, 20, 2900-2907.
2. Asahi, R; Morikawa, T; Ohwaki, T; Aoki, K; Taga, Y., *Science* **2001**, 293, 269-271.
3. Lin, Li; Lin, W; Zhu, Y; Zhao, B; Xie, Y., *Chem. Lett.* **2005**, 34, 284-285.
4. Ohno, T; Mitsui, T; Matsumura, M., *Chem. Lett.* **2003**, 32, 364-365.
5. Li, Di; Haneda, H; Labhsetwar, N. K; Hishita, S; Ohashi, N., *Chem. Phys. Lett.* **2005**, 401, 579-584.
6. Hong, X; Wang, Z; Cai, W; Lu, F; Zhang, J; Yang, Y; Ma, N; Liu, Y., *Chem. Mater.* **2005**, 17, 1548-1552.
7. Sun, H; Bai, Y; Cheng, Y; Jin, W; Xu, N., *Ind. Eng. Chem. Res.* **2006**, 45, 4971-4976.
8. Cong, Y; Chen, F; Zhang, J; Anpo, M., *Chem. Lett.* **2006**, 35, 800-801.
9. Li, D; Haneda, H; Hishita, S; Ohashi, N., *Chem. Mater.* **2005**, 17, 2588-2595.
10. Ozaki, H; Iwamoto, S; Inoue, M., *Chem. Lett.* **2005**, 34, 1082-1083.
11. Sakatani, Y; Ando, H.; Okusako, K; Koike, H; Nunoshige, J; Takata, T; Kondo, J. N; Hara, M; Domen, K., *J. Mater. Res.* **2004**, 19, 2100-2108.
12. Zhao, W; Ma, W; Chen, C; Zhao, J; Shuai, Z., *J. Am. Chem. Soc.* **2004**, 126, 4782-4783.
13. Sakatani, Y; Nunoshige, J; Ando, H; Okusako, K; Koike, H; Takata, T; Kondo, J. N; Hara, M; Domen, K., *Chem. Lett.* **2003**, 32, 1156-1157.
14. Liu, H; Gao, L., *Chem. Lett.* **2004**, 33, 730-731.
15. Tryba, B; Morawski, A. W; Inagaki, M; Toyoda, M., *J. Photochem. Photobiol. A: Chem.* **2006**, 179, 224-228.
16. Bettinelli, M; Dallacasa, V; Falcomer, D; Fornasiero, P; Gombac, V; Montini, T; Romano, L; Speghini, A., *J. Hazar.Mater.* **2007**, 146, 529-534.
17. Yang, X; Cao, C.; Hohn, K.; Erickson, L.; Maghirang, R.; Hamal, D.; Klabunde, K., *J. Catal.* **2007**, 252, 296-302.
18. Hamal, D. B.; Klabunde, K. J., *J. Colloid Interf. Sci.* **2007**, 311, 514-522.
19. Klosek, S.; Raftery, D., *J. Phys. Chem B* **2001**,105, 2815-2819

20. Shi, J. Y.; Leng, W. H.; Zhu, W. C.; Zhang, J. Q.; Cao, C. N., *Chem. Eng. Technol.* **2006**, 29, 146-154.

21. Othman, I.; Mohamed, R. M.; Ibrahem, F. M., *J. Photochem. Photobiol. A: Chem.* **2007**, 189, 80-85.

22. Zhu, J.; Chen, F.; Zhang, J.; Chen, H.; Anpo, M., *J. Photochem. Photobiol. A: Chem.* **2006**, 180, 196-204

23. Iwasaki, M.; Hara, M.; Kawada, H.; Tada, H.; Ito, S., *J. Colloid Interf. Sci.* **2000**, 224, 202-204.

24. Chen, S.; Zhang, S.; Liu, W; Zhao, W., *J. Hazar. Mater.* **2008**, 155, 320-326.

25. Colon, G.; Maicu, M.; Hidalgo, M. C.; Navio, J. A., *Appl. Catal. B: Environ.* **2006**, 67, 41-51.

26. Jing, L.; Xin, B.; Yuan, F.; Xue, L.; Wang, B.; Fu, H., *J. Phys. Chem B* **2006**, 110, 17860-17865.

27. Martyanov, I. N.; Uma, S.; Rodrigues, S.; Klabunde, K. J., *Langmuir* **2005**, 21, 2273-2280.

28. Kapoor, P. N.; Uma, S.; Rodriguez, S.; Klabunde, K. J., *J. Mol. Catal. A: Chem.* **2005**, 229, 145-150.

29. Long, M.; Cai, W.; Cai, J.; Zhou, B.; Chai, X.; Wu, Y., *J. Phys. Chem* B **2006**, 110, 20211-20216.

30. Wu, Y.; Lu, G.; Li, S., *J. Photochem. Photobiol.* A: Chem. **2006**, 181, 263-267.

31. Li, Ji-G.; Buchel, R.; Isobe, M.; Mori, T.; Ishigaki, T., *J. Phys. Chem. C* **2009**, 113, 8009-8015.

32. Zhang, Y.; Chen, Y.; Wang, T.; Zhou, J.; Zhao, Y., *Microporous Mesoporous Mater.* **2008**, 114, 257-261.

33. Hirakawa, T.; Nosaka, Y., *Langmuir* **2002**, 18, 3247-3254

34. Yu, J.; Wang, Wenguang; Cheng, Bei; Su, Bao-Lian. *J. Phys. Chem. C* **2009**, 113, 6743-6750.

35. Yang, X.; Cao, C.; Erickson, L.; Hohn, K.; Maghirang, R.; Klabunde, K., *J. Catal.* **2008**, 260, 128-133.

CHAPTER 4 - Development of Gallium, Indium and Platinum Codoped Nanosized Anatase TiO_2 Photocatalysts for Carbon Monoxide Oxidation under UV-Visible Light Irradiation

4.1 Introduction

As discussed in chapter one, titanium dioxide based heterogeneous photocatalysis has been proven to be a promising technology for the degradation of undesirable chemical - organic and inorganic- pollutants from the environment. Still, the optimum photocatalytic attributes of TiO_2 has not been fully exploited due to the fast charge-carrier recombination and slow interfacial charge-transfer process even under band gap excitation with UV light. These shortcomings can be improved by introducing a foreign impurity within the band gap of TiO_2. In this context, doping of metal ions into TiO_2 seems to be the first choice of research quest because metals are naturally more abundant than nonmetals. Furthermore, metal doping offers a wide range of valence electronic configurations that can be introduced into TiO_2 allowing researchers to systematically understand their influences on phototocatalytic properties and to design materials with desired properties.

Group 13 metals (Al, Ga and In) appears to be important and attractive for further investigation in designing and developing nanosized TiO_2 photocatalysts because these metal oxides (single or mixed) are chemically nontoxic and environmentally friendly. Al_2O_3 and Ga_2O_3 have been widely used as catalytic support materials for noble metals (Au, Pd, Pt, Ir and Ru) in aerobic alcohol oxidation,[1] methanol decomposition,[2] crotonaldehyde hydrogenation,[3] and ethylene hydrogenation.[4] Most interestingly, over the past years, researchers have shown that the Al-TiO_2

nanopowders,[5] Ga_2O_3 films[6] and In_2O_3 nanocrystals[7] possess good sensing properties for CO and O_2, CO, and O_3, respectively. However, very little research work has been focused on the photocatalytic properties of TiO_2 doped with Al, Ga and In ions. For example, Park et al.[8] reported that Al-doping increases the thermal stability of anatase TiO_2 nanoparticles (less than 150 nm) even after thermal treatment at 800^o C. The activity results showed that the photodecomposition of benzene was enhanced in Al/TiO_2 compared to pure TiO_2, esp. with H_2O addition. Zhou et al.[9] reported the Ga-doped TiO_2 photocatalyst system that exhibited the highest photoactivity for the degradation of benzoic acid under UV light. This enhancement in UV photoactivity has been ascribed to the good dispersion of Ga dopant onto the surface of TiO_2, adequate surface area, and decrease of charge-carrier recombination. Shchukin et al.[10] synthesized nanocrystalline bicomponent TiO_2-In_2O_3 powders by the sol-gel technique and found enhanced UV activity for 2-chlorophenol degradation in water due to In_2O_3, which boosted a better separation of photogenerated charge carriers, an improved oxygen reduction and an increased surface acidity allowing a higher adsorption of the water pollutant on to the active sites. Moreover, these research findings suggest that TiO_2 photocatalyst doped with Al, Ga, and In ions could substitute pure TiO_2 photocatalysts for the environment clean-up even for UV light as energy input. Logically, it seems interesting to pursue a research work on how doping/codoping Al, Ga, and In ions affect textural and photocactalytic properties of TiO_2.

Besides the photomineralization of highly toxic organic pollutants into less toxic products, the oxidation of CO to CO_2 is an important reaction for hydrogen production from the water-gas shift reaction ($CO + H_2O = CO_2 + H_2$).[11] Furthermore, it is required that a trace level of CO be removed from the H_2-stream before feeding into fuel cells.[12] The oxidation of CO to CO_2 has

been reported to be carried out both thermally and photocatalytically. Supported noble metals, such as Au[13-16] and Pt,[17-20] have been extensively investigated in the oxidation of CO to CO_2 under dark conditions (without input of light energy). On the other hand, the photocatalytic oxidation of CO to CO_2 is also possible to achieve the same goal even though the process may be kinetically slow. Hwang et al.[21] studied the effects of nanosized Pt (3 wt. %) deposits on various TiO_2 supports and found that the degree of Pt-induced UV activity enhancement strongly depended on the kind of TiO_2 substrate. Interestingly, these authors concluded that not hydroxyl radicals (that are major oxidants in many photocatalytic processes, but dioxygen is responsible for the quantitative photoconversion of CO. They also revealed that the role of Pt nanoparticles in enhancing the CO photooxidation rate is provided by the surface sites on which active oxygen species photogenerated from adsorbed O_2 are stabilized. Einaga et al.[22] reported that Pt-TiO_2 is more active than pure TiO_2 photocatalyst under UV light irradiation, concluding that the deposited Pt acts as the active sites on which CO molecules are chemically adsorbed and oxidized to CO_2 upon UV light excitation in the presence O_2. Zhang et al.[23] demonstrated that the doped Pt particles facilitate the transfer of photogenerated electrons from TiO_2 to Pt particles thereby resulting in the enhancement of photocatalytic activity of CO oxidation. Li et al.[24] pointed out that upon UV light excitation, the triggered oxidation of CO on Pt-TiO_2 system is attributed to the dissociative chemisorption of O_2, decrease of contact resistance on the interfacial region and increased migration velocity of photoinduced charge-carrier. From these research works, we conclude that Pt doping offers many advantages and is important for improving photoactivity of TiO_2 for CO oxidation.

To our knowledge, however, no research works have been so far directed towards the design and development of new generation of nanosized anatase TiO_2 photocatalysts that contain an appropriate combination of both gas sensing and catalytically active metals for CO oxidation. In this chapter, at first, we synthesize and characterize gallium and indium codoped nanosized anatase TiO_2 photocatalysts for heterogeneous photocatalysis that involved both organic and inorganic pollutants in air/water under UV light irradiation. In an attempt to improve the photoactivity for CO oxidation further in visible region, the effect of codoping noble metal (platinum) into (Ga, In)- TiO_2 nanosized photocatalyst is also presented.

4.2 Experimental Section

4.2.1 Chemical Reagents

Titanium(IV) isopropoxide (97% Aldrich), toluene, methanol, nitric acid (63%), aluminum(III) nitrate, gallium(III) nitrate, indium(III) nitrate, silver(I) nitrate, gold(III) chloride, palladium(II) acacetylacetonate, platinum(II) acetylacetonate and ruthenium(III) acetylacetonate were used as-received without further purification.

4.2.2 Photocatalyst preparations

In a typical synthesis procedure, 10 mL titanium isopropoxide (0.033 moles) was dissolved into 60 mL toluene and 40 mL methanol. To this mixture was added 2.26 mL deionized H_2O and 0.2 mL HNO_3 (15.8N) at once under vigorous stirring at room temperature. After stirring less than a minute, a solid gel was obtained. The solid gel was then transferred into a stainless steel autoclave and heated under N_2 atmosphere (initial pressure, 100 psi) from room temperature to 265^o C. When the temperature reached at 265^o C, the autoclave was suddenly vented to remove the solvent vapors and was allowed to cool naturally. The as-synthesized nanopowders were annealed at 500^o C for 2h in air at a heating rate of 2^o C/min to obtain pure TiO_2 photocatalyst. To prepare metal-doped or codoped TiO_2 samples, a desired amount of each metal precursor was added into the mixture of titanium isopropoxide, toluene and methanol before hydrolysis, and the same experimental procedure was followed for the rest of steps.

4.2.3 Characterization

Powder X-ray diffraction (XRD) patterns of samples were recorded on a Scintag XDS 2000 D8 diffractometer with Cu-Kα radiation of wavelength of 1.5406 Å and were analyzed from 15^{o}–75^{o} (2θ) with a step size of 0.05^{o} to determine the crystalline phase. The specific surface areas were determined from the N_2 adsorption–desorption isotherms recorded on a Quantachrome Instrument (NOVA 1000 Series) at liquid nitrogen temperature (77K) by using the Brunauer-Emmett- Teller (BET) method. The Barrett-Joyner- Halenda (BJH) method was used to determine the pore size distributions derived from the BJH desorption isotherms. The UV-Vis absorption spectra were recorded from 200 nm to 800 nm on a Cary 500 Scan UV-Vis NIR Spectrometer with an integrating sphere attachment using PTFE powder as a reference. X-ray photoelectron spectroscopy (XPS) data were recorded with a Perkin–Elmer PHI 5400 electron spectrometer using acrochromatic AlKα radiation (1486.6 eV). All spectra were obtained under vacuum at a pressure of about 3.0×10^{-8} Torr. The XPS binding energies were measured with a precision of 0.1 eV. The analyzer pass energy was set to 17.9 eV, and the contact time was 50 ms. The TEM images were recorded on a Philips CM 100, operating at 100kV.

4.2.4 Photocatalytic Activity Test

In a typical photoactivity test, 0.1025 g (0.00128 moles) sample was placed in a circular disc mounted into a 305 mL cylindrical air-filled static glass reactor. 100 µL of acetaldehyde is placed and allowed to equilibrate for 40min at room temperature. Before UV light illumination, 35 µL of gaseous mixture from the reactor was extracted and analyzed by a Shimadzu GCMS QP500. UV photocatalysis was performed using optical filters that transmit a broad band UV

light of wavelength, λ, 320 - 400 nm. Several other organic pollutants were also photocatalyzed in the same way. For liquid-phase UV photocatalysis, methyl orange (MO) dye was used as a probe. 0.15 g photocatalysts was dispersed into aqueous MO solution (Initial concentration = 1 x 10^{-4} M), sonicated for 10 min, and stirred for 30 min in dark. The degradation of MO was followed by UV-vis measurement of MO dye at 465 nm. For gas-phase CO photooxidation, a certain volume of pure CO gas was injected into the reactor and stirred at room temperature for 40 minutes in the dark and its photodegradation was followed by determining the amount of evolved CO_2. For visible light photocatalysis, combined optical glass filters that transmit visible light of wavelength, λ > 420 nm. The photoactivities of samples were expressed in terms of evolved CO_2.

4.3 Results and Discussion

4.3.1 Characterizations

The aero-gel prepared TiO_2 samples were characterized various techniques. Figure 4.1 shows the powder X-ray diffraction patterns of the doped and undoped TiO_2 samples that contain only anatase phase with the average crystallite size in the range of 8.5 – 10.9 nm. This observation is in good agreement with the TEM analysis of 1% (Ga, In)-TiO_2 sample (Fig.4.2). Furthermore, the TEM image (Figure 4.2a) confirms that the nanoparticles with mean particle size of 11.7 ± 3.5 nm (Figure 4.2b) form porous network-like structures. Figure 4.3 proves that there was no segregation of Ga_2O_3 and In_2O_3 phases even for heavily doped TiO_2 samples that are still composed of nanoparticles of crystallite sizes < 10 nm. Thus, the dopants (B, Al, Ga, and In) are homogeneously dispersed in the nanosized anatase TiO_2.

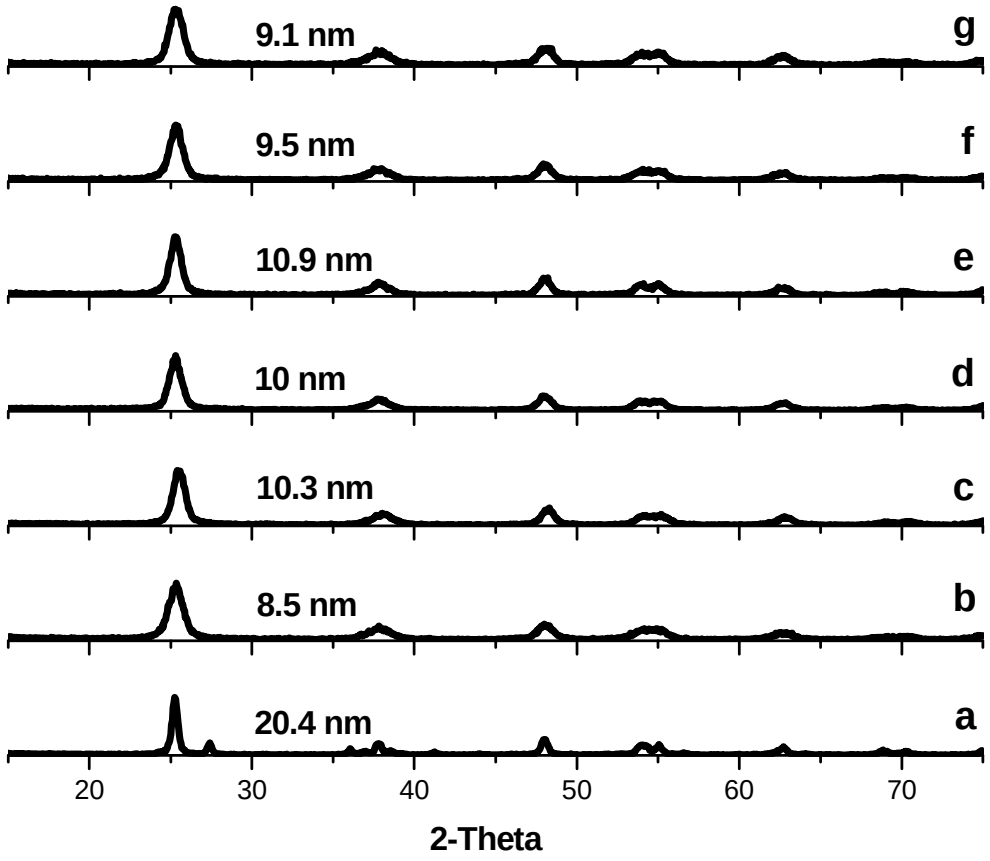

Figure 4.1 Powder X-ray diffraction patterns of (a) TiO_2-P25, (b) TiO_2, (c) 1% B-TiO_2, (d) 1% Al-TiO_2, (e)1% Ga-TiO_2, (f) 1% In-TiO_2, and (g) 1% (Ga, In)-TiO_2

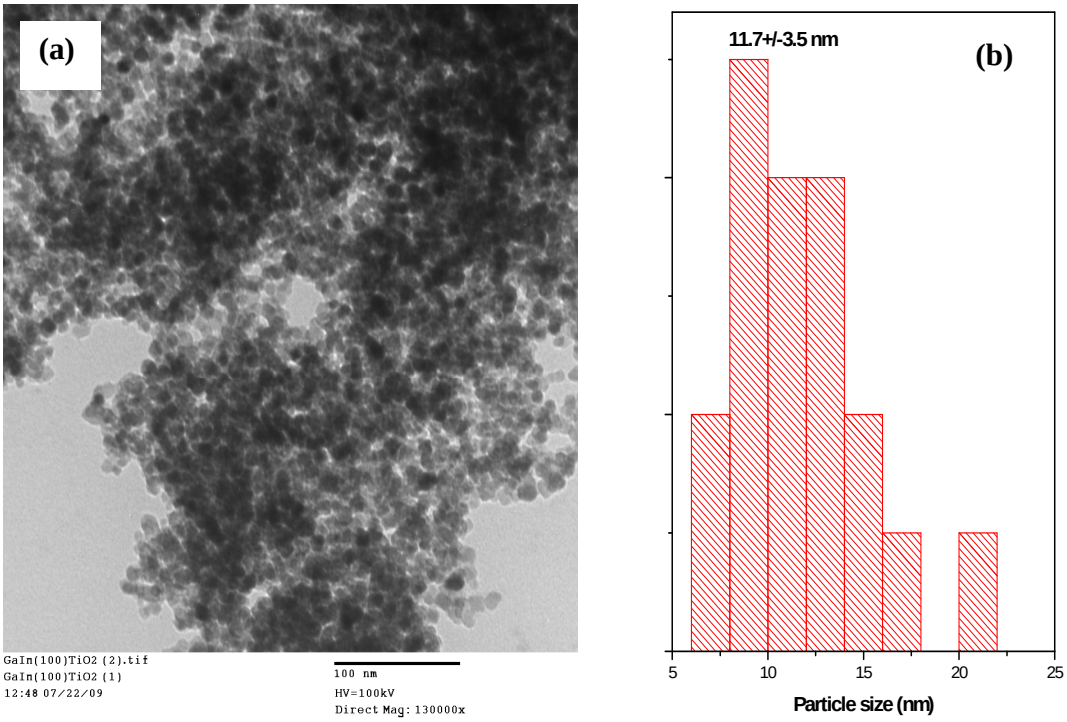

Figure 4.2 (a) TEM image and (b) particle size distribution of 1% (Ga, In)-TiO_2 sample

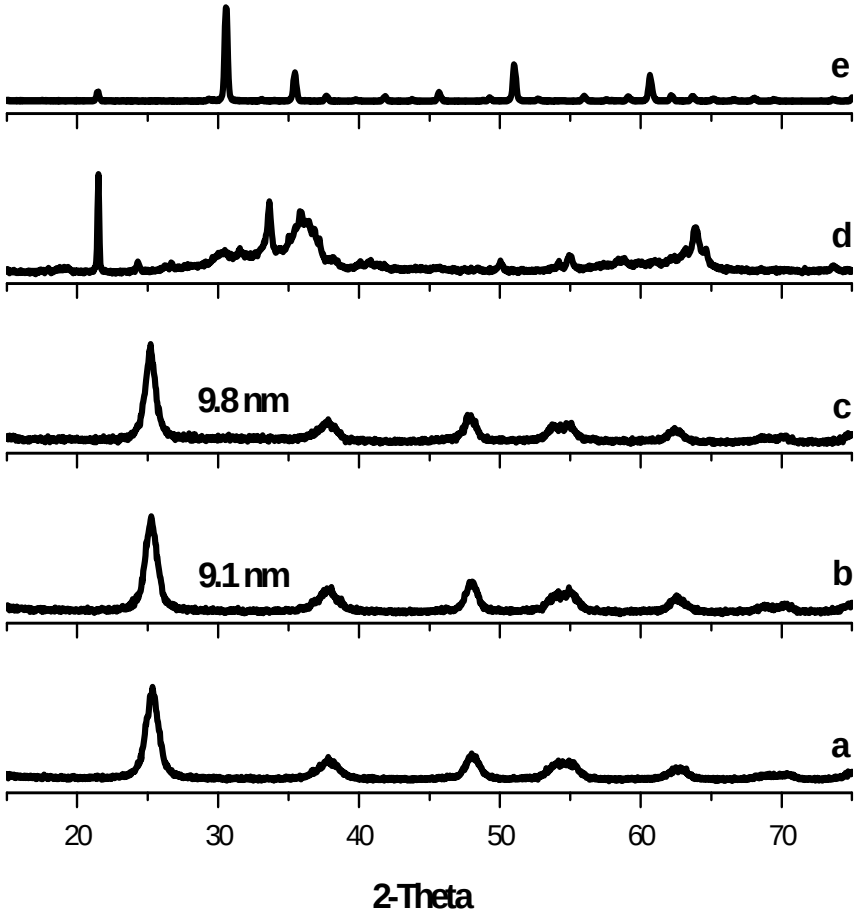

Figure 4.3 Powder X-ray diffraction patterns of (a) TiO_2, (b) 10% Ga-TiO_2, (c) 10% In-TiO_2, (d) Ga_2O_3, and (e) In_2O_3

Figure 4.4 shows the UV-vis absorption spectra of the doped and codoped samples as compared with undoped TiO_2 samples. Only boron doping shifts the onset of the absorption edge into the visible region (Eg = 2.22 eV), whereas other dopants (Al, Ga, and In) produce no red shift in the UV-vis spectra. Consequently, the band-gap energies of the doped and codoped TiO_2

samples nearly remained the same as that of pure TiO_2 (3.2 eV). Thus these metal doped/codoped TiO_2 samples could serve as UV-light-active photocatalysts. Again, UV-vis results show that dopants (B, Al, Ga , and In) in TiO_2 are homogenous and uniformly dispersed. This can be clearly seen in 1% Ga and/or In codoped TiO_2 samples, which exhibit neither a blue-shift nor a red-shifts. This indicates that there was no formation of bulk Ga_2O_3 and In_2O_3.

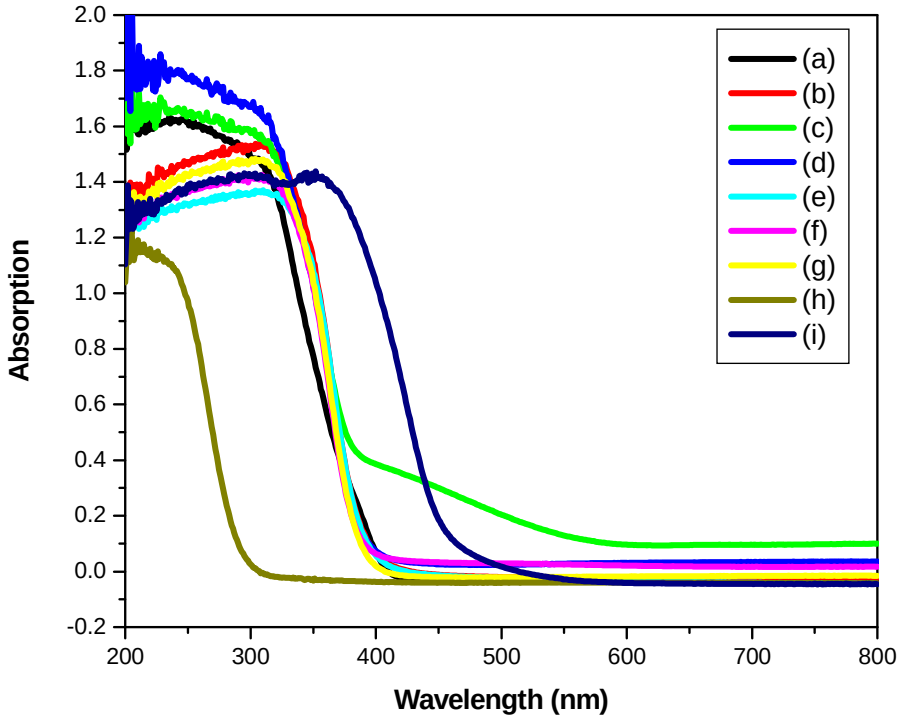

Figure 4.4 UV-visible optical absorption spectra of (a) TiO_2-P25, (b) TiO_2, (c) 1% B-TiO_2, (d) 1% Al-TiO_2, (e) 1% Ga-TiO_2, (f) 1% In-TiO_2, (g) 1% 1% (Ga, In)-TiO_2, (h) Ga_2O_3, and (i) In_2O_3

Table 4.1 shows the textural properties of the doped and undoped TiO_2 samples derived from N_2 adsorption-desorption isotherms. It is obvious that the aero-gel prepared samples exhibit high surface areas (100 – 133 m^2/g), high pore volumes (0.41 – 1.03 cc/g), and wide pore sizes (7.82 – 15.74 nm) as compared with a commercial standard, TiO_2-P25. These improved textural properties of nanosized anatase TiO_2 samples, both doped and undoped, are useful for photocatalysis.

Table 4.1 Specific surface areas, pore volumes and pore diameters of doped and undoped TiO_2 samples

Catalyst	Surface area (m^2/g)	Pore Volume (cc/g)	Pore Diameter (nm)
TiO_2-P25	51	0.14	2.3
TiO_2-AP	104	0.75	7.8
1% B-TiO_2	121	0.88	15
1% Al-TiO_2	117	0.79	10.6
1% Ga-TiO_2	103	0.41	9.6
1% In-TiO_2	133	0.86	12
1% (Ga, In)-TiO_2	132	1.03	15.7

4.3.2 Photocatalytic degradation of organic pollutants in air/water under UV light

Here, we have chosen some representative air/water pollutants in order to explore the photoactivities of aero-gel prepared doped and undoped TiO_2 samples. Figure 4.5 shows the evolution of carbon dioxide gas from acetaldehyde over various photocatalysts under UV light irradiation. The results indicate that all aero-gel prepared samples both doped and undoped TiO_2 samples exhibit higher activities than a commercial standard, TiO_2-P25. This proves that high-

surface areas are needed for enhanced photomineralization of air pollutant, such as acetaldehyde. Among the doped samples, 1% In-TiO_2 photocatalyst displays the highest rate of degradation/mineralization of acetaldehyde under UV light irradiation (Table 4.2); but is comparable to that of the aero-gel prepared undoped TiO_2. At least, acetaldehyde degradation/mineralization kinetic results support prove that improved textural properties, such as surface areas, pore volumes, and pore diameters, lead to an increased photocatalysis (Compare with TiO_2-P25).

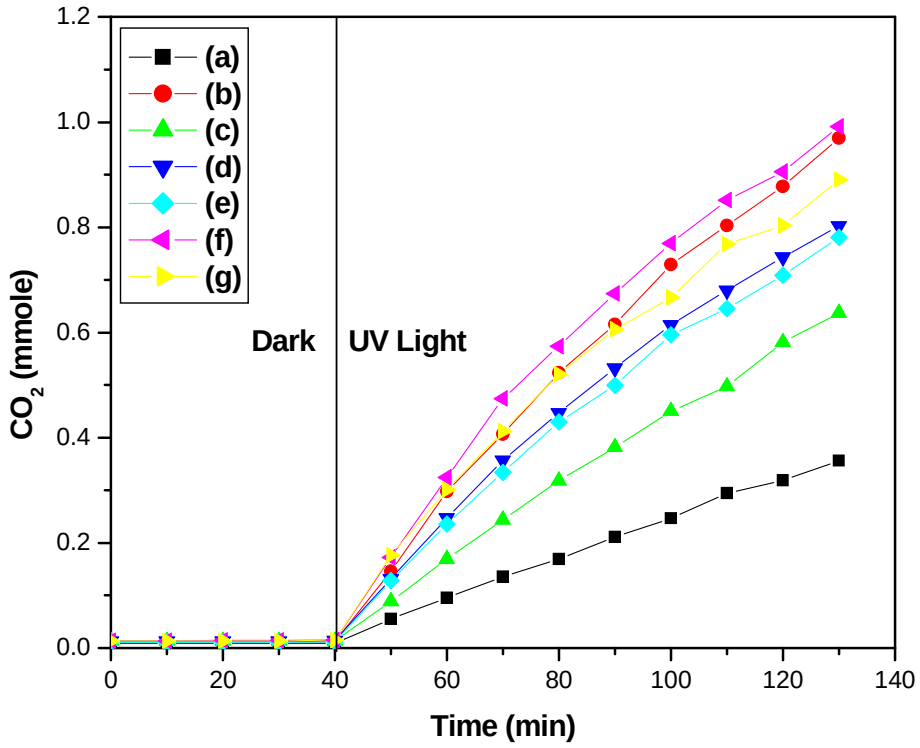

Figure 4.5 Evolution of CO_2 from CH_3CHO degradation over (a) TiO_2-P25, (b) TiO_2, (c) 1% B-TiO_2, (d) 1% Al-TiO_2, (e) 1% Ga-TiO_2, (f) 1% In-TiO_2, and (g) 1% (Ga, In)-TiO_2 photocatalysts under UV light irradiation

Table 4.2 Initial rate (mmole/min) of CH_3CHO degradation and CO_2 formation under UV light

Samples	CH_3CHO	CO_2
TiO_2-P25	5.0×10^{-3}	4.0×10^{-3}
TiO_2	21×10^{-3}	13×10^{-3}
1% B-TiO_2	14×10^{-3}	7.6×10^{-3}
1% Al-TiO_2	17×10^{-3}	11×10^{-3}
1% Ga-TiO_2	19×10^{-3}	10×10^{-3}
1% In-TiO_2	19×10^{-3}	14×10^{-3}
1% (Ga, In)-TiO_2	19×10^{-3}	13×10^{-3}

However, we are very interested to examine whether or not the codoping of two metals is effective for enhanced photocatalytic activity of pure TiO_2. It is well-known that activity of a photocatalyst depends upon the nature of the pollutants to be degraded. Here, the degradation of trichloroethylene is chosen as a probe reaction to compare the activities of three photocatalysts, codoped vs undoped. Again, for this reaction, the aero-gel prepared undoped TiO_2 exhibit the highest activity for photomineralization of trichloroethylene under UV light (Figure 4.6). However, high-surface area 1% (Ga, In)-TiO_2 samples still display an impressive activity as compared to low-surface area TiO_2-P25. Furthermore, UV-light-activity of 1% (Ga, In)-codoped TiO_2 system was tested for organic compounds with various functional groups (Figure 4.7). Here it was found that acetic acid and formaldehyde were degraded nearly to the same extent**;** but pyridine and benzene were least degraded. These results clearly prove that the activity of Ga and In codoped system depends upon the nature of the air pollutants. Table 4.3 summarizes the initial rate of degradation of various organic pollutants over 1% (Ga, In)-TiO_2 sample under UV light irradiation.

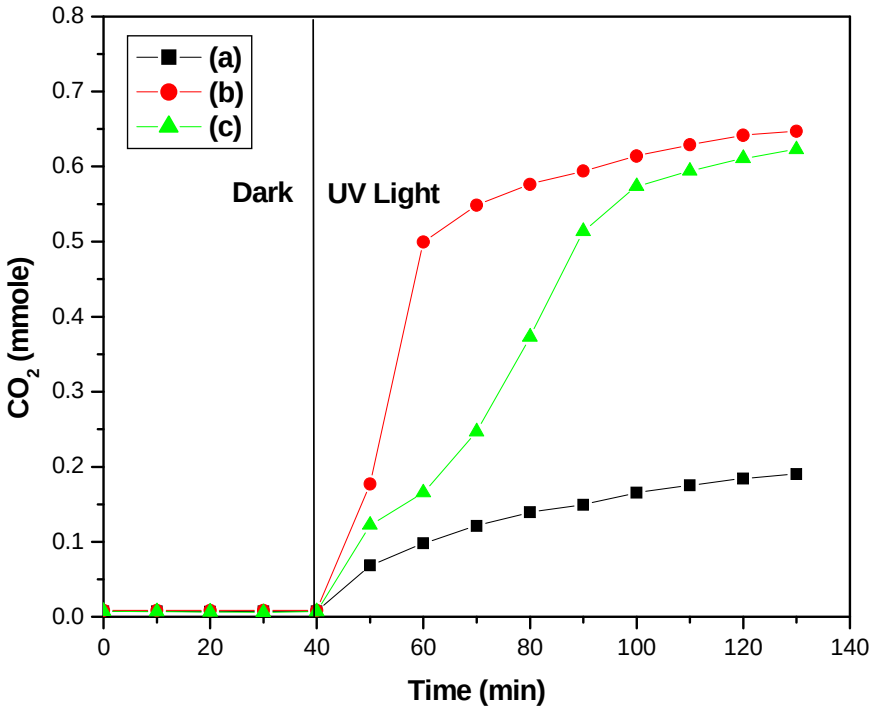

Figure 4.6 Evolution of CO_2 from $Cl_2C=CHCl$ degradation over (a) TiO_2-P25, (b) TiO_2, and (c) 1% (Ga, In)-TiO_2 photocatalysts under UV light

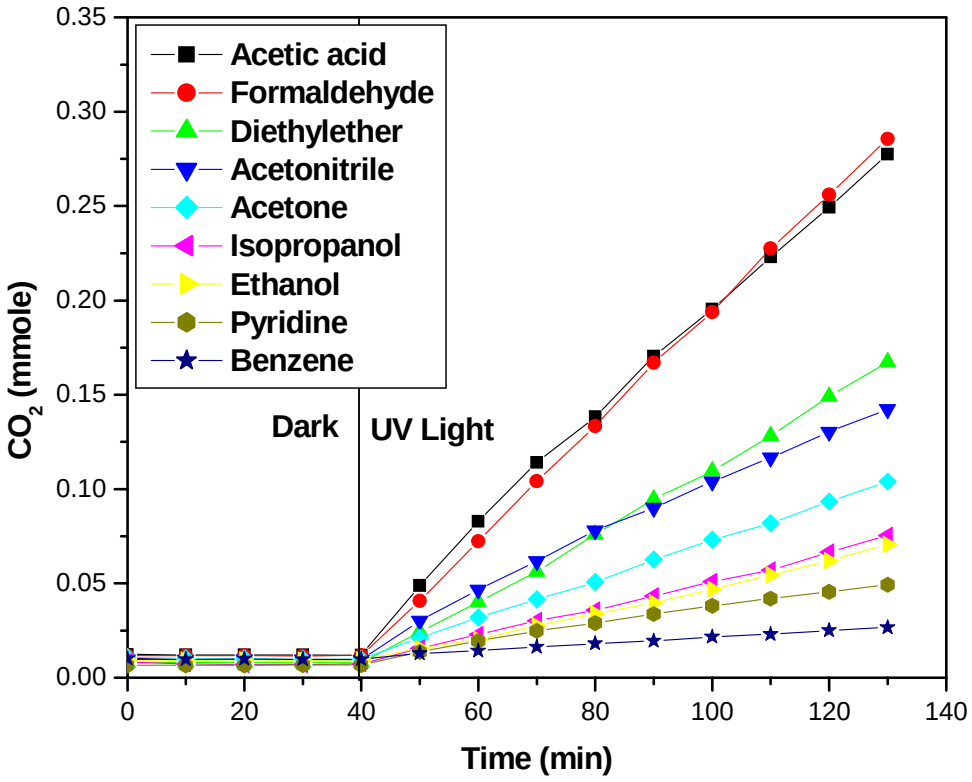

Figure 4.7 Evolution of CO_2 from organic compounds with various functional groups over 1% (Ga, In)-TiO_2 photocatalysts under UV light

Table 4.3 Initial rate (mmole/min) of mineralization of organic pollutants with various functional groups over 1% (Ga, In)-TiO_2 under UV light

Pollutant	CO_2
Acetaldehyde	13×10^{-3}
Trichoroethylene	8.6×10^{-3}
Acetic acid	3.1×10^{-3}
Formaldehyde	3.1×10^{-3}
Diethylether	1.7×10^{-3}
Acetonitrile	1.7×10^{-3}
Acetone	1.0×10^{-3} [4]
Isopropanol	7.2×10^{-4}
Ethanol	6.1×10^{-4}
Pyridine	5.6×10^{-4}
Benzene	2.0×10^{-4}

Now, it is obvious that for 1% (Ga, In)-TiO_2 photocatalyst system, the photoactivity seems to be a function of the nature of the substrates to be degraded or mineralized. Until now, we have examined only gas-phase heterogeneous photocatalysis over Ga and In-codped TiO_2 system. It is interesting to know whether or not this system display photoactivity in liquid-phase. For this purpose, we studied the photodegradation of methyl orange dye, which is stable under UV light irradiation (Figure 4.8a). However, the MO dye degrades almost completely in aqueous dispersion of TiO_2-P25 for 90 min UV light irradiation (Figure 4.8b), whereas it takes 135 min for complete degradation in 1% (Ga, In)-TiO_2 photocatalyst (Figure 4.8c). The value of the pseudo-first-order rate constant, k, indicates that the undoped TiO_2-P25 photocatalyt degrades the MO dye two time faster than the codoped photocatalyst, 1% (Ga, In)-TiO_2 (Figure 4.8d), which was active for acetaldehyde degradation more than three times (Table 4.1).

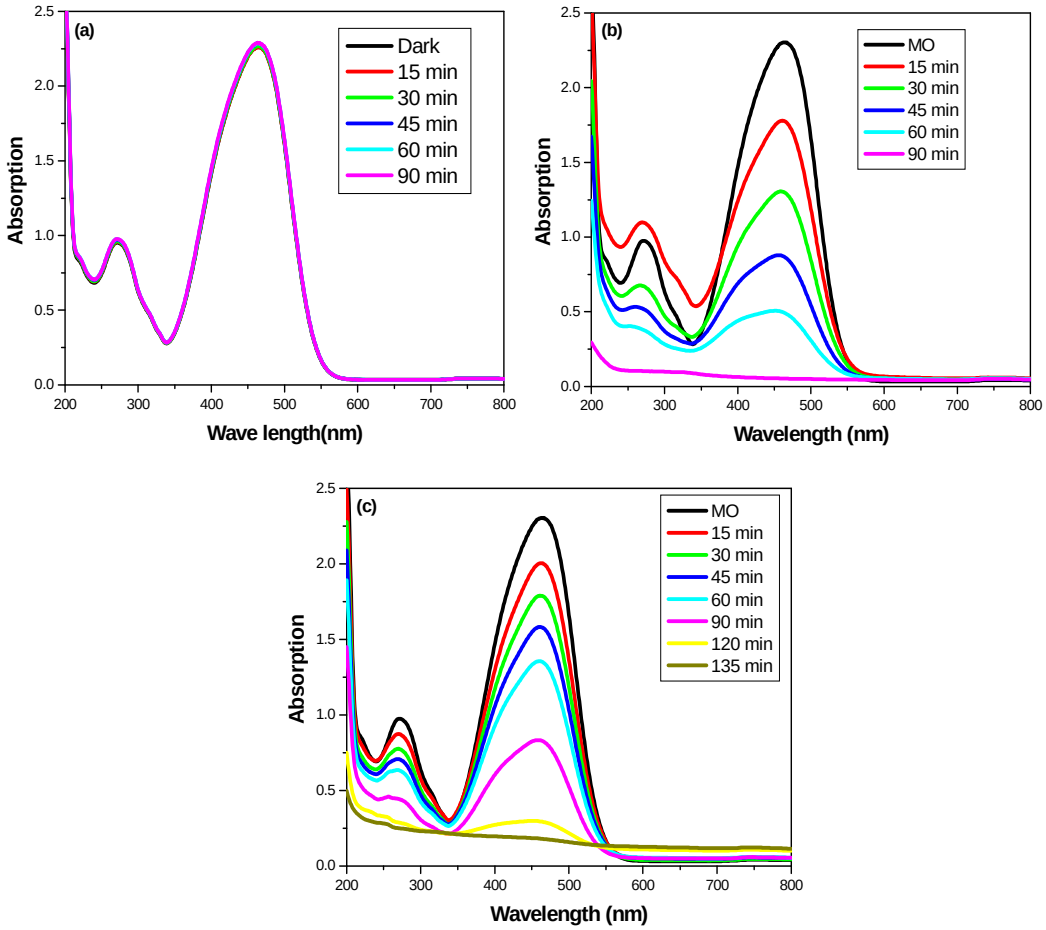

Figure 4.8 (a) Effect of UV light on UV-vis absorption of methyl orange dye (MO) in absence of a photocatalyst, (b) Effect of UV light + TiO_2-P25 on UV-vis of MO, and (c) Effect UV light + 1% (Ga, In)-TiO_2) (Initial concentration of dye = 1 x 10^{-4} M; photocatalyst = 0.15 g, total solution volume = 150 mL)

Finally, UV-light-induced heterogeneous photocatalysis results prove that the nature of the substrate and the medium of catalysis have important role in defining the activity of photocatalyst systems.

4.3.3 Photocatalytic oxidation of carbon monoxide under UV light and visible light

To this point, we observed that either aero-gel prepared undoped (TiO_2) or a commercial standard (TiO_2-P25) photocatalyst system outperformed the codoped photocatalyst system, 1% (Ga, In)-TiO_2. A question still remains unanswered as to why codoping is needed for enhancing photoactivity. To answer this question, we are interested to examine the photoactivities for CO oxidation reaction over various TiO_2 systems, both doped and undoped, under UV light illuminations. CO is the simplest inorganic compound of carbon, and its oxidation product is only CO_2. In addition, CO contains a very strong triple bond. Therefore, CO oxidation kinetics can provide useful information for future photocatalyst developments.

Figure 4.9 shows the evolution of CO_2 from CO over various photocatalyst systems under UV light irradiation. Under UV light irradiation, CO photodegradation is exceptionally triggered over 1% (Ga, In)-TiO_2 sample compared with single metal-doped and undoped TiO_2 samples. It is important to note that 1% In-TiO_2 sample is the most active for CO oxidation to CO_2, and 1% Al-TiO_2 sample is the least active. Table 4.4 shows the initial rate of CO_2 production from CO under UV-induced-photocatalysis. On the basis of initial rates for CO_2 production, we observed that 1% (Ga, In)-TiO_2 photocatalyst is 4.5, 3.4 and 2 times more active than pure TiO_2, TiO_2-P25 and 1% In-TiO_2 samples, respectively. Moreover, the results shown in Figure 4.10 prove that 1% (Ga, In)-TiO_2 sample is reproducible, photostable and sensitive to CO environment.

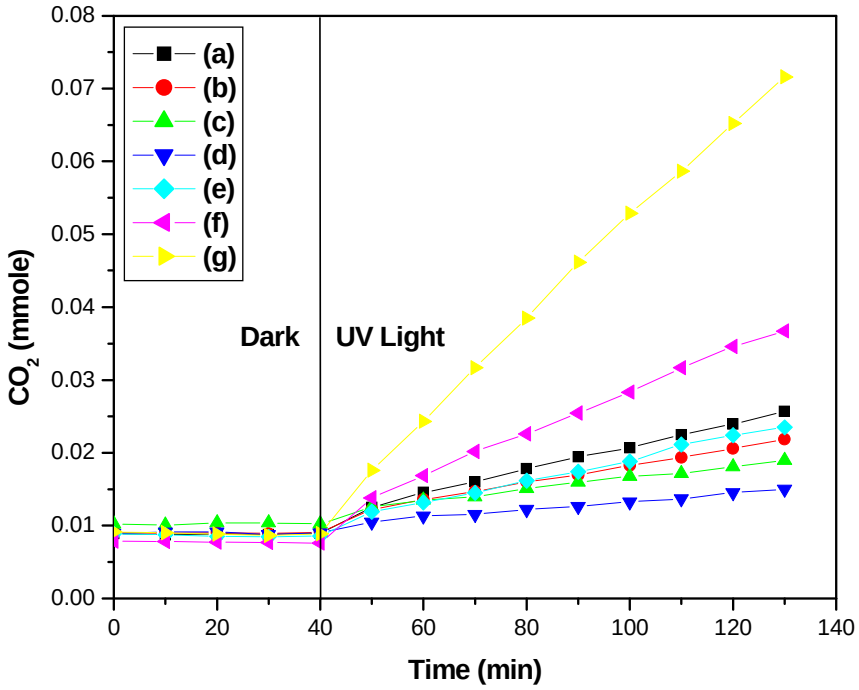

Figure 4.9 Evolution of CO_2 from CO oxidation under UV light over (a) TiO_2-P25, (b) TiO_2, (c) 1% B-TiO_2, (d) 1% Al-TiO_2, (e) 1% Ga-TiO_2, (f) 1% In-TiO_2, and (g) 1% (Ga, In)-TiO_2

Table 4.4 Initial rate (mmole/min) of CO_2 production from CO oxidation over various photocatalysts under UV light

Sample	CO_2
TiO_2-P25	2.1×10^{-4}
TiO_2	1.6×10^{-4}
1% B-TiO_2	1.1×10^{-4}
1% Al-TiO_2	7.5×10^{-5}
1% Ga-TiO_2	1.8×10^{-4}
1% In-TiO_2	3.6×10^{-4}
1% (Ga, In)-TiO_2	7.3×10^{-4}

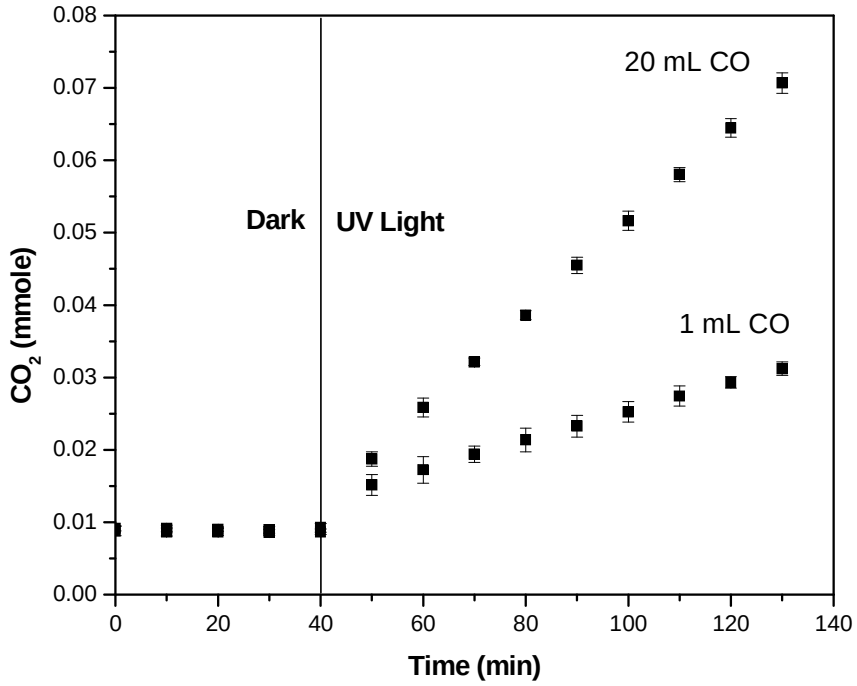

Figure 4.10 Reproducibility, photostability, and sensitivity test for 1% (Ga, In)-TiO_2 photocatalyst for CO_2 evolution from CO oxidation under UV light

Although 1% (Ga, In)-TiO_2 photocatalyst system exhibits commendable activity for CO oxidation under UV light, it does not work under visible light for the same reaction. To enhance its activity both in UV and visible light, codoping of platinum was carried out. X-ray powder diffraction patterns analysis shows that 0.1% platinum codoped 1% (Ga, In)-TiO_2 system has only anatase TiO_2 with small crystallite sizes < 11 nm (Figure 4.11).

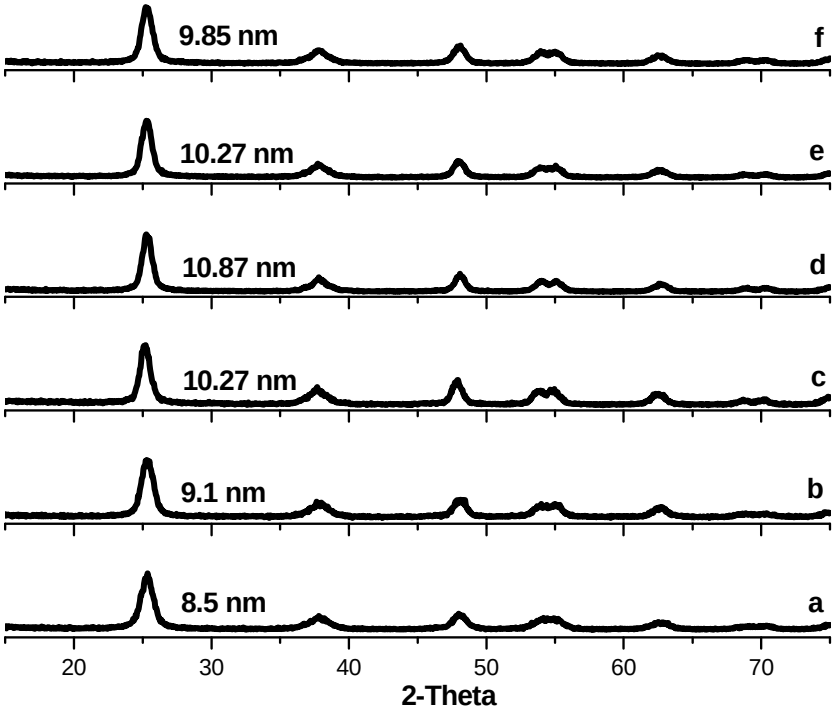

Figure 4.11 Power X-ray diffraction patterns of (a) TiO_2, (b) 1% (Ga, In)-TiO_2, (c) 0.1% Pt/TiO_2, (d) 0.1% Pt/Ga-TiO_2, (e) 0.1% Pt/In-TiO_2, and (f) 0.1% Pt/(Ga, In)-TiO_2

This X-ray observation is further confirmed by the TEM analysis (Figure 4.12). The UV-visible diffuse reflectance measurement shows that platinum codoping does not shift the onset of the band edge of TiO_2 photocatalyst in visible region, but displays increased absorption plateaus at wavelength, $\lambda > 400$ nm (Figure 4.13). The BET measurements show that platinum doped/codoped TiO_2 samples have high surface area, high pore volumes and mesopores, which are advantageous for photocatalytic applications (Table 4.5).

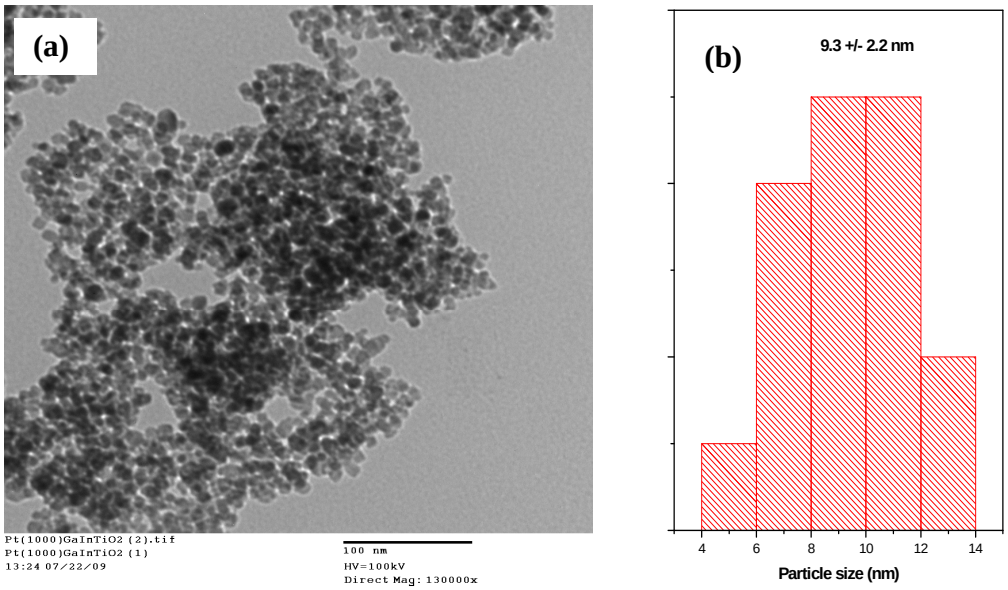

Figure 4.12 (a) TEM image and (b) particle size distribution of 0.1% Pt/(Ga, In)-TiO_2 sample

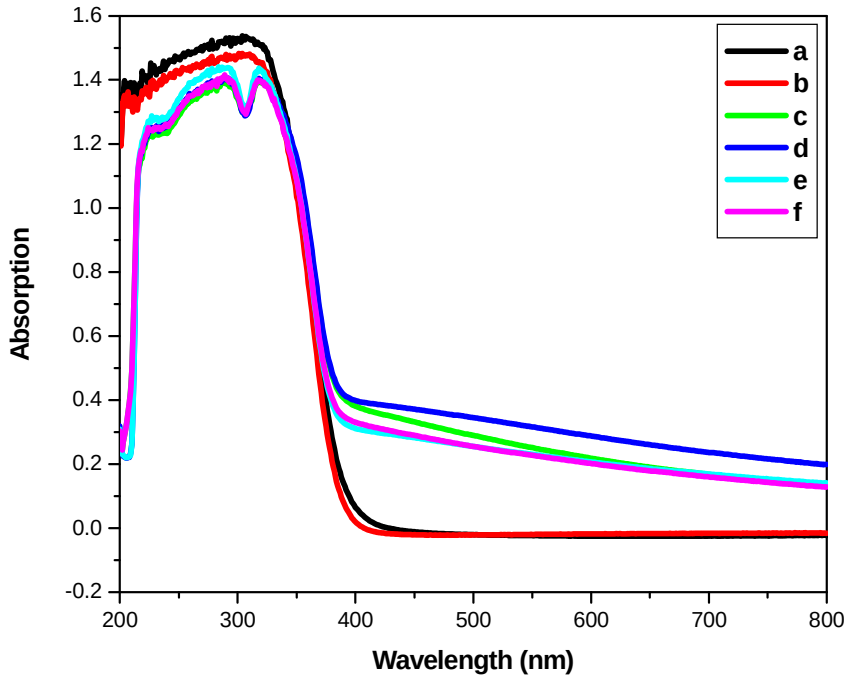

Figure 4.13 UV-visible optical absorption spectra of (a) TiO2, (b) 1% (Ga, In)-TiO_2, (c) 0.1% Pt/TiO_2, (d) 0.1% Pt/Ga-TiO_2, (e) 0.1% Pt/In-TiO_2, and (f) 0.1% Pt/(Ga, In)-TiO_2

Table 4.5 Specific surface areas, pore volumes and pore diameters of TiO_2 samples doped with Pt, Ga, and In

Sample	Surface area (m^2/g)	Pore volume (cc/g)	Pore diameter (nm)
0.1% Pt/TiO_2	111	0.54	9.67
0.1% Pt/$GaTiO_2$	110	0.21	9.64
0.1% Pt/$InTiO_2$	142	0.66	20.9
0.01% Pt/(Ga, In)-TiO_2	111	0.65	12
0.1% Pt/(Ga, In)-TiO_2	132	0.69	12.2
1% Pt/(Ga, In)-TiO_2	130	0.71	15.7

Figure 4.14 depicts that 0.1% Pt/(Ga, In)-TiO_2 sample exhibits enhanced activity for CO oxidation under both UV and visible light irradiations, with a prominent dark activity. Even though 0.1% Pt/In-TiO_2 sample is visible light active for CO oxidation in the initial stage of light activation, it deactivates after 30 min visible light irradiation. From the results, it appears that Ga is necessary for sustained activity of 0.1% Pt/(Ga, In)-TiO_2 system. The long-run experiment confirmed that the 0.1% Pt/(Ga, In)-TiO_2 system is photostable for prolonged time (50h) of visible light irradiation (Figure 4.15a) only if a fresh amount of CO is injected into the reactor. Thermodynamically, CO photooxidation reaction appears to be reversible one. However, the equilibrium seemed to shift the product side if UV light is irradiated for 6h (Figure 4.15b). This observation implies that CO oxidation would proceed faster if CO_2 is removed from the reactor.

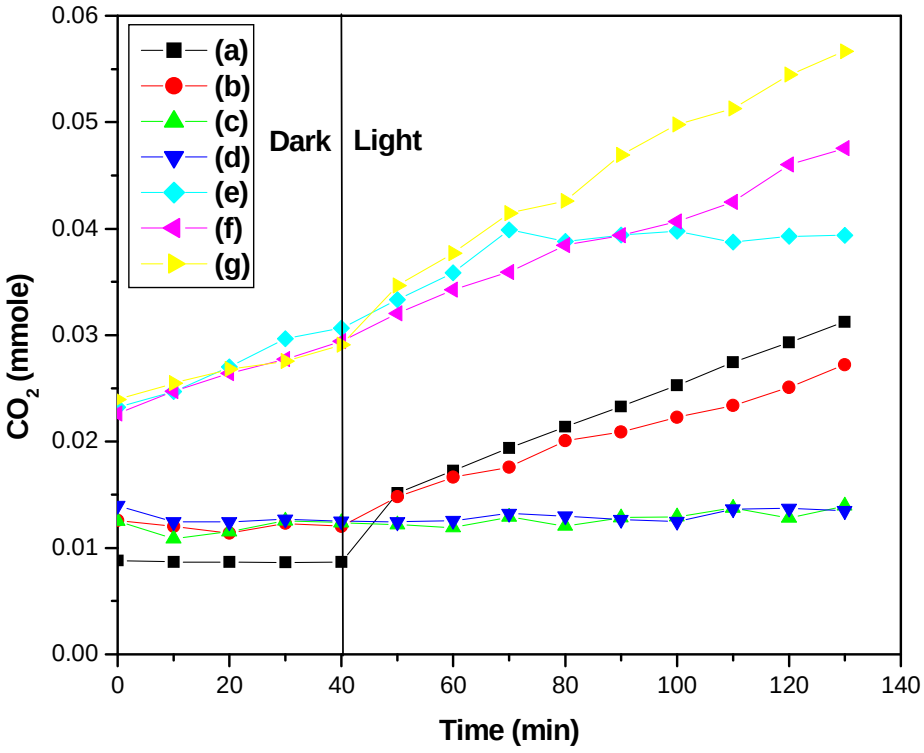

Figure 4.14 Evolution of CO_2 from CO oxidation over (a) 1% (Ga, In)-TiO_2 + UV light, (b) 0.1% Pt-TiO_2 + UV light, (c) 0.1% Pt-TiO_2 + Visible light, (d) 0.1% Pt/Ga-TiO_2 + Visible light, (e) 0.1% Pt/In-TiO_2 + Visible light, (f) 0.1% Pt/(Ga, In)-TiO_2 + Visible light, and (g) 0.1% Pt/(Ga, In)-TiO_2 + UV light (Initial amount of CO = 1 mL)

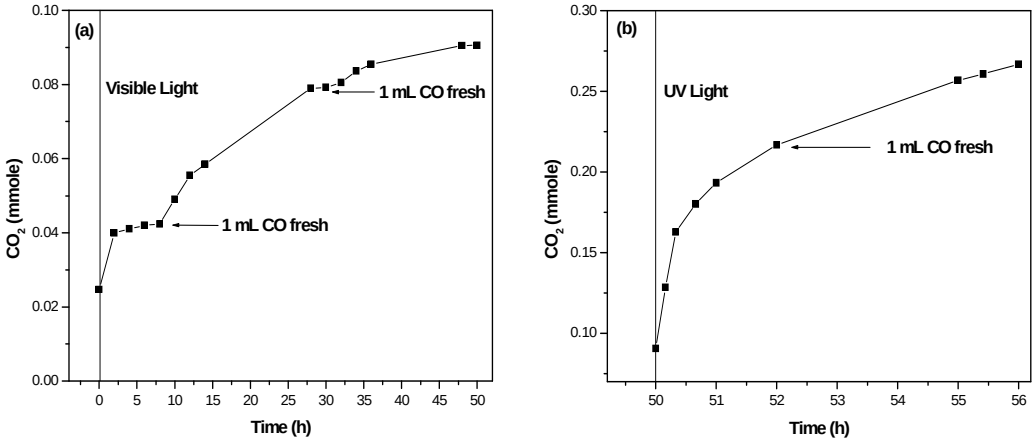

Figure 4.15 Long-run test for CO_2 from CO oxidation over 0.1% Pt/(Ga, In)-TiO_2 Photocatalyst under (a) Visible light and (b) UV light irradiation

What could be plausible explanations for visible-light-induced photocatalysis, especially for CO oxidation? Stoichiometrically, CO needs just one O atom to be oxidized; the reduction and dissociation of molecular oxygen at room temperature is not as easy as one can expect. Particularly for this reaction, adsorption and dissociation of O_2 onto active surface sites of a photocatalyst seem to be indispensable for CO oxidation. The active surface sites could be the formation of oxygen vacancies,[25] presumably by codoping of Ga[26] and In[27] into TiO_2. Understandably, when a trivalent metal ion is doped into TiO_2, oxygen vacancies are likely to be formed in order to maintain the charge neutrality onto the surface or in the bulk of TiO_2 (O- T^{4+} - O + M^{3+} = O- Ti^{3+} - M^{3+} + V_O). The formation of oxygen vacancy depends upon the size of ionic radii. The ionic radii of In^{3+}, Ga^{3+}, and Ti^{4+} ion are 0.86 nm, 0.08 nm, 0.062 nm, and 0.061 nm, respectively. Conceptually, codoping of platinum, indium and gallium produce more V_O

(oxygen vacancy) sites, where the dissociation of O_2 molecules is favored. Also note that Ti^{3+} species act as strong reducing agent. If this happens, adsorbed CO molecules interact with dissociated O atoms to form CO_2 product. Even for dilute amount of CO, carbon dioxide formation triggers if dopants possesses CO gas sensitivities and selectivities. Logically, Ga and In dopants have the abilities to accomplish these criteria to some extent.[5-7] To support these logical explanations, XPS measurements for selected samples were carried out.

The core level XPS analysis revealed that the oxidation states of Ti, O, Ga, and In in 1% (Ga, In)-TiO_2 sample + 4, - 2, + 3, and + 3, respectively (Figure 4.16). The observed binding energy values for $Ti2p_{3/2}$, O1s, $Ga2p_{3/2}$, and $In3d_{5/2}$ are a bit higher than the reported values.[28-32] This indicates that dopants experience strong interactions with each other. In the case of indium, two additional peaks appeared at 447.8 and 449.9 eV. The appearance of these two peaks implies that indium could have a mixed valence state: In^{2+} and In^{3+}. For $Pt4f_{7/2}$, the core level XPS analysis shows that platinum in 0.1% Pt/ (Ga, In) before and after CO oxidation is present as Pt^{4+} (Figure 4.17). This value is somewhat higher than the reported value.[33]

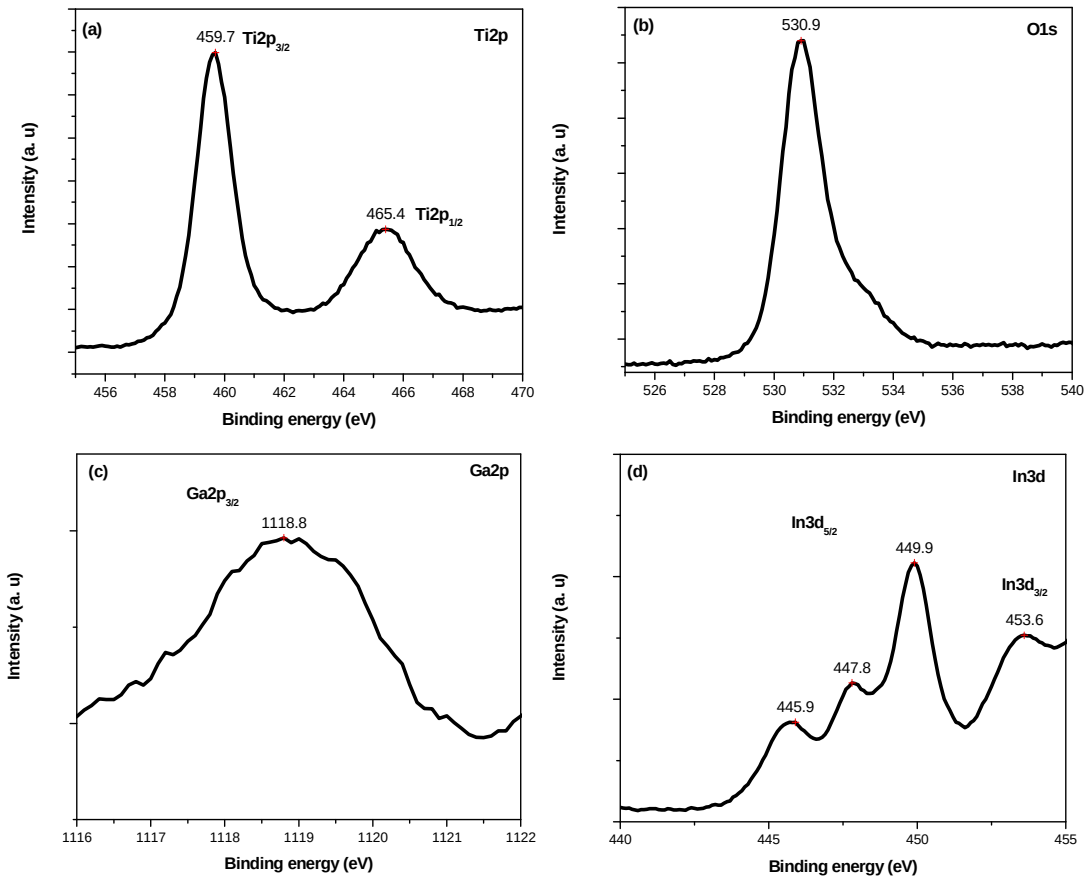

Figure 4.16 XPS core level spectra of (a) Ti, (b) O, (c) Ga, and (d) In present in 1% (Ga, In)-TiO_2 sample

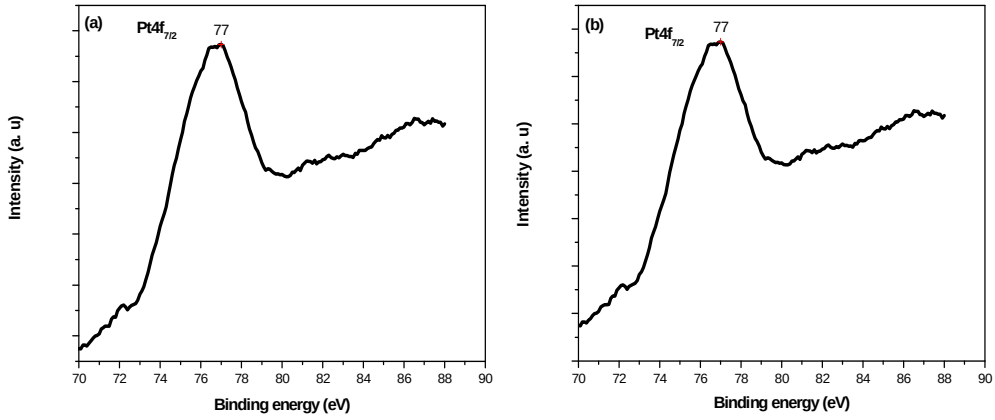

Figure 4.17 Pt4f7 core level XPS spectra of 0.1% Pt/ (Ga, In)-TiO_2 sample (a) before and (b) after CO oxidation reaction under visible light

Based on the above results and discussion, we believe that in 0.1% Pt/(Ga, In)-TiO_2 system, codoping of Ga and In induces oxygen vacancies as sites for the dissociation of molecular oxygen, and the codoped platinum species acts as sites for CO adsorption[22] as well as electron-hole trap.[34] As a consequence, CO photooxidation was enhanced over 0.1% Pt/(Ga, In)-TiO_2 system. However, future works are necessary to add detail for enhanced photocatalytic oxidation of CO over nanosized anatase TiO_2 photocatalyst codoped with gallium, indium, and platinum.

4.4 Conclusions

Metal(s)-doped or codoped anatase TiO_2 nanoparticle photocatalysts with small crystallite sizes (> 11 nm), high surface areas (> 100 m^2/g), high pore volumes (> 0.41 cc/g), and average pore diameters (> 7.82 nm) were synthesized by the aero-gel method and characterized by various spectroscopic techniques. Except boron, doping/codoping of metals (Al, Ga, In) has no effect on the optical absorption and the band-gap of TiO_2 host. The photocatalytic studies reveal that activities of these nanomaterials were found to be substrate dependent. At least for acetaldehyde degradation, all single metal-doped TiO_2 photocatalysts have higher photodegradation and photomineralization abilities than TiO_2-P25, but comparable to that of the pure anatase TiO_2. Very interestingly, among the dopants studied, indium demonstrated very impressive enhancement effects both in textural and photocatalytic properties. Moreover, codoping of gallium and indium into TiO_2 resulted in an outstanding performance in the CO oxidation reaction under UV light. More importantly, codoping of platinum into In-TiO_2 and (Ga, In)-TiO_2 induced exceptional photostabilities and UV-visible-light-activities at least for CO photooxidation reaction. Moreover, Pt/(Ga, In)-TiO_2 photocatalyst system could have promise for hydrogen production from water-gas shift reaction ($CO + H_2O = H_2 + CO_2$). Future works are needed to explore these possibilities. Overall, the current findings suggest that the photocatalytic properties of the pristine TiO_2 can be enhanced by codoping of an appropriate combination of nontoxic metals.

4.5 References

1. Su, F. Z.; Liu, Y. M.; Wang, L. C.; Cao, Y.; He, H. Y.; Fan, K. Nian., *Angew. Chem. Int. Ed.* **2008**, 47, 334-337.

2. Collins, S. E.; Baltanas, M. A.; Bonivardi, A.L., *Appl. Catal. A: General* **2005**, 295, 126-133.

3. Gebauer-Henke, E.; Farbotko, J.; Touroude, R.; Rynkowski, J., *Kinet. Catal*. **2008**, 49, 574-580.

4. Dominguez, F.; Carruyo, G.; Andrade, R.; Solano, R.; Rodriguez, D.; Sanchez, J.; Arteaga, G., *Catal. Lett.* **2008**, 123, 207-212.

5. Choi, Y. Jin; Seeley, Z.; Bandyopadhyay, A.; Bose, S.; Akbar, S. A., *Sensors and Actuators, B: Chemical* **2007**, B124, 111-117.

6. Schwebel, T.; Fleischer, M.; Meixner, H.; Kohl, C. D., *Sensors and Actuators, B: Chemical* **1998**, B49, 46-51.

7. Epifani, M.; Comini, E.; Arbiol, J.; Diaz, R.; Sergent, N.; Pagnier, T.; Siciliano, P.; Faglia, G.; Morante, J. R., *Sensors and Actuators, B: Chemical* **2008**, B130, 483-487.

8. Park, S. H; Lee, S. C.; Kang, M.; Choung, S. J., *J. Ind. Eng. Chem.* **2004**, 10, 972-981.

9. Zhou, J.; Zhang, Y.; Zhao, X. S.; Ray, A. K., *Ind. Eng. Chem. Res.* **2006**, 45, 3503-3511.

10. Rodriguez-Gonzalez, V.; Moreno-Rodriguez, A.; May, M.; Tzompantzi, F.; Gomez, R., *J. Photochem. Photobio. A: Chem*. **2008**, 193, 266-270.

11. Ladebeck, J. R. and Wagner, J. P., *Handbook of Fuel Cells – Fundamentals, Technology and Applications;* **2003**, Volume 3, Part 2, pp 190–201, John Wiley & Sons, Ltd, Chichester

12. Ruettinger, W.; Ilinich, O.; Farrauto, R. J., *J. Power Sources* **2003,** 118, 61-65.

13. Hutchings, G. J.; Hall, M. S.; Carley, A. F.; Landon, P.; Solsona, B. E.; Kiely, C. J.; Herzing, A.; Makkee, M.; Moulijn, J. A.; Overweg, A.; Fierro-Gonzalez, J. C.; Guzman, J.; Gates, B. C. *J. Catal.* **2006**, 242, 71-81.

14. Zhu, H.; Liang, C.; Yan, W.; Overbury, S. H.; Dai, S., *J. Phys. Chem. B* **2006**, 110, 10842-10848.

15. Zhong, Z.; Lin, J.; Teh, S. P.; Teo, J.; Dautzenberg, F. M., *Adv. Funct. Mater*. **2007**, 17, 1402-1408.

16. Denkwitz, Y.; Geserick, J.; Hoermann, U.; Plzak, V.; Kaiser, U.; Huesing, N.; Behm, R., J. *Catal. Lett*. **2007**, 119, 199-208.

17. Bourane, A.; Bianchi, D., *J. Catal*. **2003**, 220, 3-12.

18. Bourane, A.; Bianchi, D., *J. Catal*. **200**4, 222, 499-510.

19. Alexeev, O. S.; Chin, S. Y.; Engelhard, M. H.; Ortiz-Soto, L.; Amiridis, M. D., *J. Phys. Chem. B* **2005**, 109, 23430-23443.

20. Narkhede, V. V.; De Toni, A.; Narkhede, V. S.; Reichinger, M.; Birkner, A.; Hans-Niemantsverdriet, J. W.; Gruenert, W.; Gies, H., *J. Materi Sci.* **2009**, 44, 6701-6709.

21. Hwang, S.; Lee, M. C.; Choi, W., *Appl. Catal. B: Environ.* **2003**, 46, 49-63.

22. Einaga, H.; Harada, M.; Futamura, S.; Ibusuki, T., *J. Phys. Chem. B* **2003**, 107, 9290-9297.

23. Zhang, M.; Jin, Z.; Zhang, J.; Zhang, Z.; Dang, H., *J. Mol. Catal. A: Chem*. **2005**, 225, 59-63.

24. Li, Q.; Wang, K.; Zhang, S.; Zhang, M.; Yang, J.; Jin, Z., *J. Mol. Catal. A: Chem*. 2006, 258, 83-88.

25. Kim, H. Y.; Lee, H. M.; Pala, R. G. S.; Shapovalov, V.; Metiu, H., *J. Phys. Chem. C* **2008,** 112, 12398-12408.

26. Okajima, T.; Yamamoto, T.; Kunisu, M.; Yoshioka, S.; Tanaka, I.; Umesaki, N., *J. Appl. Phys. Part 1* **2006**, 45, 7028-7031.

27. Neri, G.; Bonavita, A.; Micali, G.; Rizzo, G.; Pinna, N.; Niederberger, M., *Sensors and Actuators, B: Chem.* **2007**, 27, 455-462.

28. Ohno, T; Mitsui, T; Matsumura, M., *Chem. Lett.* **2003**, 32, 364-365.

29. Li, Di; Haneda, H; Labhsetwar, N. K; Hishita, S; Ohashi, N., *Chem. Phys. Lett.* **2005**, 401, 579-584.

30. Hong, X; Wang, Z; Cai, W; Lu, F; Zhang, J; Yang, Y; Ma, N; Liu, Y., *Chem. Mater.* **2005**, 17, 1548-1552.

31. Schoen, G., *J. Electron Spectrosc. Relat. Phenom.* **1973**, 2, 75

32. Cahen, D., Ireland, P.J., Kazmerski, L.L., Thiel, F.A., *J. Appl. Phys*. **1985**, 57, 4761

33. Mouvier G., Hoogewijs M., Leclere C., *J. Catal.* **1977**, 48, 217

34. Kim, S.; Hwang, S. J.; Choi, W., *J. Phys. Chem. B* **2005**, 109, 24260-24267

CHAPTER 5 - A Multifunctional Biocide/Sporocide and Photocatalyst Based on Titanium Dioxide (TiO_2) Codoped with Silver, Carbon, and Sulfur

5.1 Introduction

There is an urgent need for the design and development of eco-friendly and cost-effective antibacterial and antiviral nanomaterials to counteract dangerous pathogens. Of the materials so far studied, TiO_2 remains as an excellent starting material for academic and industrial purposes due to its stability, non-toxicity, low-cost and commendable UV light photoactivity. Furthermore, discoveries in the past decades demonstrated that UV light excited TiO_2 particles exhibited potent killing ability for pathogens.[1-3] These results indicate that photocatalytic sterilization with TiO_2 is due to the generation and the reaction of photoinduced excitons (e^- + h^+) with adsorbed O_2 and H_2O to form O_2^- ions, $^{\cdot}OH$ radicals and H_2O_2 molecules, which oxidize the complex proteins and inhibit the enzymatic functions of the bacterial cells, thereby leading to ultimate cell death.

Recently, several authors reported strong inhibitory and antimicrobial abilities of silver nanoparticles[4-8] and silver ions,[9-11] (for example against *Escherichia coli* and *Staphylococcus aureus*) without the presence of TiO_2. It is clear that silver ions are antibacterial species and the controlled release rate of silver ions from the active surface sites of the silver nanoparticles is a key mechanistic factor. Besides silver nanoparticles and silver ions, studies on silver doped TiO_2 systems also demonstrated the destruction of pathogenic bacteria [12-17] and spores [18] by exploiting

the biocidal dexterity of silver and UV excited TiO_2 photocatalysis together. These works motivated several researchers to prepare proficient visible–light-driven photoactive biocides such as S-TiO_2,[19] N-TiO_2,[20] C-TiON,[21] AgI-TiO_2,[22] AgBr-TiO_2,[23] Ag-AgBr-TiO_2[24] and Apatite-Coated Ag-AgBr-TiO_2.[25] These literature results uncovered that the enhanced photocatalytic destruction of both Gram-positive and Gram-negative pathogens with the doped photoactive TiO_2, stemmed from an interplay of the reactive oxygen species with the proteinaceous compounds of the cell wall and cell membrane. Regrettably, these systems are not active in the dark. Previously, we reported the influence of silver doping on the visible light activity of sulfur and carbon-codoped TiO_2 nanoparticle photocatalysts for photooxidation of organic air pollutants.[26] However, to the best of our knowledge, there has been no report on the influence of silver doping on biocidal-sporocidal activities of carbon and sulfur codoped TiO_2 nanoparticles. Therefore, herein we report on Ag/(C, S)-TiO_2 nanoparticles, and their promise as an effective photocatalyst in visible light for degrading air pollutants, and as an effective biocide/sporocide in the dark, and compare our findings with commercially available, universally accredited P25-TiO_2 reference sample.

5.2 Experimental Section

5.2.1 Chemicals and Biocidal Cultures

Degussa P25 TiO_2 was purchased from Degussa. Titanium (IV) isopropoxide (97% Sigma-Aldrich), Ammonium thiocyanate (97.5% Alfa Aesar), silver nitrate (99.9+%, Alfa Aesar), Ethanol (Absolute, 200 Proof, Aaper Alcohol and Chemical Co.), and ammonium hydroxide (29.9%, Fisher) were used as received. *Escherichia coli* strain C3000 was obtained from ATCC. *Bacillus subtilis* spores ATCC6633 were purchased from Raven Biological Labs. *E. coli* was grown in tryptic soy broth before the experiment, while the *B. subtilis* spore suspension was used as received.

5.2.2 Ag/(C, S)-TiO_2 sample preparation

Typically, 0.124 moles (9.44 g) of NH_4SCN were dissolved in 200 mL of C_2H_5OH, and 0.031 moles (8.5 g) of $Ti[OCH(CH_3)_2]_4$ were added under vigorous stirring. A desired amount of $AgNO_3$ (Ag = 0, 0.5, 1, 2, 10, and 20 mol %) was dissolved in 0.125 moles (2.25 g) of deionized water and one mL (0.0148 moles) of NH_4OH solution. This mixture was added drop-wise into the titanium isopropoxide-ammonium thiocyanate solution, stirred for 5 min at room temperature; the solvent was then removed in a rotavapor. The samples were dried overnight, annealed at 500°C/2h in air.

5.2.3 TEM sample preparation

The control and nanoparticle-treated cells were immersion fixed with 2 % glutaraldehyde overnight. The samples were then washed with sodium cacodylate buffer and post-fixed with a 1 % osmium tetraoxide solution for 1.5 hrs and washed again. The samples were then gradually dehydrated with increasing concentrations of acetone and later embedded in resin. The samples were placed in an oven overnight and later cut with a microtome diamond knife and viewed in the electron microscope. The TEM images were recorded on a Philips CM 100, operating at 100kV.

5.2.4 Sample Characterization

Scanning Electron Microscope (S-3500N) and adsorbed Electron Detector (S-6542) (Hitachi Science Systems, Ltd.) were used to measure the EDX spectrum and to determine the surface composition of the annealed samples under conditions of 20 keV and 4000x magnification. Nitrogen adsorption-desorption isotherms of TiO_2–P25 and Ag/(C, S)-TiO_2 (Ag = 0, 0.5, 1, 2, 10 and 20 mol %) were recorded at 77 K on a NOVA-1200 Instrument from Quantachrome Corporation. The Brunnauer-Emmett-Teller (BET) and Barrett-Joyner-Halenda (BJH) methods were used to determine the specific surface area, pore-volume and pore-diameter of samples. Nicolet NEXUS 670 FTIR was used to record transmittance IR spectra of samples by pelletizing with KBr as reference. XRD patterns were measured by means of a Scintag XDS 2000 (D8) diffractometer with Cu Kα monochromatic radiation of 0.15406 nm wavelength. The Scherrer equation, $t = 0.89\lambda/\beta Cos\theta$, was used to estimate the mean crystallite size. Cary 500 Scan UV-vis

NIR spectrometer was used to measure the UV-visible diffuse reflectance spectra of samples from 800 nm to 200 nm using PTFE reference.

5.2.5 Photoactivity Test

100µL of liquid acetaldehyde was placed in a 305 mL cylindrical air-filled static glass reactor containing 0.1025 g sample placed in a circular disc, mounted into the reactor. After 40 min stirring in the dark and before UV or visible light illumination, 35 µL of gaseous mixture from the reactor was extracted and analyzed by a Shimadzu GCMS QP500. UV and visible light photocatalytic tests were performed using two separated cut-off filters, one $320 < \lambda < 400$ nm and another $\lambda > 420$ nm, respectively. The amount of carbon dioxide evolved from acetaldehyde photodegradation was determined.

5.2.6 Biocidal Test

Vegetative cells and spores were diluted in Millipore water to between 10^4 and 10^9 CFU/mL. 50 mg each of the Ag/(C, S)-TiO_2 was added to 2 mL of bacteria or spore solution in a sterile test tube, vortexed and aged for 5 or 30 minutes. The samples were then centrifuged at 2500 rpm at 4°C for about 2 minutes and three aliquots of 100 µL were extracted from each supernatant and plated on Petri dishes, containing nutrient agar. The agar plates were incubated for 24 hrs at 37°C, the colonies formed were counted and log reduction values calculated (Log Reduction = Log_{10} (c_0/c), where c_0 = initial concentration of cells/spores used for the experiment, and c = concentration of cells/spores after treatment with metal oxides at measured time). The counts on

the three plates were averaged. The experiment was performed at least two times. The standard log deviations for all samples were less than ±0.5.

5.2.7 X-ray photoelectron spectroscopy (XPS) measurement

X-ray photoelectron spectroscopy (XPS) data were recorded with a Perkin–Elmer PHI 5400 electron spectrometer using acrochromatic AlKα radiation (1486.6 eV). All spectra were obtained under vacuum at a pressure of about 3.0×10^{-8} Torr. The XPS binding energies were measured with a precision of 0.1 eV. The analyzer pass energy was set to 17.9 eV, and the contact time was 50 ms.

5.3 Results and Discussion

We synthesized Ag/(C, S)-TiO_2 nanoparticles following an earlier procedure[26] which involves silver loadings of 0, 0.5, 1, 2, 10 and 20 mole%. In addition to silver, EDX measurements showed the presence of carbon and sulfur as dopants in the TiO_2 (Figure 5.1 and Table 5.1). However, we observed that the amount of silver determined from the EDX is far less than that of the initial silver loading, implying that only a small fraction of the doped silver remained on the surface, and the rest of it could have occupied the titania lattice space.

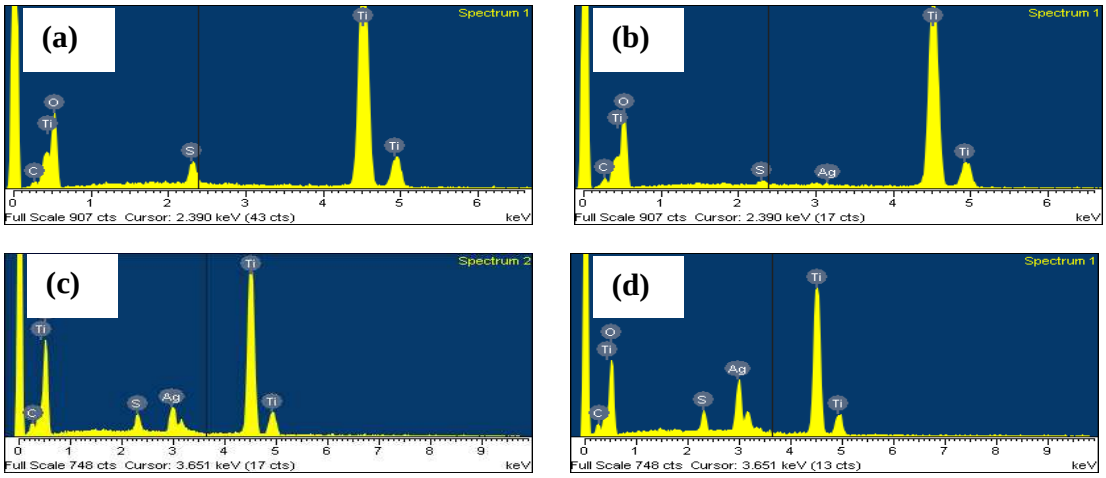

Figure 5.1 EDX spectrum of Ag/(C, S)-TiO_2 sample with initial silver doping (a) 0, (b) 1, (c) 10 and (d) 20 mol%

Table 5.1 Amount of carbon and sulfur codoped with silver in TiO_2 samples after heat treatment at 500 °C for 2h in air

Initial Ag^+ loading (mol %)	Ag (at. %)	C (at. %)	S (at. %)
0	0	4.8	1.8
1	0.30	5.8	1.6
10	1.76	10	1.4
20	3.57	9.9	1.7

The N_2 adsorption-desorption isotherms indicated that all the doped samples have mesoporous structures with BET specific surface areas in the range of 35-92 m^2/g (Fig.5.2 and Table 5.2).

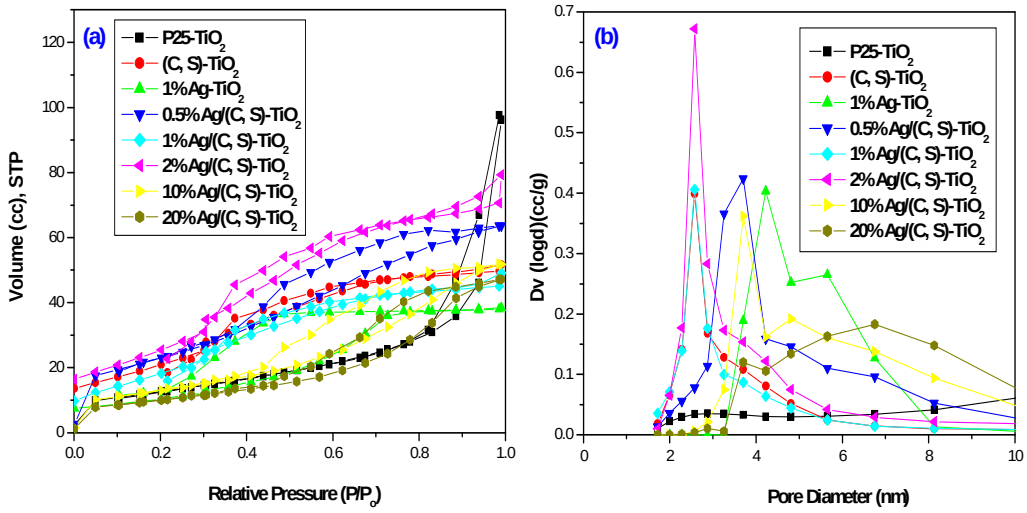

Figure 5.2 (a) Nitrogen adsorption-desorption isotherms and (b) pore-size distribution of the doped and undoped TiO_2 samples

Table 5.2 Specific surface-areas, pore volume and pore diameter of the samples

Samples Ag/(C, S)-TiO_2	BET Area (m^2/g)	Pore Volume (cc/g)	Pore Diameter (nm)
TiO_2-P25	45	0.15	2.3
(C, S)-TiO_2	70	0.09	3.4
1% Ag-TiO_2	34	0.07	3.8
0.5% Ag/(C, S)-TiO_2	83	0.1	3.7
1% Ag/(C, S)-TiO_2	68	0.06	3.4
2% Ag/(C, S)-TiO_2	92	0.13	3.4
10% Ag/(C, S)-TiO_2	46	0.09	3.7
20% Ag/(C, S)-TiO_2	36	0.08	3.7

Furthermore, the powder X-ray diffraction patterns confirmed that the Ag/(C, S)-TiO_2 nanoparticles were in the anatase crystalline phase with less than 10 nm crystallite size (Figure 5.3a). A thorough analysis of the XRD results showed that there was no detectable amount of Ag_2CO_3 or Ag_2SO_4 at silver loading less than 10 mole %; however, the formation of Ag^0 and Ag_2SO_4 could be seen in 20 mole % Ag/(C, S)-TiO_2 (Figure 5.3b).

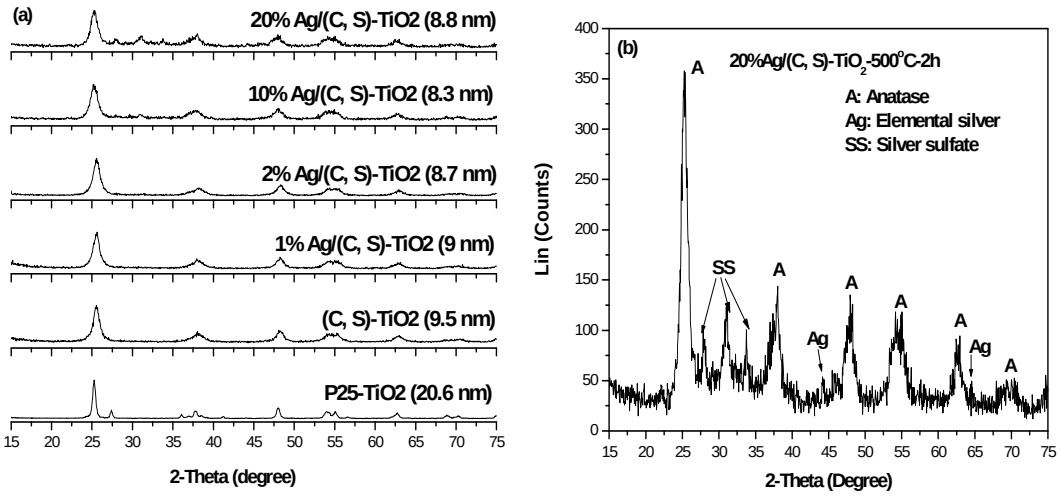

Figure 5.3 (a) XRD patterns of the doped and undoped TiO_2 nanoparticles and (b) an enlarged view of the XRD pattern of 20% Ag/(C, S)-TiO_2

The FT-IR measurement shows characteristic peaks at 1113.1 cm^{-1} and 1053.69 cm^{-1}, assigned to the stretching mode of S-O bonds in SO_4^{2-} species on the surface of (10-20)% Ag/(C, S)-TiO_2 samples (Figure 5.4). The UV-Vis diffuse-reflectance absorption spectra shows that the Ag/(C, S)-TiO_2 nanomaterials exhibit a pronounced visible light absorption at $\lambda > 420$ nm (Figure 5.5).

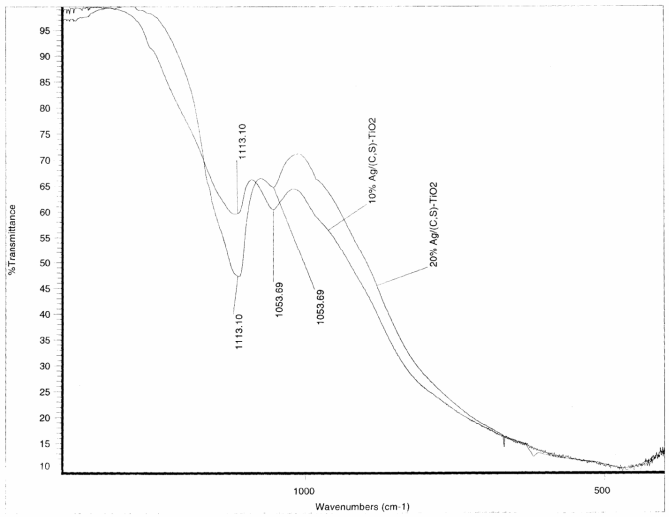

Figure 5.4 FT-IR spectrum of sulfate species present in 10 and 20 mol% silver doped (C, S)-TiO_2 samples obtained with KBr reference

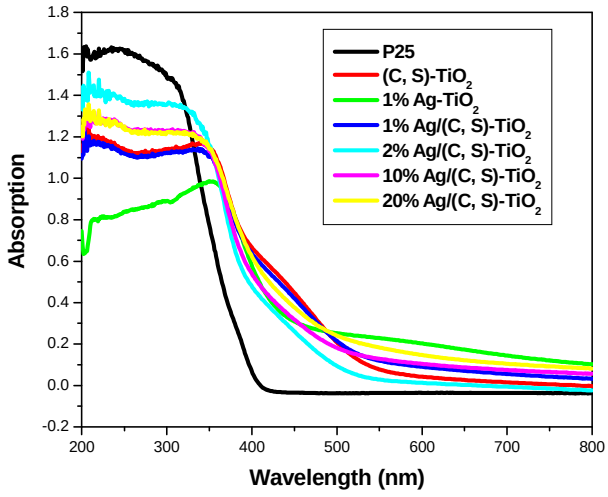

Figure 5.5 UV-visible diffuse reflectance photoabsorption spectra of the doped and undoped TiO_2 nanoparticles

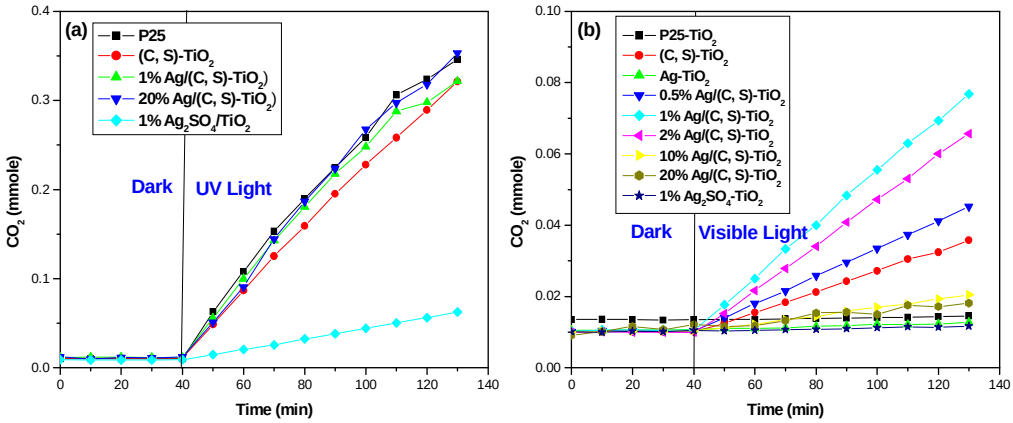

Figure 5.6 Evolution of CO_2 from acetaldehyde degradation with the doped and undoped TiO_2 nanoparticles under (a) UV light and (b) visible light excitation

Figure 5.6a and 6b display the CO_2 evolution from gas-phase CH_3CHO degradation with various catalysts under UV- and visible light illumination, respectively. Under UV light excitation, the TiO_2 photocatalysts co-doped with Ag, C, S, have activities, comparable to that of P25-TiO_2, for CH_3CHO mineralization, except for a control experiment sample of Ag_2SO_4 impregnated TiO_2. However, under visible light excitation, we observed that the (1% and 2 %) Ag/(C, S)-TiO_2 photocatalysts exhibited remarkably higher activities for acetaldehyde mineralization. From these results, we conclude that the co-doping of carbon and sulfur into TiO_2 is necessary for the visible-light-induced photocatalysis, as supported by the CO_2 evolution data obtained for the 1% Ag-TiO_2, 1% Ag_2SO_4-TiO_2 and (C, S)-TiO_2 control samples, that were inactive. Therefore, the optimal low loading, we assume, is due to very high dispersion of the silver species (the visible

light chromophore), which would mean more sites for photon absorption, and, perhaps, suppression of exciton (electron-hole) recombinations.

The ultimate goal of our present work has been to obtain a multipurpose, safe-to-handle material that could serve as a visible light photocatalyst and as a virulent biocide-sporocide capable of killing bacteria and spores without UV light irradiation. Figure 5.7 illustrates the log reduction value for the antibacterial efficacy of the various nanoparticle formulations to kill *E. coli* cells. These results have unequivocally demonstrated higher antibacterial efficacies of the Ag/(C, S)-TiO_2 (log_{10} kill > 6) nanoparticles than that of Degussa TiO_2 (log_{10} kill = 5.2) for 30 minute exposures. In an attempt to understand the effect of codoped carbon and sulfur in the bactericidal action of silver, we determined the amount of codoped carbon and sulfur present in TiO_2 biocide samples (Table 5.1) by EDX analysis. The elemental analysis shows that average amount of codoped carbon is 4.8, 5.8 and 10 at. % and that of codoped sulfur is 1.8, 1.6 and 1.4 at. %, when 0, 1 and 10 mole% silver is loaded. The presence of both of these dopants, carbon and sulfur, seems to be necessary for better photocatalytic properties (See Figure 5.6) and biocidal action (See Figure 5.7 and Figure 5.8). Especially note Figure 5.8 where 1% Ag-TiO_2 is not as effective as 1% Ag/(C, S)-TiO_2. Also, the larger amounts of carbon may help the bactericidal effect of 10% Ag/(C, S)-TiO_2 (8.9 log kill) as compared with 0.5% Ag/(C, S)-TiO_2 (6.7 log kill) and 1% Ag/(C, S)-TiO_2 (6.8 log kill). Obviously, the Ag/(C, S)-TiO_2 nanoparticle formulations with heavily doped silver (> 0.5%) exhibited very impressive spore kill rates (log_{10} kill = 3.3-5.8), compared with the P25-TiO_2 (3.2 log_{10} kill) and other silver doped (< 1%) formulations (1.6-2.5 log_{10} kill) for 30 min exposures. These results clearly show that for *E. coli*, even small amounts of silver have beneficial effects and that heavier loadings are best, where even in 5 min

exposures complete kills were found. However, for *B. subtilis* spores, Ag/(C, S)-TiO_2 formulations with lower loadings of silver were less effective, but higher loadings were quite effective, especially at 30 min exposures. Overall, the time studies (Figures 5.7 and 5.8) on both *E. coli* cells and *B. subtilis* spores suggest that the biocidal effect of silver present in the Ag/(C, S)-TiO_2 samples can remain in action for the prolonged time periods depending on the nature and type of pathogens present. Further work is necessary to determine overall lifetimes.

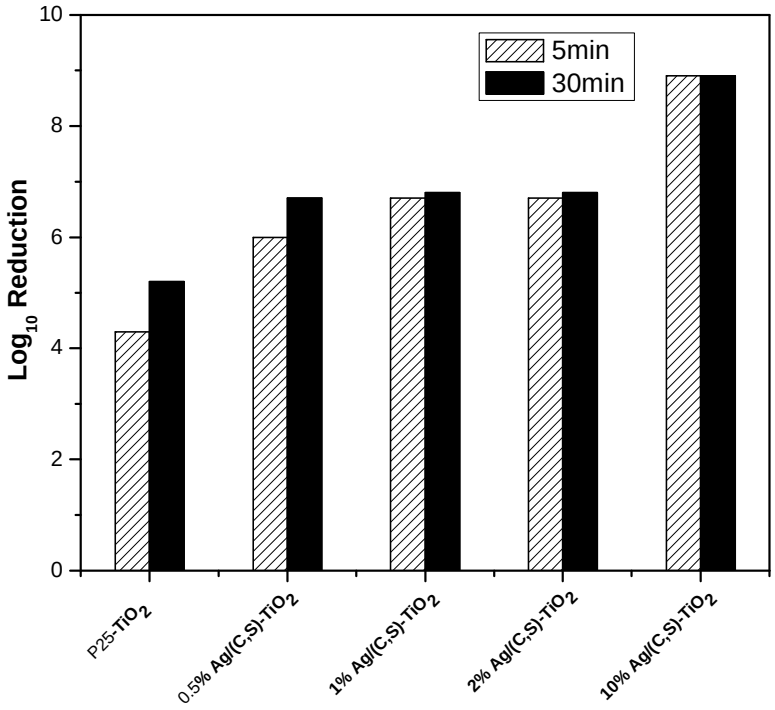

Figure 5.7 Histogram of log_{10} kill values for *Escherichia coli* cells after treatment with the doped and undoped TiO_2 nanoparticles for 5 and 30 minute exposures

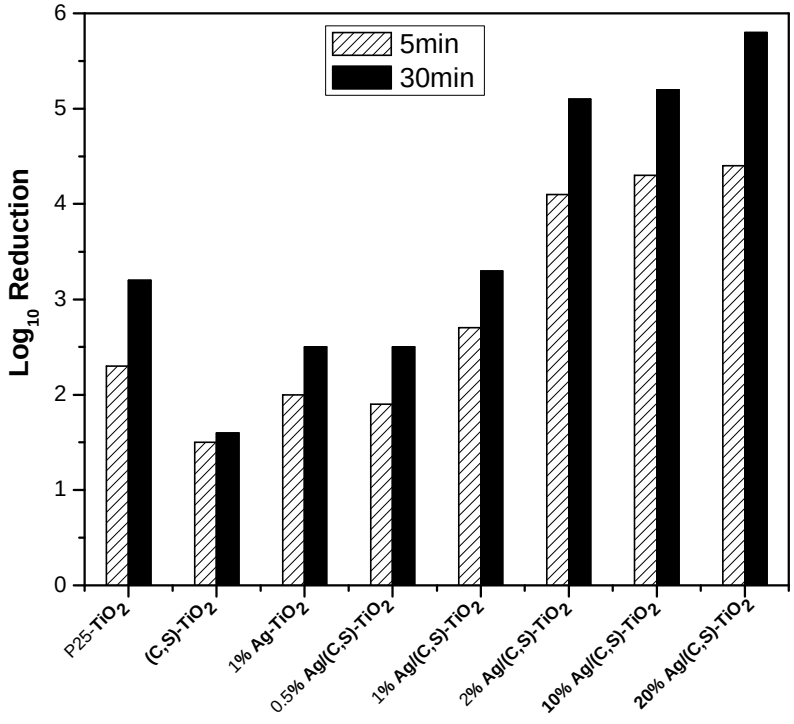

Figure 5.8 Histogram of log_{10} kill values for *Bacillus subtilis* spores after treatment with the doped and undoped TiO_2 nanoparticles for 5 and 30 minute exposures

A plausible reason for the effectiveness of Ag/(C, S)-TiO_2 nanoparticles in the destruction of *E. coli cells* and *B. subtilis* spores may depend on two synergistic factors: (i) Ag^+ ion effect and (ii) (C, S)-TiO_2 support effect. First, since the antimicrobial test was performed without UV or visible light excitation, we ruled out the formation and the involvement of the reactive oxygen species (O_2^- ions, $^{\cdot}OH$ radicals and H_2O_2) in the destruction of the bacterial cells and spores. To validate the key mechanistic role of silver ions, we examined the TEM images of the *E. coli* cells before and after treatment with 10% Ag/(C, S)-TiO_2 nannoparticles (Figure 5.9). We observed

the presence of the heavy electron-dense granules (approximately 10-20nm in size) in the treated *E. coli* (Figure 5.9b) as compared with untreated cells (Figure 5.9a). The morphological differences can be attributed to a facile release of silver ions from the Ag/(C, S)-TiO_2 nanoparticles into the viable *E. coli* cells and their concomitant reduction to silver atoms (and subsequent aggregation to nanoparticles) by thiol groups (-SH) present in enzymes and proteins, thereby inhibiting the respiration process and leading to the ultimate cell death.[8] Indeed, it is generally accepted that silver ions have a great tendency to interact with thiol groups (-SH) in the peptidoglycan layer and the cytosol, which then cause destruction of the cell wall and inactivation of crucial metabolic proteins.[27,28] Feng and co-workers[9] reported electron-dense granules (similar to Figure 5.9b), and analysis showed that they consisted of silver and sulfur. Smetana et al. have also observed this phenomenon with pure silver nanoparticles.[8] In addition, bacteria and spores carry a negative surface charge at biological pH due to the carboxylic acid groups in the proteins, whereas the silver ions are positively charged. This electrostatic interaction increases the contact between the cells/spores and the silver doped TiO_2 nanoparticles. Therefore, our antibacterial results concurred with the recent study that concluded that silver ions were the actual biocidal species.[8] Also, the biocidal activity of silver species (Ag^0 and Ag^+ ions) depends upon the source of Ag^+ ions ($AgNO_3$, AgI, AgBr, AgCl, Ag_2CO_3, Ag_2SO_4),[9,22,23,29-31] size and shape of Ag^0 nanoparticles,[5,6,8] and nature of support materials (carbon aerogels, Al_2O_3, SiO_2 and TiO_2).[27,28,30,32] Therefore, we assume that the exceptionally high biocidal-sporocidal efficacy of silver ions released from 10%Ag/(C, S)-TiO_2 and 20%Ag/(C, S)-TiO_2 nanoparticles might have attributed to the synergistic effects of the codoped carbon and sulfur. In our previous work, [26] we have shown the existence of the synergistic effects of co-doped carbon and sulfur in photodecomposition of gas-phase acetaldehyde with S-TiO_2

and (C, S)-TiO_2 photocatalysts. However, in the current study, we observed that the sporocidal activity of 1% Ag/(C, S)-TiO_2 (3.3 log kill) is higher than that of (C, S)-TiO_2 (1.6 log kill) and 1% Ag-TiO_2 (2.5 log kill), again indicating the existence of a synergistic effect of co-doped carbon, sulfur and silver.

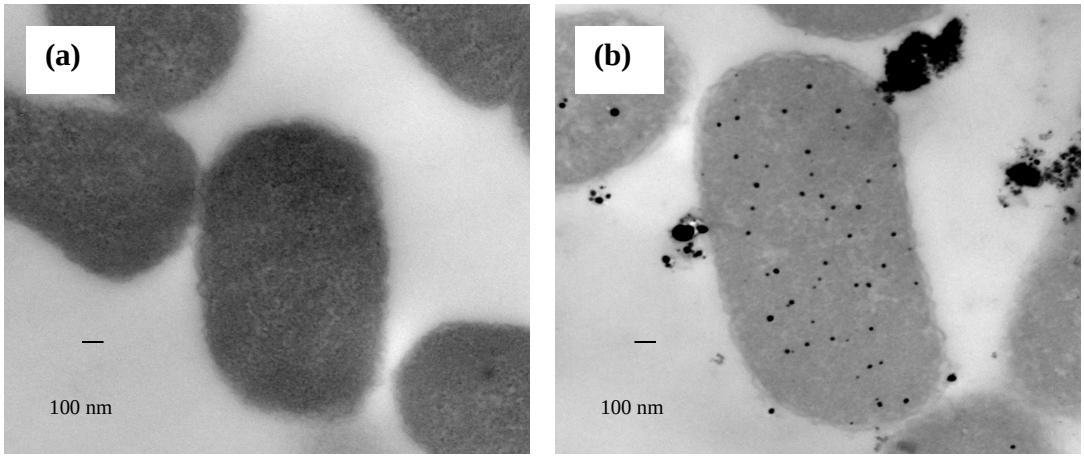

Figure 5.9 The TEM images of *E. coli* cells before (a) and after (b) treatment with 10% Ag/(C, S)-TiO_2 nanoparticles

To elucidate the chemical state and the role of dopants in antibacterial mechanism, the high-resolution, depth-profile XPS spectra of the doped and undoped TiO_2 samples were measured (Figure 5.10). The chemical status of Ti, O, C, S and Ag was determined from their corresponding core-level binding energies (Table 5.3). From the Ti2p and O1s XPS spectra, core-level binding energies in the range of 458.3 – 459.1 eV and 529.8 – 530.4 eV are assigned to $Ti2p_{3/2}$ of Ti^{4+} in pure TiO_2 anatase and lattice oxygen in Ti-O in bond, respectively.[33-35] The

C1s XPS spectrum of the (C, S)-TiO_2 (without silver) sample showed one peak at 284.5 eV and another shoulder peak at 288.6 eV, assigned to elemental carbon and surface-bound CO_3^{2-} species.[36] It appears that Ti-C bonds were not present, as evidenced by the absence of a peak around 281 eV (which arises from the substitution of carbon atoms for lattice oxygen atoms in TiO_2). The C1s XPS spectra of Ag/(C, S)-TiO_2 samples confirmed the presence of elemental carbon but not the carbonate species. The $S2p_{3/2}$ XPS spectra showed broad peaks of surface bound SO_4^{2-} species, with binding energies from 168.4 to 169 eV.[37,38] This rules out the formation of Ti-S bonds (164.8 eV). Finally, the $Ag3d_{5/2}$ XPS binding energy values in the range of 367.4 – 368.1 eV confirmed that the co-doped silver was mostly present as silver ions. However, the distinction between Ag^0 and Ag^+ species become, sometimes, more complicated from the measured $Ag3d_{5/2}$ binding energy values that depend upon the surrounding chemical environments, especially counter anions and supports.[39-41] This is supported with the observed $Ag3d_{5/2}$ B. E in pure Ag_2O and Ag_2SO_4 samples. On the other hand, it is likely that during the annealing step at 500 ^oC, the thermal decomposition of $AgNO_3$ (m. p. 212 ^oC), Ag_2O (m. p. 230 ^oC), or Ag_2CO_3 (m. p. 218 ^oC) could result in the formation of the Ag^0 species. Indeed, Ag^0 was detected in the deconvoluted XRD pattern of the 20% Ag loaded sample at $2\Theta = 44.2^o$; 64.5^o (Figure 1b) without any surface plasmon resonance (SPR) in the UV-Vis spectrum.[42-44] Meanwhile, Ag^0 particles can also get oxidized to Ag_2O species due to oxygen-rich environments. This is supported with the $Ag3d_{5/2}$ B. E. values for the Ag/(C, S)-TiO_2 samples above 1% loading. Unfortunately, we could not detect the presence of the Ag_2O species at 2Θ = 38.04; 54.4^o in the XRD profiles of the samples under current study. Probably the Ag_2O species was in the form of highly dispersed amorphous phases so that the X-ray beams could not detect them. Nevertheless, a certain amount of Ag^+ ions as Ag_2SO_4 could remain in a separate

crystalline phase on the surface of the TiO_2 support, due to the thermal stability of silver sulfate (m. p. 657 ^oC). This was in good agreement with the FT-IR and XRD results.

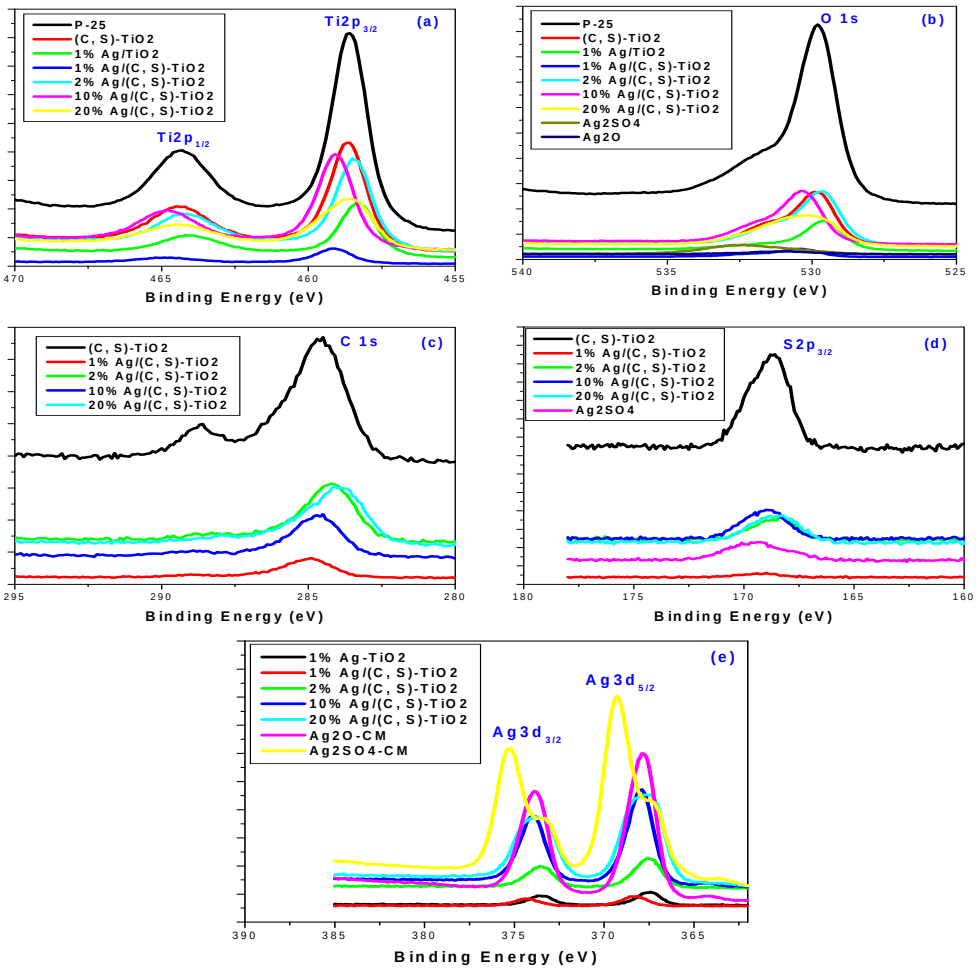

Figure 5.10 Core level XPS spectra of (a) Ti2p, (b) O1s, (c) C1s, (d) S2p, and (e) Ag3d present in various samples

Table 5.3 XPS core level binding energies of Ti, O, C, S, and Ag present in various samples

Sample	Ti $2p_{3/2}$	O1s	C1s	$S2p_{3/2}$	$Ag3d_{5/2}$
P-25	458.6	529.8	-		-
(C, S)-TiO_2	458.6	529.9	284.5; 288.6	168.6	-
1% Ag/TiO_2	458.3	529.6	-		367.4
1% Ag/(C, S)-TiO_2	459.1	530.3	284.9	169	368.1
2% Ag/(C, S)-TiO_2	458.5	529.6	284.2	168.4	367.6
10% Ag/(C, S)-TiO_2	459.1	530.4	284.5	169	367.9
20% Ag/(C, S)-TiO_2	458.6	530.3	284.1	168.5	367.4
Ag_2O	-	531.1	-		367.9
Ag_2SO_4	-	532.4	-	169.4	369.3

Furthermore, the possible importance of the electrostatic attraction forces in antimicrobial action was investigated by zeta potential measurements in aqueous medium (Table 5.4). Herein, we found that the undoped P25-TiO_2 particles carried a substantial amount of positive charge compared with the doped TiO_2 particles. Probably, electrostatic attraction of bacteria is important for pure TiO_2. However, TiO_2 nanoparticles doped with Ag, C, S exhibited smaller positive/negative charges, and the antimicrobial properties of these materials probably cannot be attributed to electrostatic attraction forces. Some other factors that contribute to antimicrobial mechanisms must be considered. As is known, the *E. coli* and *B. subtilis* spores exhibit both hydrophilic and hydrophobic properties. A balance or compromise between hydrophilic and hydrophobic properties is highly desirable to achieve an effective, safe-to-handle, virulent biocide/sporocide.[45] It is well-known that *B. subtilis* spores are more resistant towards silver

biocides than *E. coli* cells due to the presence of spore coat that prevents the penetration of Ag^+ ions through outer and inner membranes. Very interestingly, the observed $\log_{10}$ kill values for *B. subtilis* spores, treated with (C, S)-TiO_2 (1.6), 1% Ag-TiO_2 (2.5) and 1% Ag/(C, S)-TiO_2 (3.3), indicate that the (C, S)-TiO_2 support can elevate the sporocidal properties of Ag^+ ions, most probably with enhanced hydrophobic interactions. In present situation, a straight-forward determination of the exact magnitude of hydrophobic interactions seems rather a complex task; however, the measured zeta potential values (Table 5.4) allow us to estimate partly the hydrophobic properties of the doped TiO_2 biocides. The results show that zeta potential values of (C, S)-TiO_2 (+0.611 mV), % Ag-TiO_2 (-2.76 mV) and 1% Ag/(C, S)-TiO_2 (-2.13 mV) nanoparticles are much smaller than that of P25-TiO_2 (+31.4 mV). This indicates that the doped TiO_2 nanoparticle surfaces could possibly be hydrophobic in nature. Further, on the basis of zeta potential data, it seems logical to say that higher sporocidal activity of the 1% Ag/(C, S)-TiO_2 (3.3 log kill) than that of 1% Ag-TiO_2 (2.5 log kill) without C, S could be attributed to an interplay of hydrophobic interactions induced by carbon and sulfur codoping in particular. The details regarding how this happens can only be speculated upon. It may be that the carbon imparts a hydrophobic nature, as discussed above, and perhaps the sulfur (as dispersed sulfate) controls or moderates silver ions release. Thus, we believe that the (C, S)-TiO_2 support and Ag species (Ag^0, Ag^+) acted synergistically during deactivation of both *E. coli* and *B. subtilis* spores.

Table 5.4 Zeta potentials of the doped and undoped TiO_2 samples measured at pH = 3

Sample	Zeta potential (mV)
P25-TiO_2	+31.4
(C, S)-TiO_2	+0.611
1% Ag-TiO_2	-2.76
0.5% Ag/(C, S)-TiO_2	+1.27
1% Ag/(C, S)-TiO_2	-2.13
2% Ag/(C, S)-TiO_2	+1.17
10% Ag/(C, S)-TiO_2	-5.52
20% Ag/(C, S)-TiO_2	-3.75

Despite recent studies on light and dark biocidal activities of cationic conjugated polyelectrolytes,[46,47] future work is necessary to determine if visible light irradiation can further improve the biocidal effects of the lighter loading of silver in Ag/(C, S)-TiO_2 nanomaterials.

5.4 Conclusions

Overall, the following interesting findings have been made: (1) the TEM images show that silver ions have migrated into the cell, which indicates that the doped silver has an important role. (2) An increase in the destruction of cells/spores with an increasing amount of the doped silver has been observed. (3) This enhanced biocidal effect of silver against both cells and spores could be attributed to the synergistic effect of the TiO_2 support co-doped with carbon and sulfur, as supported by the data obtained for Ag-TiO_2 without C, S. (4) This Ag/(C, S)-TiO_2 nanocomposite can serve as a potent biocide/sporocide at higher loadings, and a photocatalyst under visible light at lower loadings. It would seem that this system has promise as a multifunctional system. (5) Further work is needed to add detail to the synergetic effects of all these components, especially the effect of visible light on enhancement of sporocidal activity.

5.5 References

1. Matsunaga, T.; Tomoda, R.; Nakajima, T.; Nakamura N.; Wake, H., *FEMS Microbiol. Lett.* **1985,** 29, 211-214.

2. Matsunaga, T.; Tomoda, R.; Nakajima, T.; Nakamura N.; Komine T., *Appl. Environ. Microbiol*. **1988,** 54, 1330-3.

3. Maness, P. C.; Smolinski, S.; Blake, D. M.; Huang, Z.; Wolfrum, E. J.; Jacoby, W. A., *Appl. Environ. Microbiol*. **1999**, 65, 4094-4098.

4. Sondi, I.; Salopek-Sondi, B., *J. Colloid Interface Sci.* **2004**, 275, 177-182.

5. Morones, J. R.; Elechiguerra, J. L.; Camacho, A.; Holt, K.; Kouri, J.B.; Ramirez, J.T.; Yacaman, M. J., *Nanotechnology* **2005,** 16(10), 2346-2353

6. Pal, S.; Tak, Y.K.; Song, J.M., *Appl. Environ. Microbiol*. **2007**, 73(6), 1712-1720.

7. Kumar, A.; Vemula, P. K.; Ajayan, P. M.; John, G., *Nat. Mater.* **2008,** 7, 236-241.

8. Smetana, A. B.; Klabunde, K. J.; Marchin, G. R.; Sorensen, C. M., *Langmuir* **2008**, 24, 7457-7464.

9. Feng, Q. L.; Wu, J.; Chen, G. Q.; Kim, T. N.; Kim, J. O., *J. Biomed. Mater. Res.* **2000**, 52, 662-668.

10. Yamanaka, M.; Hara, K.; Kudo, J., *Appl. Environ. Microbiol*. **2005**, 71, 7589-7593.

11. Jung, W. K.; Koo, H. C.; Kim, K. W.; Shin, S.; Kim, S. H.; Park, Y. H., *Appl. Environ. Microbiol*. **2008,** 74, 2171-2178.

12. Sokmen, M.; Candan, F.; Sumer, Z., *J. Photochem. Photobiol. A* **2001**, 143, 241-244.

13. Zhang, L.; Yu, J. C.; Yip, H. Y.; Li, Q.; Kwong, K. W.; Xu, A. W.; Wong, P. K., *Langmuir* **2003**, 19, 10372-10380.

14. Vohra, A.; Goswami, D. Y.; Deshpande, D. A.; Block, S. S., *Appl. Catal. B **2006***, 64, 57-65.

15. Guin, D.; Manorama, S. V.; Latha, J. N. L.; Singh, S., *J. Phys. Chem. C* **2007**, 111, 13393-13397.

16. Liu, Y.; Wang, X.; Yang, F.; Yang, X., *Microporous Mesoporous Mater.* **2008,** 114, 431-439.

17. Reddy, M. P.; Venugopal, A.; Subrahmanyam, M., *Water Res.* **2007**, 41, 379-386.

18. Vohra, A.; Goswami, D. Y.; Deshpande, D. A.; Block, S. S., *J. Ind. Microbiol. Biotechnol.* **2005**, 32, 364-370.

19. Yu, J. C.; Ho, W.; Yu, J.; Yip, H.; Wong, P. K.; Zhao, J., *Environ. Sci. Technol*. **2005**, 39, 1175-1179.

20. Wong, M. S.; Chu, W. C.; Sun, D. S.; Huang, H. S.; Chen, J. H.; Tsai, P. J.; Lin, N. T.; Yu, M. S.; Hsu, S. F.; Wang, S. L.; Chang, H. H., *Appl. Environ. Microbiol*. **2006**, 72, 6111-6116.

21. Li, Qi; Xie, R.; Li, Y. W.; Mintz, E. A.; Shang, J. K., *Environ. Sci. Technol*. **2007**, 41, 5050-5056.

22. Hu, C.; Guo, J.; Qu, J.; Hu, X., *Langmuir* **2007**, 23, 4982-4987.

23. Lan, Y.; Hu, C.; Hu, X.; Qu, J., *Appl. Catal. B* 2007, 73, 354-360.

24. Hu, C.; Lan, Y.; Qu, J.; Hu, X.; Wang, A., *J. Phys. Chem. B* **2006**, 110, 4066-4072.

25. Elahifard, M. R.; Rahimnejad, S.; Haghighi, S.; Gholami, M. R., *J. Am. Chem. Soc.* **2007**, 129, 9552-9553.

26. Hamal, D. B.; Klabunde, K. J., *J. Colloid Interface Sci*. **2007**, 311, 514-522.

27. Zhang, S.; Wu, D.; Wan, L.; Tan, H.; Fu, R., *J. Appl. Polym. Sci*. **2006**, *102*, 1030-1037**.**

28. Kim, Y. H.; Lee, D. K.; Cha, H. G.; Kim, C. W.; Kang, Y. S., *J. Phys. Chem. C* **2007**, *111*, 3629-3635.

29. Corbett, R. J., *Int. J. Cosmetic Sci.* **1996**, 18, 151-165.

30. Buckley, J. J.; Gai, P. L.; Lee, A. F.; Olivi, L.; Wilson, K., *Chem. Commun.* **2008**, 34, 4013-4015.

31. Peng, B.; Yuan, C.; Chai, L. Y.; Wei, S. W.; Yu, Y. F.; Su, W. F., *Trans. Nonferrous Met. Soc. China* **2005**, 15, 1156-1160.

32. Liu, H. R.; Lin Y.; Ye, R. F.; Song, Li.; Chen, Q., *Key Eng. Mater.* **2007**, 330-332, 995-998.

33. Joung, S. K.; Amemiya, T.; Murabayashi, M.; Itoh, K., *Chem. Eur. J.* **2006**, 12, 5526-5534.

34. Guin, D.; Manorama, S. V.; Latha, J. N. L.; Singh, S., *J. Phys. Chem. C* **2007**, 111, 13393-13397.

35. Park, M. S.; Kang, M., *Mater. Lett.* **2008**, 62, 183-187.

36. Shi, Z. M.; Ye, X. Y.; Liang, K. M.; Gu, S. R.; Pan, F., *J. Mater. Sci. Lett.* **2003**, 22, 1255-1258.

37. Li, X.; Xiong, R.; Wei, G., *Catal. Lett.* **2008**, 125, 104-109.

38. Sun, H.; Liu, H.; Ma, J.; Wang, X.; Wang, B.; Han, L., *J. Hazar. Mater*. **2008**, 156, 552-559.

39. Bowering, N.; Croston, D.; Harrison, P. G.; Walker, G. S., *Inter. J. Photoenergy* **2007**, 1, 90752/1-90752/8.

40. Li, Y.; Zhang, H.; Guo, Z.; Han, J.; Zhao, X.; Zhao, Q.; Kim, S. J., *Langmuir* **2008**, 24, 8351-8357.

41. Shah, M. S. A. S.; Nag, M.; Kalagara, T.; Singh, S.; Manorama, S. V., *Chem. Mater.* **2008**, 20, 2455-2460.

42. Zhang, H.; Wang, G.; Chen, D.; Lv, X.; Li, J., *Chem. Mater.* **2008**, 20, 6543-6549.

43. Li, H.; Duan, X.; Liu, G.; Liu, X., *J. Mater. Sci.* **2008**, 43, 1669-1676.

44. Liu, Y.; Wang, X.; Yang, F.; Yang, X., *Microporous Mesoporous Mater.* **2008**, 114, 431-439.

45. Klibanov, A. M., *J. Mater. Chem.* **2007**, 17, 2479-2482.

46. Chemburu, S.; Corbitt, T. S.; Ista, L. K.; Ji, E.; Fulghum, J.; Lopez, G. P.; Ogawa, K.; Schanze, K. S.; Whitten, D.G., *Langmuir* **2008,** *24*, 11053-11062.

47. Corbitt, T. S, Ding, L.; Ji, E.; Ista, L. K.; Ogawa, K.; Lopez, G. P.; Schanze, K. S.; Whitten, D. G., *Photochem. Photobiol. Sci.* **2009**, 8, 998-1005.